ENHANCEMENT OF COOLING TOWER PERFORMANCE BY MANIPULATION OF RAIN ZONE DROP SIZE

by

Henry Randolph Oosthuizen

Thesis presented in partial fulfilment of the requirements for the degree Master of Engineering at the University of Stellenbosch.

Thesis Supervisor: Prof. P.J.Erens

Department of Mechanical Engineering
University of Stellenbosch
March 1995

DECLARATION

I, the undersigned, hereby declare that the work contained in this thesis is my own work and has not previously in its entirety or in part been submitted at any university for a degree.

Signature Date

This thesis is dedicated to my parents,
Ronnie and Hannetjie Oosthuizen

ABSTRACT

The possibility of improving the heat transfer in the rain zone of large natural draft wet cooling towers, by decreasing the mean drop diameter in this region, has been investigated.

Experimental studies were aimed at determining typical drop size distributions under trickle packs and obtaining actual performance data for packing and rain zone combinations in a cooling tower test facility. A photography-based method, which utilizes image processing techniques, was developed to determine the drop size distributions found in the test facility. A computer simulation program developed by Dreyer [94DR1] was used to theoretically predict rain zone performance data (i.e., transfer coefficients and drop size distribution data) for comparison with and evaluation of the experimental data.

It was found that by placing a layer of splash grids beneath a trickle pack the mean drop diameter in the rain zone was decreased, resulting in corresponding increases in transfer characteristic. Using a computer simulation program it was calculated that this arrangement could increase the thermal capacity of a large natural draft cooling tower by up to 5 %.

Keywords : Cooling tower, rain zone, drop size measurement, image processing

OPSOMMING

Die moontlikheid om die warmteoordrag in die reënsone van 'n natuurlike trek nat koeltoring te verbeter deur die gemiddelde druppel diameter van die sproei te verminder is ondersoek.

Eksperimentele werk was daarop gerig om tipiese druppelgrootte verspreidings onder druppakking te bepaal, asook die verkryging van werklike verrigtings-data vir verskillende pakking en reënsone kombinasies in 'n koeltoring toetsfasiliteit. 'n Fotografiese metode wat gebruik maak van beeldverwerkingstegnieke is ontwikkel om die druppelgrootte verspreidings wat in die koeltoring toetsfasiliteit gevind word te bepaal. 'n Rekenaar simulasieprogram wat ontwikkel is deur Dreyer [94DR1] is verder gebruik om reënsone verrigtingsdata (oordragskarakteristieke en druppelgrootte verspreidings) teoreties te voorspel, vir vergelyking met en evalusie van die eksperimentele resultate.

Dit is bewys dat die plasing van 'n laag spatroosters reg onder druppakking die gemiddelde druppeldiameter in die reënsone verminder het, wat gelei het tot 'n ooreenstemmende toename in oordragskarakteristiek. Met die gebruik van 'n rekenaar simulasie program is bereken dat hierdie opstelling die termiese kapasiteit van 'n koeltoring met tot 5 % kan verbeter.

Sleutelwoorde : Koeltorings, reënsone, druppelgrootte verspreidings, beeldverwerking

ACKNOWLEDGMENTS

I would like to thank my thesis supervisor Prof. P.J. Erens for his advice and encouragement throughout this investigation.

I would also like to thank Mr. C. Zietsman for his valuable technical assistance.

TABLE OF CONTENTS

NOMENCLATURE

Symbols

A	Area, m^2
a	Surface area per unit volume, m^2/m^3
C_D	Drag coefficient, *dimensionless*
c_p	Specific heat (heat capacity), *J/kgK*
d	Diameter, *m*
d_{30}	Mass mean diameter, defined in Equation 2.8, *m*
d_{32}	Sauter mean diameter, defined in Equation 2.7, *m*
d_{RR}	Scale parameter for Rosin-Rammler distribution, *m*
E	Drop deformation, *dimensionless*
e	Eccentricity, *dimensionless*
g_{YS}	Correction factor defined by Yao [74YA1], *dimensionless*
G	Air mass flux, kg/m^2s
g	Gravitational acceleration, m/s^2
h_c	Convection heat transfer coefficient, W/m^2K
i	Enthalpy, *J/kg*
k	Thermal conductivity, *W/mK*
K	Mass transfer coefficient, kg/m^2s
KaV/L	Transfer characteristic, *dimensionless*
$KaZ/\dot{M}_w$	Transfer characteristic, *dimensionless*
L	Merkel notation for $\dot{M}_w$, kg/m^2s
m	Mass flow rate, *kg/s*
$\dot{M}_w$	Water mass flux, kg/m^2s
n	Number, *dimensionless*
n_{RR}	Shape parameter for Rosin-Rammler distribution, *m*
N_p	Pressure loss coefficient (Number of pressure heads), m^{-1}
Δp	Pressure drop, *Pa*
$\dot{Q}$	Heat transfer rate, *W*
R	Cumulative mass fraction, *dimensionless*
R^2	Correlation coefficient, *dimensionless*
t	Time, *s*
T	Temperature, ℃
v	Velocity, *m/s*
V	Merkel notation for Z, *m*
w	Humidity of air, (*kg water/kg dry air*)
x_{RR}	Additional parameter for Rosin-Rammler distribution, m^{-1}

z	Vertical height or fall distance, *m*
Z	Packing thickness, *m*

Greek symbols

ρ	Density, kg/m^3
σ	Surface tension, *N/m*

Subscripts

a	Air
as	Saturated air
f	Fluid
g	Gas
i	Interface
j	Summation index
m	Maximum
rz	Rain zone
sg	Splash grid
sz	Spray zone
tp	Trickle pack
T	Terminal
w	Water

Dimensionless groups

Eo	Eotvos number,	$\frac{g(\rho_p - \rho_l)d^2}{\sigma}$
Le	I ewis number,	$\frac{\alpha}{D}$ or $\frac{Sc}{Pr}$
Le_f	Lewis factor	$\frac{h_c}{K c_{pm}}$
$M_{\dot{z}}$	Acceleration modulus,	$\frac{(\partial v / \partial t)d}{v^2}$
Nu	Nusselt number,	$\frac{h_c d}{k}$
Re	Reynolds number,	$\frac{\rho v d}{\mu}$

Sh	**Sherwood number,**	$\frac{h_D d}{D}$

CHAPTER 1

INTRODUCTION

Evaporative cooling towers are commonly used for the cooling of water in many industrial processes. They are used extensively in the power generation industry, as well as industries such as steel making, food processing, industrial refrigeration, air conditioning, the chemical industry, plastics, the dairy industry, breweries, distilleries and the petrochemical industry. Cooling towers have evolved quite considerably since the simple spray pond with many different types of cooling towers being currently used in various industries. In the power generation industry, large natural draught wet cooling towers are still used extensively, despite the developments in dry cooling and hybrid cooling. Natural draught cooling towers combine the advantages of relatively low construction and operation costs and the ability of cooling large amounts of water. The large concrete hyperbolodial shape of these towers is a familiar sight in the industrial landscape of this country.

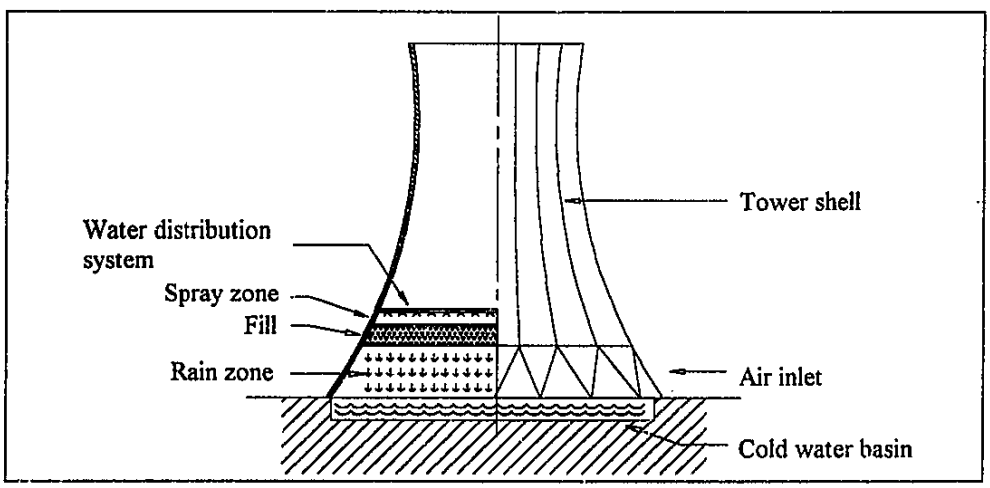

***Figure 1.1** Natural draft counterflow cooling tower.*

In natural draft cooling towers the kind of fill used is usually of the splash pack or trickle pack type. These towers have a large rain zone beneath the fill, due to the large inlet height required to reduce air inlet flow losses. The cooling occuring in this area can contribute as much as 20% to the total cooling capacity of the tower. It is therefore advantageous to have droplets of small size in the rain zone since this would increase the cooling in this region, due to an increase in interfacial area and drop residence times. Whereas some packing material produce small drops in the rain zone others, particularly film packs and trickle packs tend to produce

larger drops reducing the amount of cooling attainable in the rain zone. These packs, however, have other advantages such as low height (therefore less pumping power) and high strength.

In this project the possibility of reducing the drop size in the rain zone is investigated in order to retain the advantages of film packs and trickle packs while increasing the rain zone performance. Experimental studies were aimed at detecting typical drop size distributions under trickle packs and obtaining actual performance data. A mathematical model developed by Dreyer [94DR1] was used to theoretically predict rain zone performance data (i.e., transfer coefficients and drop size distribution data) for comparison with and evaluation of the experimental data.

CHAPTER 2
LITERATURE SURVEY

In this chapter the literature relevant to cooling tower analysis and drop size measurement is reviewed. Section 2.1 gives an overview of cooling tower theory and the determination and calculation of transfer characteristics. Section 2.2 discusses methods of drop size measurement and data abstraction as well as methods of classifying drop size distributions and calculation of average drop sizes. Section 2.3 summarises the literature survey and outlines the conclusions drawn.

2.1 COOLING TOWER ANALYSIS

2.1.1 Cooling tower theory

In a cooling tower both heat and mass transfer are utilised to cool the water. A mathematical statement of the cooling process may be expressed as :

$$d\dot{Q} = h_c(T_i - T_a)dA + K(w_{asi} - w_a)i_g dA, \qquad (2.1)$$

with the first term on the right giving the heat transfer and the second the mass transfer. The first attempts at the modelling of this heat and mass transfer process were made at the turn of the century. Various papers were presented on the subject (See McKelvey [59Mc1]), but it was only when Merkel [26ME1] developed a simplified relation for heat and mass transfer that a method was found that gained widespread approval in the analysis of wet cooling towers. The greatest merit of the Merkel theory is its simplicity. His analysis characterises the sensible- and latent- heat transfer as a combined heat and mass transfer process based on a driving force created by the enthalpy difference between the moist air and the air on the surface of the water droplets. Since the moist air is heated and saturated as it passes through the tower, the temperature, and thus enthalpy, of both moist air and also the water droplets is a function of location in the tower.

Merkel hypothesised that a film of saturated air exists adjacent to the water surface at a temperature between that of the mainstream air and the liquid water. During steady-state conditions the heat and mass transfer from the water surface to the saturated air film must be equal to the heat and mass transfer from the saturated air film to the main air stream. The Merkel equations express this energy balance and describe the simultaneous mass and heat transfer through the Lewis relation. The assumptions made in the Merkel analysis can be summarised as follows :

1) The interfacial film between water and air is saturated at water temperature T_w.
2) The interfacial film offers no resistance to heat or mass transfer from the water to the bulk air.
3) The vapour contents in the film and bulk air are proportional to the respective partial pressures.
4) The Lewis factor is equal to one, i.e. , $Le_f = h_c/c_{pm}K = 1$.
5) The specific heat of water, c_{pw} is constant over the temperature range T_w to T_a.
6) Water mass flow rate per unit area is constant, i.e., the effect of evaporation is negligible.

With the help of these assumptions the relation for the cooling process then becomes

$$d\dot{Q} = K(i_{asw} - i_a)dA \tag{2.2}$$

Noting that $\dot{m}_a\, di_a = \dot{m}_w\, c_{pw}\, dT_w$, integration of Equation (2.2) between the water inlet and outlet positions of a cooling tower yields the following integral

$$\frac{KaZ}{\dot{M}_w} = \int_z \frac{c_{pw}\,dT}{(i_{asw} - i_a)} \tag{2.3}$$

$KaZ/\dot{M}_w$, or KaV/L as it is more commonly known, is the well-known Merkel number, or transfer characteristic. Equations (2.2) and (2.3) are known as the Merkel equations. Given the inlet water and air conditions the Merkel equations predicts the enthalpy (hence wet-bulb temperature) of the outlet air, but not its humidity. The equations also predict the required number of transfer units (NTU), or the transfer characteristic (KaV/L, also known as number of diffusion units) needed to accomplish the process. Both these numbers give an indication of the performance of the packing in a wet cooling tower. Historically, the use of the packing characteristic has been favoured over the transfer unit method.

Subsequent research in cooling tower modelling has been aimed at investigating the effect of the assumptions made in the Merkel model on the accuracy of cooling tower performance prediction as well as devising methods to compensate for several of these assumptions and approximations.

Mickley [49MI1] introduced temperature and humidity gradients, heat and mass transfer coefficients from water to interfacial film, and from film to air. Cribb [59CR1] showed that the liquid film resistance does exist, but that it can be considered negligible for practical design purposes of direct contact coolers. Baker and Mart [52BA1] based their analysis on a unit-volume coefficient, which is a fraction of a transfer unit. They also developed a "hot water

correction factor" which reduced scatter in their test data. Baker and Shryock [61BA2] discussed the errors in the model due to the assumptions and describe methods to minimise them. These include the use of a *true* potential difference based on a temperature gradient as well as taking into consideration the effect of evaporation losses. No attempt was made to evaluate these improvements. Nahavandi et al. [74NA1] determined the effect of evaporation losses in counterflow cooling towers. His analysis shows an error introduced by ignoring evaporation losses as high as 12%. Marseille et al. [91MA1] describes a liquid-side film resistance model. The theory is similar to that of Baker and Shryock [61BA1], based on a difference between true and apparent driving potential. Marseille et al. shows that surface temperature has a greater impact on the enthalpy difference across air side film as the temperature of the interface increases. The model thus avoids the use of hot water correction techniques that have been used to account for apparent dependence of the mass transfer coefficient on temperature. Lefevre [84LE1] presents a detailed analysis of the Merkel assumptions as well as traditional calculation methods such as the Chebycheff method of integration. He concluded that it is not clear whether the temperature correction factor can be replaced by eliminating the Merkel assumptions. Ninic and Vehauc [92NI1] investigated the effect of the choice of enthalpy zero point on cooling tower design. They showed that shifting the water enthalpy zero point from 0°C to the tower outlet water temperature increases the accuracy of the computation. This method basically eliminates the assumption of negligible evaporation.

Despite the shortcomings of the Merkel theory, it provided the basis for cooling tower modelling through the years as well as being sufficiently accurate for design purposes. However, since the advent of computers and improved numerical methods, more precise models could be developed and implemented. The emphasis in research changed from simplified methods of cooling tower analysis to comprehensive and detailed models for computerized analysis of cooling towers. These models include those developed by Poppe [84PO1], Bourillot [83BO1], Sutherland [83SU1], Webb [88WE1] and Feltzin and Benton [91FE1]. A detailed analysis of the different cooling tower models is given by Dreyer [88DR1].

2.1.2 Transfer characteristic

The transfer characteristic, KaV/L (or NTU) plays an important role in the performance evaluation of cooling towers. It is usually associated only with the fill material. Standard cooling tower design depends on experimentally determined values of the transfer characteristic for the fill material. These values, as well as approximations of the characteristics for the spray and rain zones, are then used for evaluation purposes. Recently attempts have

been made at determining the transfer characteristic for splash packing from basic principles [94DR1]. The theoretical modelling of transfer characteristics will be discussed later in this section.

a) Fill material transfer characteristic

The value of KaV/L depends on several factors, such as the geometry of the packing, the water loading and the air mass flow rate through the tower. As have been stated previously, this value cannot be calculated theoretically and has to be determined experimentally for each type of packing material. The calculated transfer characteristic is then correlated as a function of air and water mass flow rates or air/water mass flow ratio. The conventional procedure is to evaluate the transfer characteristic by means of Merkel's equation, using experimental data.

The experimentally determined values for the transfer characteristic can then be correlated by relations of the form

$$\frac{KaV}{L} = c_1\left(\frac{L}{G}\right)^n \tag{2.4}$$

or

$$\frac{KaV}{L} = c_2 L^m G^n \tag{2.5}$$

These correlations in effect describe the performance of a packing material which can then be used for design purposes. Various investigators measured and correlated experimental transfer characteristic and pressure drop data for different types of packing material. Lowe and Christie [62LO1] carried out the pioneering work in this field, and provided the basis for subsequent investigations into packing performance. Cale [82CA1] also completed a thorough investigation and more recently Johnson [90JO1] obtained transfer and pressure drop data for eight crossflow and eight counterflow fills.

The above correlations state that the transfer characteristic is dependent on the water and air mass flow rates. The evaporation of water, however, results in the transfer characteristic not being constant throughout the packing material. The evaporation of a portion of the water causes a smaller water mass flow rate at the cooling tower air inlet, or a smaller (L/G) ratio. The exponent n in equation (2.4) is negative and hence a smaller (L/G) ratio will result in a larger transfer characteristic. The correlation of the transfer characteristic only as a function of air and water mass flow rates will therefore result in an over prediction of the performance of packing material.

Tezuka et al. ([73TE1],[75TE1],[86FU1]) correlated the transfer characteristic as a function of the packing depth and hydraulic diameter, as well as the air and water mass flow rates.

The transfer characteristic is also dependent on the water temperature. Although it is desirable that the transfer characteristic be correlated in such a way that it is independent of the water temperature, this cannot be achieved. This was first noticed and investigated by Kelly and Swenson [56KE1], Lefevre [85LE1], Kametani et al. [87KA1] and Webb [88WE1] also investigated the errors associated with ignoring the temperature dependency of the transfer characteristic. Experience has shown that the transfer characteristic decreases with increased water inlet temperature. Schultz and Erens [90SC1] investigated the performance of packing material at low temperatures for bulk air coolers.

One of the shortcomings of available literature on correlations of the transfer characteristic is a lack of information regarding the size of the spray zone and the rain zone below the packing for which the transfer characteristic was measured. The degree to which 'wall effects' had been eliminated, as well as initial drop size distributions, are also not known. Baker and Mart [52BA1] commented on the effect of water cooling on the test cooling tower walls but concluded that no correction was necessary in their research. Lowe and Christie used an experimental tower with a cross section of 1.216 m^2 to obtain their results. Singham [83SI1] reports that cross sections as small as 0.456 m^2 have been used to obtain packing data. It can be assumed that with cross sections this small, the effect of heat and mass transfer from the section walls may be considerable. Basson [94BA1] constructed a water collection system that independently drains water from the wall and from central area of the cooling tower test facility at the University of Stellenbosch, thereby minimising the wall effect.

The correlation of the transfer characteristic of fill is usually accompanied by correlations for the pressure loss coefficient. The pressure loss coefficient is usually expressed in a relation similar to the correlation for transfer characteristic, i.e.,

$$N_p = \frac{\Delta p}{0.5\rho_a v_a^2} = c_3 L^n G^m \tag{2.6}$$

b) Rain zone transfer characteristic

Until recent years the contribution of the rain zone to cooling tower performance had been largely neglected. A lot of work was done on correlating the transfer characteristic and pressure drop data for various packing materials as shown in the previous section. Singham [83SI1] noted that the spray zones were not accounted for in packing data. As a rule of thumb, Lowe and Christie [62LO1] suggested that, for a spray in a counter flow tower, a value of c_1

in equation (2.5) in the range 0.033-0.066 m^{-1} with n about -0.5, be used. In cooling tower design this value would then just be added to the value of KaV/L for the packing. However, individually developed correlations for the transfer characteristic in the pure droplet zones, i.e., the spray and rain zones, based on more relevant parameters, were ignored.

It has only been in the study of spray cooling towers (cooling tower without any fill) that the heat and mass transfer in droplet sprays received attention, thus making it possible to calculate the transfer characteristic of the sprays. Niederman et al. [41NI1], Lowe and Christie [62LO1], and Dutkiewicz [66DU1] have described experimental investigations while Nottage and Boelter [40NO1] have reported an analytical approach. More recently Missimer and Bracket [85MI1] and Sedina [92SE1] conducted model tests of the rain zones in natural draught cooling towers. Hollands [74HO1] modelled the operation of a spray cooling tower mathematically using basic aerodynamic, hydrodynamic and heat/mass transfer information. He concluded that a uniformly sized drop distribution would be more desirable than a wide droplet-size distribution. He also noted that the mean droplet size should be as small (between 1-2 mm) as possible for high performance. Warrington and Musselman [83WA1] reached the same conclusion in comparing the performance of a mono-dispersed (single drop size) spray to that of a poly-dispersed (distribution of drop sizes) spray.

Benton and Rehberg [86BE1], Benocci et al. [86BE1], Hoffmann and Kröger [90HO1], Rennie and Hay [92RE1] and Conradie [93CO1] used numerical models to calculate the performance of the rain zones below the packing in large natural draught cooling towers. These models all use single drop sizes to represent the actual drop size distribution. This is because modelling of individual drops would be prohibitive in terms of computing time.

The Sauter mean diameter and the mass mean diameter is usually used when modelling heat and mass transfer in disperse systems with single drop sizes. The Sauter mean diameter of a distribution of drop sizes is that diameter which has the same surface area to mass ratio as the complete distribution. Symbolically, the Sauter mean diameter, d_{32} can be expressed as

$$d_{32} = \frac{\sum_j n_j d_j^3}{\sum_j n_j d_j^2} \tag{2.7}$$

Similarly, the mass mean drop diameter is defined as

$$d_{30} = \left(\frac{\sum_j n_j d_j^3}{\sum_j n_j} \right)^{1/3} \tag{2.8}$$

The choice of a suitable representative drop size has been shown to be one of the major parameters affecting the predicted cooling tower performance. Table 2.1 shows the effect of water droplet size on cooling tower performance according to the model by Rennie and Hay.

***Table 2.1** Effects of water droplet size on cooling tower performance ([92RE1]).*

Droplet Diameter *mm*	Mean Recooled Water Temperature, ^{o}C	Mean Air Exit Temperature, ^{o}C	Tower Air Flow *kg/s*
2	18.5	23.9	9494
3	19.3	23.1	9664
4	19.7	22.6	9736
5	20.0	23.3	9789

Dreyer [94DR1] developed a computer program for the modelling of cooling tower splash pack. His analysis of the spray zones does not depend on a single representative drop size, but uses initial drop size distribution data for the computation of heat and mass transfer in the spray zones. This approach is based on a packet concept in which drops of similar properties (temperature, size, velocity) are grouped together.

2.1.3 Mathematical modelling from basic principles

Earlier attempts at analysing the performance of sprays depended on empirical or analytical correlations to predict the transfer characteristic. Later models used basic drop thermal and dynamic behaviour information to predict the transfer characteristics. The use of basic information has also been extended to the modelling of splash packing, as shown in the dissertation of Dreyer [94DR1]. This kind of approach necessitates knowledge regarding drop thermal and dynamic behaviour. The following is a short overview of available literature on the subjects of drop thermal and dynamic behaviour, which could be used in the modelling of splash pack.

a) Drop dynamic behaviour

The analysis of drop dynamic behaviour centers on the determination of the drag coefficient of drops. This is complicated by the fact that liquid drops do not behave in the same manner as solid spheres. It has been shown by Dreyer [94DR1] that the predicted terminal velocity of liquid drops based on solid sphere drag models differs from measured values considerably at larger drop diameters ($d > 3$ *mm*). As such a different approach must be taken when considering the drag coefficients of liquid drops. Such an approach would ideally take into account the effects of drop deformation, oscillation and internal circulation. Turton and Levenspiel [86TU1] used data of solid spheres falling at terminal velocity to obtain the

following correlation for the standard drag coefficient (drag coefficient of particle falling at terminal velocity)

$$C_D = \frac{24}{Re}\left(1 + 0.173Re^{0.657}\right) + \left(\frac{0.143}{1 + 16300Re^{-1.09}}\right) \tag{2.9}$$

Chen and Trezek [77CH1] proposed the following correlations for the drag coefficients of drops

$$C_D = 0.27 + \frac{24}{Re} + \frac{6}{1+\sqrt{Re}} \quad \text{for } 1 < Re < 1000 \tag{2.10}$$

$$C_D = 0.6649 - 0.2712 \times 10^{-3}\, Re + 1.22 \times 10^{-7}\, Re^2 - 10.919 \times 10^{-12}\, Re^3 \quad \text{for } 1000 < Re < 3600 \tag{2.11}$$

In both these correlations Re is evaluated at the relative drop velocity.

Several authors, such as Beard [76BE1] and Clift et al. [78CL1], have proposed models to correct solid sphere drag correlations. Dreyer [94DR1] assumed that drop deformation is the main reason for the increased drag coefficients found for liquid drops compared to solid spheres. He developed the following correlation using the drag correlation of Turton and Levenspiel [86TU1], terminal velocity data of falling drops from Gunn and Kinzer [49GU1] and drop deformation data of Beard and Clift et al. [78BE1]

$$\left(\frac{C_D}{C_{D,sphere}}\right) = 1.0 - 0.17185(1 - E_T) + 6.0392(1 - E_T)^2 - 6.605(1 - E_T)^3 \tag{2.12}$$

Drop deformation

As a drop accelerates it changes shape due to increased hydrodynamic pressure at the forward stagnation point. The usual method to describe the extent of drop deformation is to either calculate the aspect ratio

$$E = b/a \qquad \begin{array}{l} \text{oblate } E > 1 \\ \text{sphere } E = 1 \\ \text{prolate } E < 1 \end{array} \tag{2.13}$$

or the eccentricity, which for an oblate spheroid would be

$$e = \sqrt{1 - E^2} \tag{2.14}$$

where b and a is defined as shown in Figure 2.1.

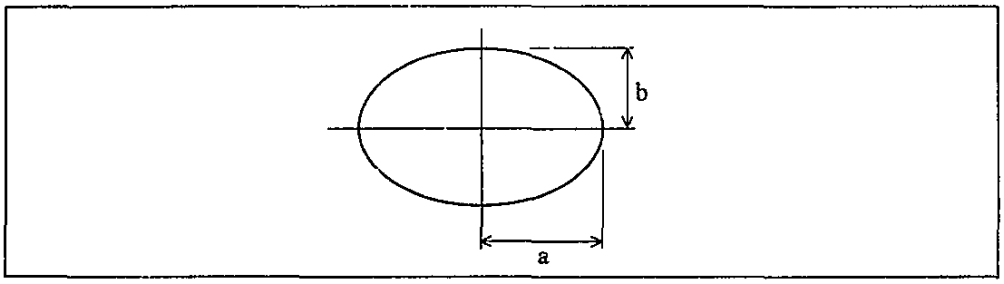

***Figure 2.1** Approximate geometry of a deformed drop.*

The amount of drop deformation is usually correlated with the use of the Eotvos number. The Eotvos number is the ratio of the maximum hydrostatic pressure head inside the drop to the surface tension forces. Various investigators, such as Pruppacher and Beard [70PR1] and Chandrasekar et al. [88CH1], have presented experimentally determined correlations for water drop deformation. Other investigators, such as Pruppacher and Pitter [71PR1] and Beard and Chuang [87BE1], calculated the deformation numerically and found good agreement with experimental data.

Dreyer [94DR1] correlated the data of Beard and Chuang [87BE1] for drop deformation in terms of the Eotvos number as follows

$$E_T = \frac{1}{1 + 0.148\,Eo^{0.85}} \quad \text{for } Eo > 0 \tag{2.15}$$

Clift et al. [78CL1] presented the following correlation

$$E_T = \frac{1}{1 + 0.18\,(Eo - 0.5)^{0.8}} \quad \text{for } 0.4 < Eo < 8 \tag{2.16}$$

and Srikrishna et al.[81SR1],

$$E_T = \frac{1}{0.146\,Eo + 1} \tag{2.17}$$

These correlations are quite similar to those of Dreyer [94DR1] and Clift et al. [78CL1] giving very similar results but the correlation of Srikrishna et al.[81SR1] only giving good agreement at lower Eotvos numbers.

Pruppacher and Beard [70PR1] approximated the aspect ratio at terminal velocity as follows

$$E_T = 1.03 - 0.062 d_e \quad \text{for } 1.0 < d < 9.0\ mm \tag{2.18}$$

Dreyer [94DR1] developed an equation for the deformation of an accelerating drop in terms of the velocity, terminal velocity and drop deformation at the terminal velocity

$$E = 1 - \left(\frac{V}{V_T}\right)^2 (1 - E_T) \tag{2.19}$$

Internal circulation and drop oscillation

Internal circulation in a drop is induced by the resultant skin friction as the drop falls through air. It can also be the result of drop detachment or drop oscillation. Drop oscillations may be initiated by deformation immediately prior to detachment. Drop oscillation may also be due to vortex shedding in the drop wake or free-stream turbulence. Clift et al. [78CL1] give a good overview of internal circulation and drop oscillation. Dreyer [94DR1] concluded that the effect of internal circulation and drop oscillation on the drag of a drop is much less pronounced than the effect of drop deformation.

b) Drop thermal behaviour

The thermal behaviour for drops evaporating is described by the mass and heat transfer coefficients, which can be calculated from the Sherwood and Nusselt numbers. The best known correlations for heat and mass transfer from small liquid drops are those presented by Frössling [38FR1]

$$Nu = 2 + 0.522\,Pr^{1/3}\,Re^{1/2} \qquad \text{for } 2 < Re < 800 \text{ and } 0.2 < d < 1.8\ mm \tag{2.20}$$

$$Sh = 2 + 0.522Sc^{1/3}\,Re^{1/2} \qquad \text{for } 2 < Re < 800 \text{ and } 0.2 < d < 1.8\ mm \tag{2.21}$$

and Ranz and Marshall [52RA1]

$$Nu = 2 + 0.6Pr^{1/3}\,Re^{1/2} \qquad \text{for } 2 < Re < 200 \text{ and } 0.6 < d < 1.1\ mm \tag{2.22}$$

$$Sh = 2 + 0.6Sc^{1/3}\,Re^{1/2} \qquad \text{for } 2 < Re < 200 \text{ and } 0.6 < d < 1.1\ mm \tag{2.23}$$

Further correlations are also presented by Beard and Pruppacher [71BE1]

$$Sh = 1.56 + 0.616Sc^{1/3}\,Re^{1/2} \qquad \text{for } Re > 2 \text{ and } 0.6 < d < 1.1\ mm \tag{2.24}$$

and Srikrishna et al. [81SR1]

$$Sh = 2 + 0.37Sc^{1/3}\,Re^{0.557} \qquad \text{for } 628 < Re < 4271 \text{ and } 2 < d < 8.4\ mm \tag{2.25}$$

As can be seen, the above two correlations agree well with those of Frössling [38FR1] and Ranz and Marshall [52RA1]. Yao and Shrock [76YA1] developed a correlation for freely

falling, oscillating and accelerating water drops based on the correlation of Ranz and Marshall [52RA1]

$$Nu = 2 + g_{YS}(0.6 Pr^{1/3} Re^{1/2}) \text{ for } 3 < d < 6\ mm \tag{2.26}$$

where

$$g_{YS} = 25\left(\frac{z}{d_e}\right)^{-0.7} \qquad \text{for } 10 < (z/d) < 600 \tag{2.27}$$

Dreyer [94DR1] re-correlated the data of Yao [74YA1], obtaining the following correlation for g_{YS}

$$g_{YS} = 2.32\left(\frac{z}{d_e}\right)^{-0.16} \qquad \text{for } 10 < (z/d) < 600 \tag{2.28}$$

or alternatively

$$g_{YS} = 0.22 + 3.15 M_{\dot{z}}^{0.2}\left(\frac{d}{d_m}\right)^{0.2} \text{ for } M_{\dot{z}} > 5.0\times10^{-4} \tag{2.29}$$

with d_m, the maximum stable drop size being given by

$$d_m = \sqrt{\frac{16\sigma}{g(\rho_w - \rho_a)}} \tag{2.30}$$

and $M_{\dot{z}}$, the acceleration modulus defined by

$$M_{\dot{z}} = \left(\frac{(\partial v / \partial t)d}{v^2}\right) \tag{2.31}$$

Mercker [93ME1] used a function similar to that of Dreyer [94DR1], correlating his data for heat and mass transfer from mono-disperse sprays as follows

$$g_{YS} = 1 + 66.54 M_{\dot{z}}^{0.8}\left(\frac{d}{d_m}\right)^{-0.1} \text{ for } M_{\dot{z}} > 3.0\times10^{-3} \text{ and } 2.5 < d < 6\ mm \tag{2.32}$$

with d_m and $M_{\dot{z}}$ defined as previously.

Any one of the above correlations can be used to calculate the average Nusselt number describing the heat and mass transfer from a drop. The mass transfer coefficient required to

calculate the heat transfer rate from a drop due to heat and mass transfer can be found from the Nusselt number and the similarity between heat and mass transfer as follows

$$K = \frac{h_c}{Le_f c_p} \quad \text{and} \quad h_c = \frac{Nu\, k_a}{d} \tag{2.33}$$

The correlations of Frössling [38FR1] and Ranz and Marshall [52RA1] were obtained by measuring the heat/mass transfer from pendant drops in a steady airstream. Since acceleration influences the drag experienced by a falling drop, it can be expected that acceleration will also influence the heat/mass transfer from/to a drop. The correlations of Yao and Shrock [76YA1] and Mercker [93ME1] were obtained using larger drops accelerating in air. It may be noted that the correlation by Mercker approaches the Ranz and Marshall correlation when the drop approaches terminal velocity (i.e., when $M_2 \rightarrow 0$).

2.1.4 Packing design and selection

One of the biggest overall differences between modern cooling towers and earlier cooling towers is the capability of getting much more cooling out of a smaller package with less energy usage. In order to achieve this higher level of performance, the various components of the tower have been refined and fine tuned to work together as a coherent system. This, of course, is an ongoing process, as well as being one the objectives of this thesis. The packing, or fill, is the heart of the water cooling tower.

Three types of packing are commonly used, namely splash packing, film packing and film-grid packing. The splash type packing is designed to break the mass of water falling through the tower into a large number of drops. As water falls through the fill droplets collide with successive layers of splash bars which causes redistribution of water and heat by the formation of fresh droplets. A further benefit is that the water residence time in the tower is increased due to lower drop velocities and by contact with the fill. Film packing differs from splash packing in that, although the purpose is again to produce a large water surface area, this is achieved not by the formation of droplets but by allowing the water to spread itself thinly over a large area of fill. Film-grid packing combines elements of both splash packing and film packing to break up the water drops whilst a relatively large grid surface area also contributes to increasing the contacting area between water and air.

A mathematical model that predicts the performance of splash packing was developed by Dreyer [94DR1]. He found that a grid with 80% open area and a slat width of less than 10 mm represents the best combination between transfer characteristic and pressure drop. He also concluded that the optimisation of the slat surface areas is of importance. As stated previously,

the wetted surface of the splash bars contribute quite significantly to the total interface area between the air and water. The so-called trickle packs make use of this property. They are essentially the same as normal splash grids, except for being much denser with smaller diameter splash bars. This results in a large wetted surface area and increased heat and mass transfer.

The most common type of packing used in medium sized modern towers is the film type packing. It is commonly referred to as cellular fill or film fill. As the name suggests, this fill generates films of water rather than droplets. The surface of the sheets in film fill supplies virtually 100% of the heat and mass transfer surface in a typical cooling tower. The big advantage of film fill is that it slows down the water passing through the tower and exposes a large area per unit volume. This allows the use of a much shorter packed section. For counterflow towers, film fills require 5-8 times less packed height compared to splash bars or grids. Another advantage of film fills is that the heat transfer surfaces are parallel to the air flow rather than perpendicular as in the case of splash bars. This allows for reduced resistance to air flows. One disadvantage of closely packed film fill is a susceptibility to fouling with deposits from the cooling water. Winter [88WI1] investigated the effects of fouling and found that it may result in a loss of cooling tower performance equivalent to around 2% on recooled water temperature. Film fill was developed initially when the need arose for more compact and efficient packings. Various investigators such as Fuller et al. [57FU1], Munters and Lindqvist [61MU1] and Renzi and Kosowski [62RE1] did work in this regard. Munters experimented with thin foils of various materials and production techniques to corrugate the foils, and started to develop light weight packs for use as cooling tower fill media. Renzi and Kozowski concluded that an efficient and compact packing would consist of layers of straight strips interlocked at right angles in egg-crate fashion.

Gosi and Bergmann [88GO1] investigated the combination of the basic types of packings in order to integrate the advantageous characteristics of the different packing types. They developed a sandwich-type structure consisting of alternate layers of film fill separated by single layers of splash grids. This configuration improves the water distribution in the fill, and also helps in redistributing maldistributed water due to a failed nozzle.

Munters [61MU1] and Lindqvist showed that for a highly efficient compact mass transfer pack, the flow diameter must be at a minimum. However, a practical limitation is set by the capacity of the channels to allow water to flow and by the resultant pressure drop. Various methods have been used to promote the drainage of water from the fill passages, such as cutting the bottom of the packing at sharp angles, or by using hexagonal tubes. This practice results in adequate drainage, but also results in a large sized drop distribution leaving the fill packing, due to dripping or jetting beneath the fill. From the viewpoint of heat and mass

transfer in the rain zone this is an undesirable effect. This effect highlights an advantage of splash packing that is usually overlooked. Because the splash packing produces smaller drop sizes, the resultant heat and mass transfer in the rain zone beneath splash packing should be larger than beneath film fill. A combination of splash and film packing should therefore result in the same amount of heat and mass transfer in the packing region associated with film fill, combined with the heat and mass transfer in the rain zone associated with splash packing. Gosi and Bergmann [88GO1] investigated the combination of film and splash packing, but only from a spatial water distribution point of view and the associated benefits of this effect, whilst overlooking the effect of this arrangement on the rain zone performance.

2.2 DROP SIZE MEASUREMENT

2.2.1 Measurement techniques

A large number of techniques have been developed for the measurement of drop-size and concentration distributions in sprays, as reviewed extensively by Azzopardi [78AZ1] and Chigier [83CH1]. These techniques can be summarised as follows :

a) Photographic and holographic methods
b) Impact methods
c) Thermal methods
d) Electrical methods
e) Optical methods
f) Time of residence methods

These methods all have certain advantages and disadvantages, as well as being applicable only in a certain environment. To a large degree, most of the methods were developed for drop sizes smaller than those found in a wet cooling tower. Drop size distributions in sprays, e.g., liquid fuel flames or spray dryers, and in annular two-phase flows have received the most attention. Table 2.2 (next page) shows the ranges of drop sizes involved. The measurement of splash phenomena has also been investigated in detail.

In the rain zone of a wet cooling tower drop sizes are much larger than those given in Table 2.2 and range to drops as large as 9 mm (9000 μm) in diameter. Due to the size of the drops, as well as the high rain densities found in a cooling tower, many of the above mentioned measuring techniques, such as the thermal, electrical and time of residence methods, cannot be used for measuring drop sizes in a cooling tower. Photographic, optical or impact methods

Table 2.2 *Ranges of drop sizes ([78AZ1]).*

Operation	Range (μm)
Combustion of liquid fuels	10 - 800
Spray drying	10 - 1000
Annular two phase flow	10 - 400

are more suitable methods for measuring large drop sprays.

Small, swiftly moving objects are difficult to photograph. However, careful consideration of the illumination and photography involved and of the measurement of images produced enables accurate results to be obtained with relative simple techniques and equipment. Impact methods involve the capture of drops on solid surfaces or in thin, viscous liquid films with slide mechanisms. The sampling slide method requires rather simple equipment; however, it has the disadvantage that the slide disturbs the flow field, and small drops bypass the sampler. Optical methods comprise scattering methods, obscuration methods and Laser-Doppler anemometer methods. Scattering methods are based on the intensity of light scattered by a particle, which depends on the intensity of the illuminating radiation, the diameter and refractive index of the particles, the wavelength and polarisation of the light and the direction of observation relative to that of the illumination. Scattering methods can be applied to multiple particles systems, given sufficient separation of the particles. Obscuration methods are based on the reduction of the amount of light that emerges from a control volume along the irradiation direction, when a particle is inserted in a light beam. These methods work well in the determination of drop velocity, as well as spatial positioning. The measurement of multiple particle systems is possible, but becomes increasingly complex and inaccurate with an increase in particle numbers. Laser-Doppler anemometers use the frequency information contained in light scattered by particles passing through an interference pattern to determine velocities and sizes. The major disadvantage of this method, as well as light scattering methods is that expensive specialised instrumentation is required.

Azzopardi [78AZ1] concluded that it is not possible to give an overall recommendation for drop size measurement. The optimum method depends on the type of mean or distribution required, and it is often necessary to examine the background to the requirement for drop size data. He also concluded that photographic methods were probably the easiest to implement, although it involved great tedium, with consequent possibility of error at the data abstraction stage. Photography is probably also best suitable for the determination of larger drop sizes. Chigier [83CH1] states that photography is a well established, reliable and accurate technique, although the manual analysis of photographs is very time consuming and subject to operator bias, thus confirming the conclusions of Azzopardi [78AZ1]. He further states that automatic

image analysis is an improvement but must be used carefully, and that it increases the cost of equipment. However, since Azzopardi's article in 1978, and that of Chigier in 1983 there have been rapid developments in electronic technology. Sophisticated digital image processing procedures and equipment are freely available, allowing the development of an accurate and relatively inexpensive procedure to analyse photographs.

In measuring local size distributions in sprays with direct photography, narrow depths of field are used to obtain detailed spatial resolution. This results in photographs being characterised by the simultaneous presence of drop images with a wide range of 'sharpness' of focus. This is not the case with bubbles (Schrodt and Saunders [81SC1]), emulsions (Kamel et al. [87KA1]) or drops suspended in oil (Dreyer [94DR1]) for which automated and/or interactive image analysis procedures have been developed and applied. Drop images are sharpest for drops lying in the plane which is focused on the photographic plate of the optical system. As this plane is infinitely thin, it is not possible to measure size distributions by counting only those drops which lie exactly in this plane. As a drop is moved away from this plane the sharpness of the image decreases, thus producing an increasingly thick blurred 'halo' around it. It is clear that the selection of the in-focus drops must be done on the basis of the thickness of this halo, thus making any analysis procedure which relies on the operators judgement extremely critical. This, together with the dependence of the image characteristics on a number of physical parameters, gives rise to the need for objective criteria and automatic procedures for the analysis of in-focus drops. But, conversely, it is precisely this problem which represents the main difficulty in the design of a fully automated procedure of drop sizing and counting.

Ramshaw [68RA1] used direct photography to obtain drop sizes in combustion chambers. He used a particle size analyzer to determine the drop sizes and suggested a method that takes into account out-of-focus drops by correctly adjusting the clipping level of the particle size analyzer. This is based on the fact that the gradients at the edges of drops reflect the degree of focus and can be used as a criterion by which drops are chosen for measurement. Fantini et al. [90FA1] developed an automatic analysis system to analyse photographs obtained by high-speed micrography. The problem of determining whether photographic images of particles are in focus or not are solved by obtaining a calibration of geometric parameters of particle images as functions both of the particle position in the camera's field of view and of the particle diameter.

The automated analysis of drop images depends on the successful detection of drops. In other words, once the image has been obtained and suitable criterion for defining in-focus drops has been decided upon, the objects of interest, i.e., in-focus drops, must be separated from the rest of the image and sized. Most recent automated analysis systems utilize various different image

processing schemes to accomplish this.

Fantini et al. [90FA1] uses a semi-automatic global thresholding technique with two threshold values to separate images into the background, halos and cores of the drops, resulting in a three-level image. A connected component detection algorithm is then used to detect and size the drops. Lin and Miller [93LI1] developed an on-line, image-based particle size analyzer for measuring coarse particle size on a conveyor belt. Three automatic thresholding techniques were evaluated, including a maximum entropy method (Kapur et al. [85KA1]), Otsu's technique [75OT1] and a hybrid method. Two detection algorithms were implemented: a seed-filling algorithm (Glassner [90GL1]) and an edge-detection algorithm (Pavlidis [82PA1]). However, no mention is made of the method used to size the particles following thresholding and detection. Yamashita et al. [93YA1] also developed an on-line image-based method for the measurement of cell size distribution and concentration of yeast in a fermentor. Images were enhanced using the Sobel operator and thresholded with Otsu's technique [75OT1]. The Hough method (as described by Gonzalez and Woods [92GO1]) is then used to detect and size the particles. Dreyer [93DR2] developed software for the measurement of drop sizes from photographs. A single threshold value based on a technique proposed by Brink [92BR1] is used to segment the image. The drops are then detected using a sequential line-by-line scan technique described by Beukman [87BE1] and Horn [87HO1]. This software is explained in greater detail in Chapter 5.

As can be seen from the cited literature a great variety of different techniques and methods abound in image processing pertaining to the detection and sizing of particles in images. It is beyond the scope of the current chapter to discuss these techniques and methods in greater detail. However, the subject of image processing is discussed in greater detail in Chapter 5 where more information on the relevant methods and techniques is given.

2.2 Drop size distributions and mean diameters

An accurate knowledge of the drop size distribution as a function of the conditions of a system is a pre-requisite for *fundamental* analysis of the heat and mass transfer in such a system. Distribution of particles is also a vital element of general particle size analysis in disperse systems. Representing the characteristics of particle assemblies, such as drop sprays, is therefore a subject that has been well researched and documented. There are several books available on the subject of particle size analysis. These include those of Stockham and Fochtman, Particle Size Analysis [77SST1], Allen, Particle Size Measurement [81AL1] and Rumpf, Particle Technology [90RU1].
Some of the most relevant topics in particle size analysis are now highlighted.

General representation of particle assemblies

The population of particles being measured is usually distributed according to some function of x, x being any measure of dispersity. In drop sprays this will be the diameter of the drops, or equivalent diameter for non-spherical drops. A *cumulative* distribution function is defined as follows

$$0 < Q_r(x) < 1 \tag{2.34}$$

$$Q_r(x_{min}) = 0 \text{ and } Q_r(x_{max}) = 1 \tag{2.35}$$

The manner in which the population is counted is designated by the subscript r. If the population is measured by number, $Q_0(x)$ is used, by lengt $Q_1(x)$, by surface area $Q_2(x)$ and by volume $Q_3(x)$. For distributions by mass the fraction undersize is designated by the complement C and the fraction oversize by the residue R. Thus $C(x) + R(x) = 1$. If the density is independent of particle size then $C(x) = Q_3(x)$. With most of the particle assemblies which occur in practice the number of particles is so large that the distribution function can be regarded as continuous and it can be differentiated as follows:

$$q_r(x) = \frac{dQ_r(x)}{dx} \tag{2.36}$$

where $q_r(x)$ is the *density* distribution function corresponding to the cumulative distribution function $Q_r(x)$. In literature Q(x) is also designated as $\phi(x)$, and q(x) as $f(x)$ or y(x).

Because size distributions follow the law of probability, the study of size distributions can be fruitfully made from the accumulated knowledge of the theory of distributions in statistics. If the distribution of the random variable x is such that a simple explicit function $g(x)$ has a well-known distribution, it becomes possible to use the results of research on the latter in studying the former distribution. The best known of such distributions is the log-normal and the Rosin-Rammler [33RO1] distributions.

The log-normal distribution is defined as follow

$$f_{LN}(z) = \frac{1}{\sigma_z\sqrt{2\pi}} \exp\left[-\frac{(z-\bar{z})^2}{2\sigma_z^2}\right] \tag{2.37}$$

where $z = \ln(x)$, $\bar{z}$ the mean of ln(x) and σ_z the standard deviation of ln(x).

The Rosin-Rammler distribution is defined as follows

$$f_{RR}(x) = nbx^{n-1} \exp(-bx^n) \tag{2.38}$$

where n and b are characteristic constants.

Both distributions have an infinite range and are skewed to the right. They also have a spread that is mode dependant, i.e., any change in the mode will result in a predetermined change in the spread and vice versa. Since real particle populations have an upper size limit determined by physical considerations and since it is at least conceptually possible that the mode and spread will vary independently, such distributions cannot be considered as generally applicable to all real particle populations. The log-normal and Rosin-Rammler distributions will totally fail to describe populations whose size distribution is skewed to the left.

To overcome some of these difficulties, various other size distribution functions have been proposed. These include the multiple parameter Nukiyama-Tanasawa, Griffith, Gaudin-Schumann and Gaudin-Meloy functions.

Simmons [77SI1] correlated the drop size distributions in fuel nozzle sprays with a nondimensional correlation similar in form to the Rosin-Rammler function. The drop size was normalized with the mass mean diameter. They showed that drop number distributions can be correlated on a nondimensional basis by cutting off the data at the extreme tails of the volume distribution. They also developed equations for calculating the distributions given only the mass mean or Sauter diameter for a spray. Tishkoff and Law [77TI1] studied the approximation of drop size data by the Nukiyama-Tanasawa, Rosin-Rammler and Griffith functions. A general four-parameter function was also considered. All functions, except the Rosin-Rammler function were applied to spray data using a logarithmic least-squares technique. They determined that the general function was the most accurate, with the Nukiyama-Tanasawa function being the least accurate of the three functions. They concluded that the Griffith function was the most desirable function due to a combination of appreciable accuracy and ease of implementation. Popplewell et al. [88PO1] presented a modified version of the beta distribution function which displays some advantages over the traditional log-normal and Rosin-Rammler functions. The main advantages of the modified beta distribution function are that it has a finite range, independent mode and spread, and the ability to describe symmetric as well as asymmetric distributions skewed either to the right or the left. Yu and Standish [90YU1] studied particle size distributions in detail and highlighted the limitations of distribution functions presented in literature. The problem of finding a universal function is explained and Johnson's S_B function is suggested to be the function that can represent all the unimodal size distributions of particles.

Mean diameters

In many mass and heat transfer processes it is desirable to work only with average diameters instead of the complete drop size distribution. This can be seen in Section 2.1.2 (b) where the rain zone of a cooling tower is discussed. Table 2.3 shows a few of the mean diameters and the fields of applications for each. In order to use these means effectively, they must be readily calculated from the drop size function. Mugele and Evans [51MU1] discussed mean diameters in detail. They define the general relation for a mean diameter as

$$\overline{x}_{qp}^{\,q-p}\int_{x_0}^{x_{in}} x^p \frac{dn}{dx}dx = \int_{x_0}^{x_{in}} x^q \frac{dn}{dx}dx \qquad (2.39)$$

Table 2.3 Mean diameters (Mugele and Evans [51MU1]).

Symbol	Name of mean diameter	Field of application
d_{10}	Linear	Comparisons,evaporation
d_{20}	Surface	Surface area controlling - e.g., absorption
d_{30}	Volume	Volume controlling - e.g., hydrology
d_{21}	Surface diameter	Adsorption
d_{31}	Volume diameter	Evaporation, molecular diffusion
d_{32}	Sauter	Efficiency studies, mass transfer, reaction
d_{43}	De Brouckere	Combustion equilibrium

2.3 DISCUSSION

- There is an abundance of literature available covering most aspects of cooling tower theory. Merkel's model has been investigated in great detail and several improved models have been presented. Merkel's model is, however, still used extensively in many cooling tower analysis, despite it's shortcomings.

- Experimentally determined transfer characteristic and pressure drop data have been obtained for a number of different type of fills. None of these fills were, however, similar to the type used in this study.

- The transfer characteristic of the spray zone can be obtained by analysis of the drop dynamic and thermal behaviour of drops. Single, representative drop sizes are usually used in this kind of analysis, although analysis based on a drop size distribution would be more accurate.

- The scientific design of fill material has not been investigated in great detail. The effect of drop size formation on the performance of the rain zone has been neglected.

- The measurement of drop sizes is well documented with photographic methods appearing to be the most applicable for measuring drop sizes in large drop sprays.

- Data abstraction from images can be automated with little expense and relative ease. No method found in literature could, however, be applied directly to this study.

- Research in drop size distributions functions has been aimed at developing a general function that can be used to describe most size distributions.

- The available literature presented enough information to conduct a thorough theoretical and experimental analysis of the generation and effect of decreased drop sizes in the rain zone of a counterflow, natural draft cooling tower.

CHAPTER 3

EXPERIMENTAL APPARATUS AND PROCEDURE

This chapter describes the experimental apparatus and procedures used in the project. As has been stated previously, performance data for cooling tower packing has to be determined experimentally. This is usually done in smaller scale test facilities which are either forced or induced mechanical draught towers. Due to a lack of standardization, performance data for packing material is often influenced by the type of testing facility used. Factors such as the size of the tower, properties of the sprays, elimination of wall effects and inlet air velocity profiles all affect the accuracy and effective interpretation of the performance data.

The Department of Mechanical Engineering at the University of Stellenbosch has at their disposal a wet/dry cooling facility designed for the evaluation of cooling tower fill material and spray-cooled heat exchangers. This facility was used for obtaining performance data and determining drop size distributions for the packing arrangements investigated in this study.

3.1 DESCRIPTION OF COOLING TOWER TEST FACILITY

3.1.1 General

A schematic layout of the cooling tower test facility is shown in Figure 3.1.

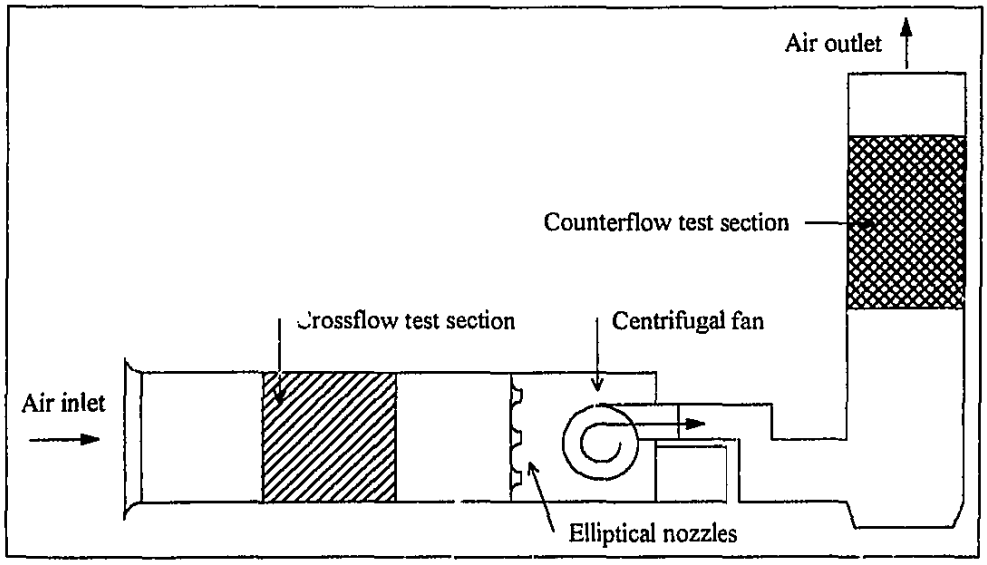

Figure 3.1 Test facility layout.

The test facility is designed to enable testing of counterflow and crossflow packing arrangements. For the purpose of this project the counterflow test section was used. Figure 3.2 shows the counterflow test section in greater detail.

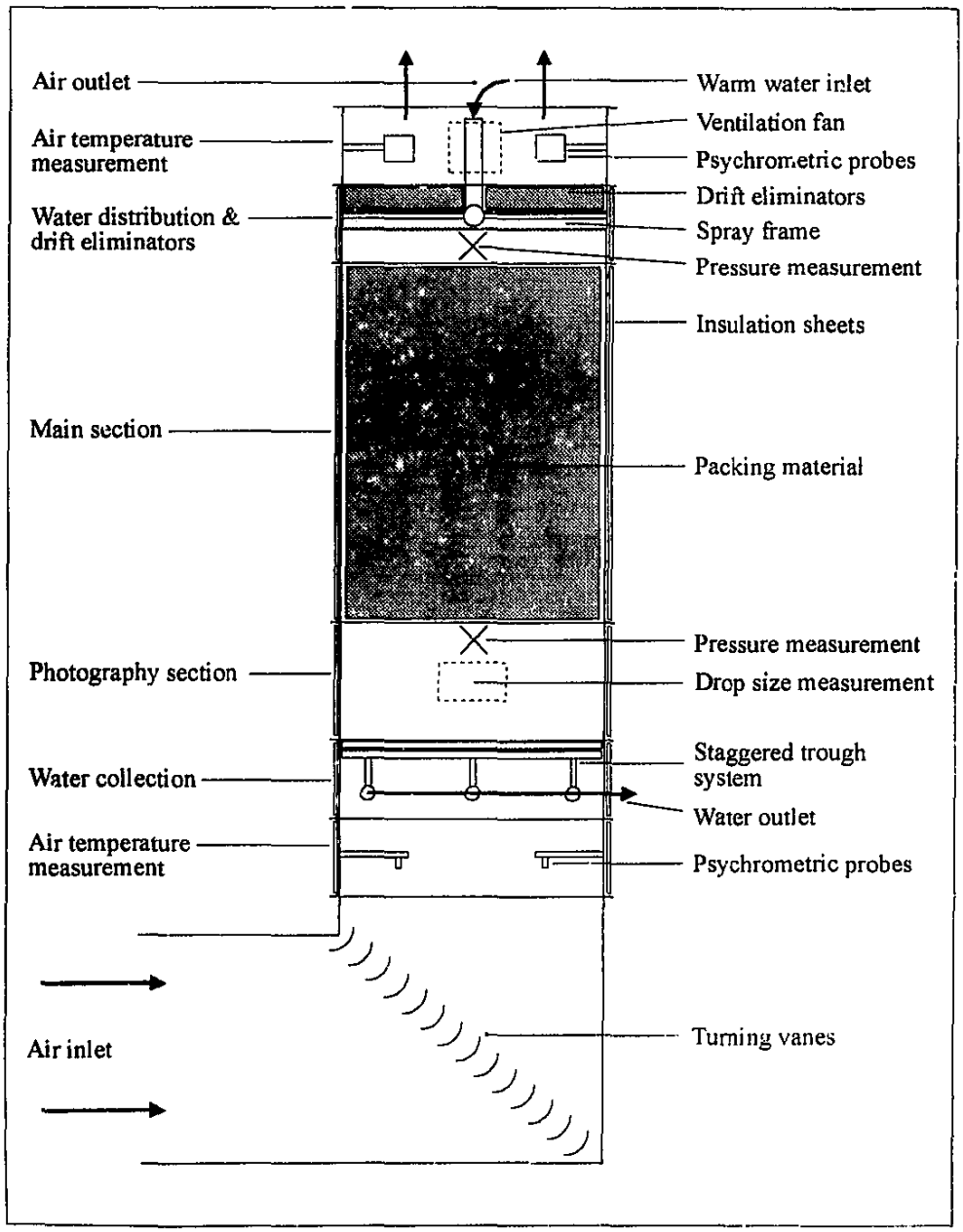

Figure 3.2 *Counterflow cooling tower test facility.*

The countertlow test section has a plan area of 1.5 m by 1.5 m and consists of several interchangeable elements. The main section is 2.25 m high with a swing door to facilitate the loading of packing material into the tower. The other interchangeable elements consist of a number of sections (0.5 m or 0.75 m high) which can be used for a variety of purposes such as adjusting the tower height or, for the purpose of this project, inserting a section for additional measurements. In this case the additional section served a twofold purpose : providing a section for additional measurement as well as increasing the tower height, thus maximizing the amount of cooling that can be measured in the rainzone. The sections are bolted together and sealed with rubber strips and silicone sealant. The sections are insulated with 25 mm thick closed cell polyurethane foam sheets to minimize heat loss to the surroundings and are described briefly below :

- 1 × 2.25 *m* main section with a swing door,
- 1 × 0.5 *m* section, directly above the main section which contains the water distribution frame and the drift eliminators,
- 2 × 0.5 *m* sections, containing probes for temperature measurement,
- 1 × 0.5 *m* section, containing the water collecting troughs, and
- 1 × 0.75 *m* section, containing the fittings for measuring drop size distributions.

Air flow

The air flow through the test section is obtained by means of a centrifugal fan with a variable speed motor. This fan produces air speeds of up to 4.5 m/s in the counterflow test section.

Water flow

The water is supplied to the test section by a distribution spray frame as shown in Figure 3.3. The spray frame consists of a manifold which distributes water to smaller distribution pipes.

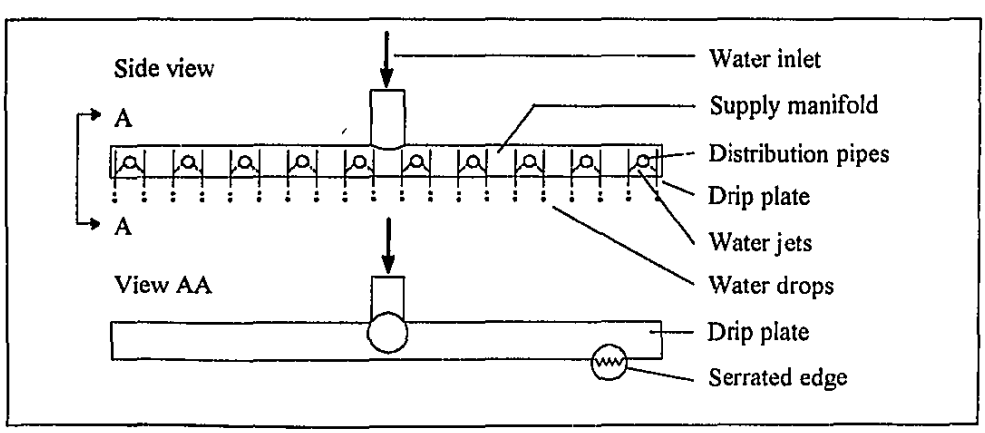

***Figure 3.3** Water distribution spray frame.*

On both sides of each distribution pipe there is a drip plate, each 1.5 m long, with a serrated edge. Water jets spray from small holes drilled in the distribution pipes and strike the drip plates. This configuration ensures an even distribution of water since the water drips from the points of the serrated edge.

Below the packing material the water is collected by a staggered trough system (See Figure 3.4) made of PVC to minimize heat transfer in the troughs. From Figure 3.4 it can be seen that the water flow is drained selectively from the trough system by dividing it into two water collecting areas. Webs in the troughs separate the collecting areas in such a way that water collected in the central area and outer perimeter is drained away separately. This arrangement eliminates the effect of water accumulating and cooling on the walls of the test section by isolating a part of the water flow that has not been in contact with the walls. The water from this test area is collected in a basin and the outlet water flow rate is measured by a V-notch arrangement, before flowing into a 200 *l* sump and pumped back to the underground water reservoir. The water from outside the test area is drained directly into the sump, before being pumped away. The outlet water pipes of the manifold collecting the water from the troughs have a 360° bend to ensure the pipes will always be filled with water thereby preventing air from being drawn into the tunnel from the outside, as well as ensuring that the thermocouples measuring water outlet temperature are always covered with water.

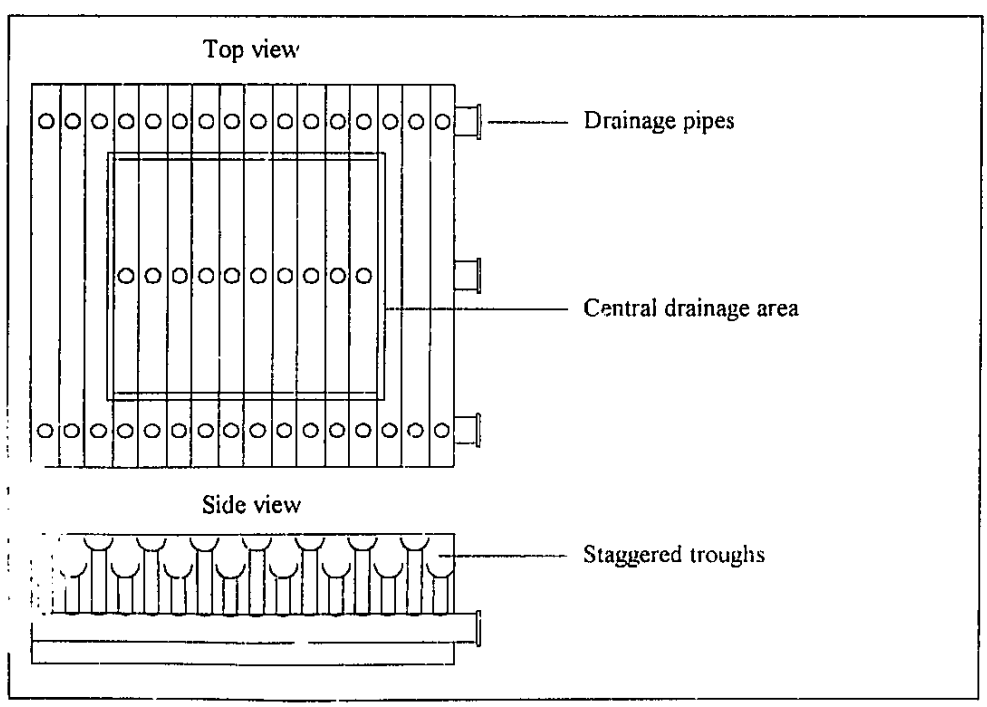

***Figure 3.4** Water collection troughs.*

Water supply

Hot water for testing is supplied from a 40 m^3 underground reservoir. This water is heated to the required inlet temperature by means of a 150 kW diesel burning water heater. Water is removed by pump from just below the reservoir surface, and returned through a narrow slot at the bottom of the reservoir. This ensures that the water in the reservoir stays stratified and provides a steady temperature at the surface from where the hot water is drawn.

3.1.2 Instrumentation

Temperature measurement

All temperature readings are made with calibrated copper-constantan thermocouples. The thermocouples are calibrated by determining the thermocouple readings at the ice melting point and water boiling point at atmospheric pressure. Each temperature reading is hence corrected according to its calibration curve.

The water temperatures are recorded by calibrated thermocouples placed in the inlet water pipe and the outlet water manifold (three measuring positions) respectively.

The inlet air temperatures to the test section are measured below the water collection system and the outlet air temperatures are measured above the drift eliminators. Both inlet and outlet air conditions are measured by a set of four ventilated psychrometric probes as shown in Figure 3.5. Air at approximately 3 *m/s* is drawn across the thermocouples by means of a small fan. All the probes are supplied with water by means of supply lines connected to water reservoirs. In order to obtain a good representative temperature reading the probes are evenly spaced over the cross-section of the tower. The probes located at the air outlet side are protected with radiation shields to avoid direct sunlight influencing temperature measurement. All the thermocouples are directly coupled to a Schlumberger data logging system.

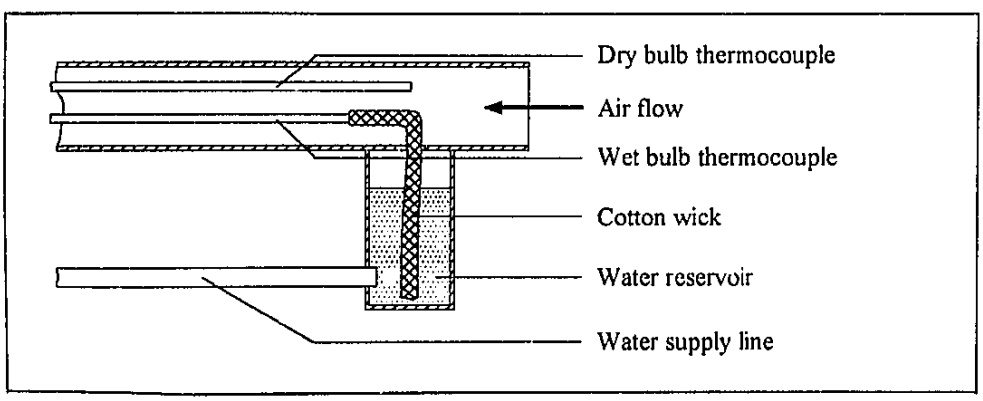

***Figure 3.5** Psychrometric probe.*

Pressure measurement

The ambient pressure is recorded before every test with a mercury column barometer. The pressure drop across the fill zone is measured with a Betz micro-manometer. Due to the high water flow rate and the slight over-pressure, conventional wall pressure tappings cannot be used to measure the local static pressure in the test section requiring the use of special pressure measuring probes, shown in Figure 3.6, to measure the local static pressure. These probes consist of two flat metal plates connected by a 20 *mm* metal tube. The static pressure point is located at the top of the tube. When the probes are positioned as shown, no water will accumulate in the pressure lines. Even when the probe is slightly inclined relative to the air flow direction water entering the tube runs out the other side without wetting the pressure point.

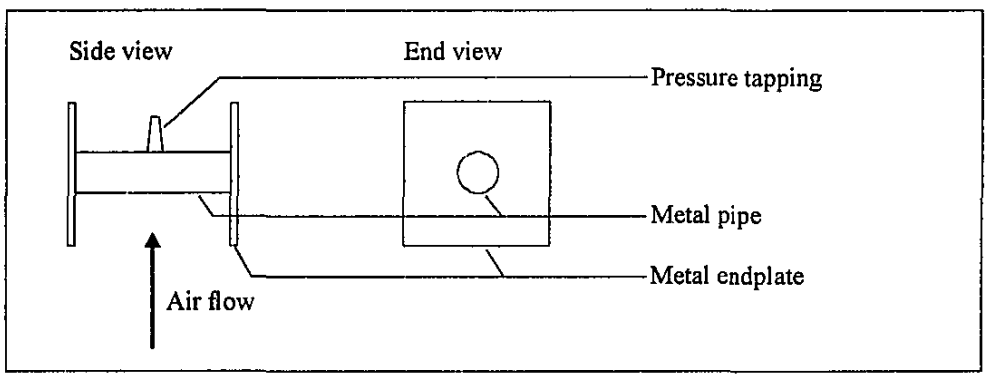

***Figure 3.6** Pressure measuring probes.*

Mass flow measurements

The inlet water flow rate is calculated from the pressure drop across an orifice plate designed according to the BS 1042 standard. The pressure difference across the orifice plate is recorded with a differential pressure transducer. The outlet water flow rate from the central drainage area is calculated from height readings recorded from a calibrated V-notch installed in the catchbasin.

The air mass flow rate through the test section is calculated from the pressure drop measured across a set of ASHRAE 51-75 elliptical flow nozzles. The pressure difference across these nozzles is recorded by a calibrated low pressure differential pressure transducer.

Data logging

All thermocouples and pressure transducers are directly connected to a multiplexing data logger, which is capable of reading all channels once per second. The data logger has an internal electronic ice point which eliminates the need for an ice bath for temperature

measurement purposes. It is programmed to convert all temperature readings from millivolts to degrees Celsius before transferring them to a personal computer. The pressure transducers convert the pressure readings to voltage signals which are transferred to the data logger. The data logger is programmed to convert this voltage signal to a pressure reading in Pascal by means of the transducer's calibration curve. The personal computer receives all temperature and pressure drop readings in the units of degrees Celsius and Pascal respectively from the data logger. This data is then used for further mass flow rate and energy balance calculations.

A Turbo Pascal program is used to read the data from the data loggers and process it immediately. The program can also continuously display time traces of the temperatures, energy balance, mass flow rates and transfer characteristic. The real-time processing of the test data makes it possible to determine when the steady-state has been reached. Once steady-state conditions are reached the data can be stored on magnetic disk for further processing.

3.2 DETERMINATION OF DROP SIZE DISTRIBUTIONS

A measurement technique, described in Chapter 5, was developed to measure drop sizes in the water sprays found in the counterflow cooling tower test facility. The technique uses digital image processing based on photographic methods to analyze the water sprays. The main advantages of this technique are the following :

- the larger drop sizes found in cooling tower sprays, as compared to the smaller sizes found in combustion processes and spray drying, can be analyzed and measured,
- the drop sizes are measured in the actual test facility, under normal operating conditions,
- little interference with the flow pattern in the test facility occur,
- the technique is robust and relatively easy to implement or adapt for other similar applications.
- the technique provides hard copies (photographs) for future re-evaluation,
- digital image processing is more accurate and less tedious than traditional data abstraction techniques.

3.2.1 Photographic technique

Small, swiftly moving objects such as water drops are difficult to photograph. The transparency of water drops also complicates the matter further. However, careful consideration of the illumination and photography involved and of the measurement of the images produced enables accurate results to be obtained with relatively simple techniques and equipment. The type of illumination used in any situation depends on the information sought and the geometry involved. The type of information usually sought from water sprays are drop

size distributions and/or the direction of motion and velocity of the drops. In this study only the drop size distributions were required. Two important effects to be considered in selecting the illumination are the illumination intensity/particle size/velocity relationships and the angular variation of scattered light. The illumination required is determined by the particle size and velocity. Azzopardi [78AZ1] established the following relationships between incident light intensity and particle size and velocity

$$I_0 \propto d_p^{-3}, \tag{3.1}$$

and

$$I_0 \propto v_p, \tag{3.2}$$

i.e., the smaller and faster the particle the more illumination required. Azzopardi also states that the illumination should be as close to 0° to the observation direction as possible (if it is 0° then shadows of objects will be recorded). In the case of water drops only the outline of the drops will be recorded due to the transparency of a water drop. As illustrated in Figure 3.8, light incident on the center of a drop passes through with no refraction. However, refraction increases as the incident light moves to the edge of the drop, with the result that the drop will

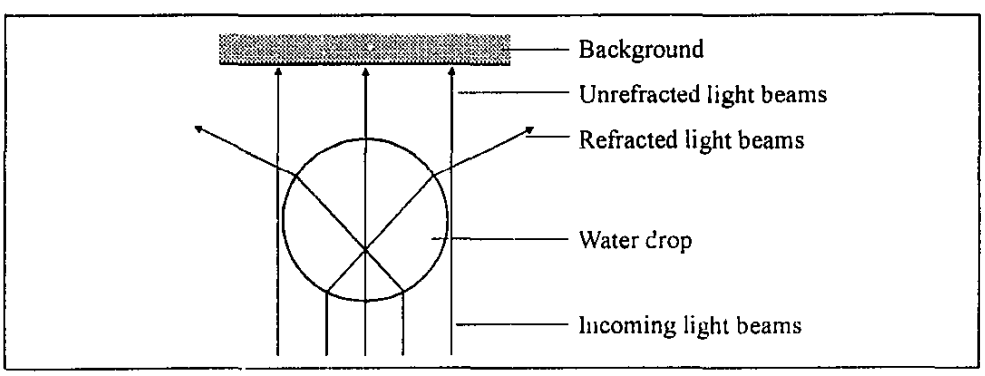

***Figure 3.8** Light passing through a water drop.*

show up as a dark circle on a white background. It is, of course, not possible to implement an angle of 0° between the illumination and observation light paths. It is for this reason that back or side illumination techniques are used. In cases where semi-automatic techniques of data abstraction are to be used (such as image processing), side illumination is not recommended because the drops may not appear as complete circles. Illuminating the background only will yield the best results, with drops appearing as dark circles on a white background. This lighting technique is called shadowgraphing, as the shadows of the drops are photographed.

For the purpose of the photographic investigation of this study the technique of shadowgraphing was employed.

The photographic equipment consisted of the following :

- NIKON FM2 camera
- MICRO NIKKOR 55 *mm* lens
- NIKON MD12 motor drive
- METZ 402 flash
- ILFORD FP4, 125 ASA film

The synchronization speed of the camera was set to 1/250 second. The flash measured the light intensity and provided illumination at an effective rate of 1/40000 second, thus *freezing* the drops and eliminating any blurring due to drop motion. The best results were obtained with a lens opening of f-5.6 , 125 ASA film and a focus distance of approximately 750 *mm*. With a longer focus distance a larger area can be photographed, but this only decreases the resolution of the image obtained, as well as resulting in increased blurring due to a larger number of out-of-focus drops in front of the focus plane. The negatives were developed using standard techniques and enlarged to 172 x 120 *mm*.

3.2.2 Experimental setup

As stated earlier the cooling tower test facility consists of a number of interchangeable elements. One of these sections was adapted for the photographic work. A schematic layout of the photography setup is given in Figure 3.9. The main elements of the photographic system are the camera and the flash. These two elements are housed in separate containers which bolted onto the adapted cooling tower section.

Camera

Container A housed the camera which was bolted onto a bracket made from PVC, and which was in turn bolted onto the container surface. This bracket allowed forward and backward, as well as lateral adjustment and rotation. The container is closed at the back by a hinged door and made as airtight as possible to prevent drops from swirling into the container because of the overpressure inside the tower. As conditions inside the tower are very turbulent, there were nevertheless still a lot of drops entering the container space. This necessitated a simple shutter arrangement at the front of the container to protect the camera. The shutter arrangement consists of a slot machined in the one side of the container and a manually operated shutter that slides in and out of the slot. Before a photograph is taken the shutter is quickly withdrawn by hand, the picture is taken and the shutter is closed again. The camera was furthermore placed

as far back as possible in the container to prevent drops falling on the camera lens. A gutter was also placed directly above the opening in the section wall as an added preventative measure to prevent drops swirling into the container space.

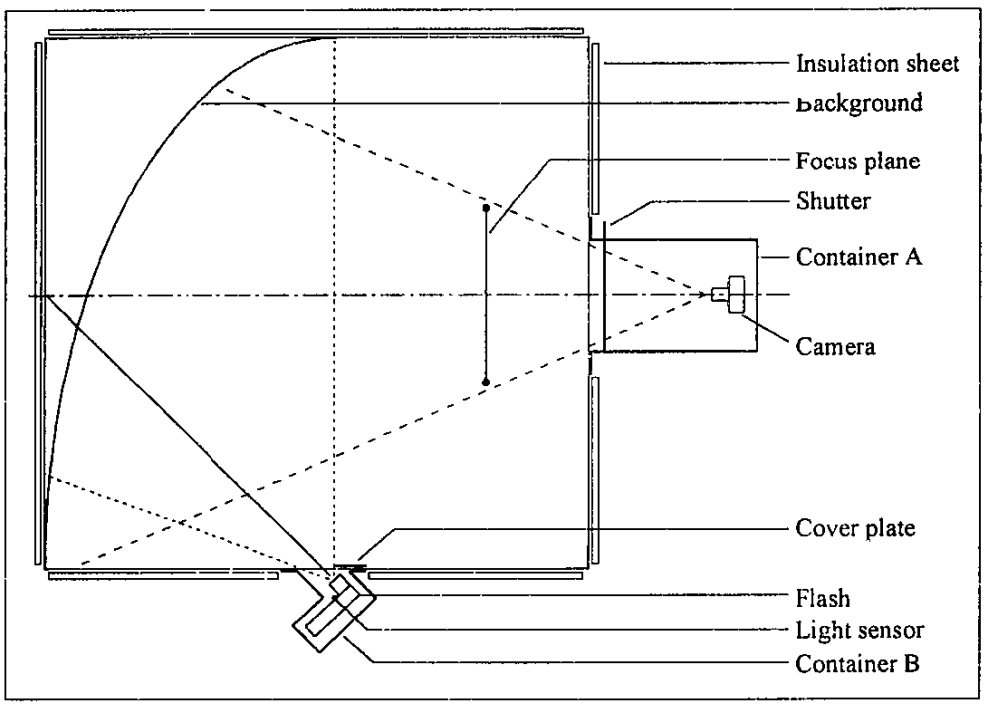

***Figure 3.9** Photographic setup.*

Flash

Container B housed the flash which was designed in such a way as to expose the flash head and the light sensor. The opening in the section wall was initially left open but this was found to be unnecessary as the opening could be covered with transparent plastic Although drops accumulated on this surface this did not influence the lighting of the backdrop surface as the drops are also transparent and only diffuses the light. A cover plate of opaque plastic was used to constrain the light to the rear section of the photographic test area.

Focusing

Two lengths of angle iron were fitted between the test section and the main section. This served as support for a grid to stand on whilst working in the tower The front length was also used to support the focusing arrangement required for the photography. This focusing frame is constructed from Meccano pieces, which proved to be a quick and versatile way of setting up the construction. For calibration purposes a number of glass beads were manufactured and

glued onto small metal rods and fitted in a comb-like arrangement which was then fitted to the focusing frame.

Background

For the background a curved metal sheet was used. This ensured a more even distribution of light intensity across the background as the distance traveled by the light from the flash to the background stayed more constant from one end to the other. The sheet was spray painted with a non-gloss white paint.

Testing

For each test run the camera and flash were installed in their respective containers. The flash was connected to a rechargeable battery pack. The camera was then focused on the focusing frame. Container A was bolted shut with only the connection with the flash and the remote trigger for the motor drive emerging from it. Container B was also closed by a cover plate to prevent light from the outside influencing light intensity measurement. The test facility was then put into operation. Photos of the spray could be taken at any time by quickly opening and closing the shutter. Sufficient time (+/- 30 seconds) had to be allowed between each shot for the flash unit to recharge.

CHAPTER 4

DATA ABSTRACTION

The abstraction of data from the photographs of the drop sprays was done through digital image processing. In this chapter the principles of digital image processing (see Gonzalez and Woods [92GO1] for a comprehensive treatment of the subject) as well as the image processing techniques used are described.

Section 4.1 gives an overview of image processing in general while Section 4.2 and 4.3 cover the methodology of the processing techniques employed. Section 4.4 describes the software used in this study and Section 4.5 gives a step-by-step description of the final processing method used to abstract the required data from the photographic images. Finally, Section 4.6 covers the correlation method employed.

4.1 GENERAL

Digital image processing consists of a number of fundamental steps, which are shown in Figure 4.1 which shows how the overall objective is to produce a result from a problem domain by means of image processing. The objective for this study is to determine the drop sizes in a water spray. The first step in the process is *image acquisition* - that is, to aqcuire a digital image. To do so requires an imaging process and the ability to digitise the image produced by such a process. In this study the imaging process was photography and the images (photographs) were digitised by a scanner. After a digital image has been obtained, the next step deals with *preprocessing* that image. The key function of preprocessing is to improve the image in ways that improve the chances for success of the other processes. In this case, preprocessing deals with techniques that improve contrast and remove noise. The next

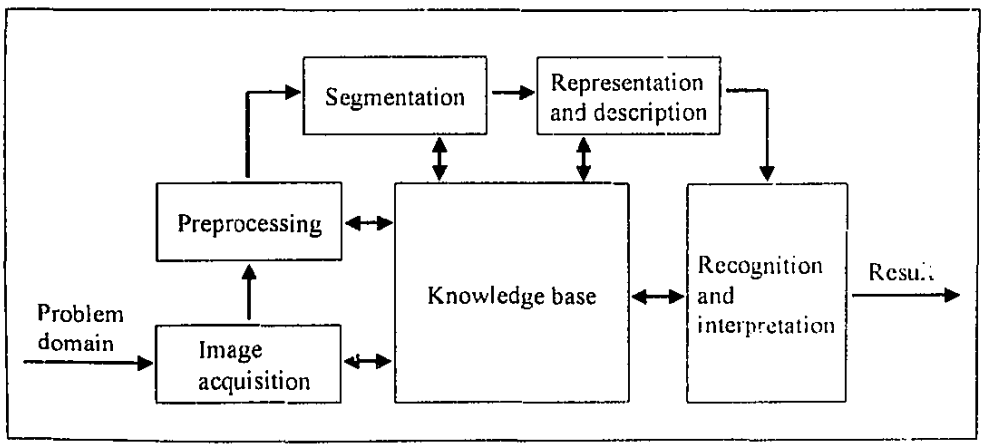

Figure 4.1 Fundamental steps in image processing

stage deals with segmentation. Broadly defined, *segmentation* partitions an input image into its constituent parts or objects. In this case the key role of segmentation is to separate individual drops from the background. The output of the segmentation stage usually is raw pixel data, constituting either the boundary of a region or all the points of the region itself. *Representation* deals with the decision of whether the data should be represented as a boundary or as a complete region. *Description* deals with extracting features that result in some quantitive information of interest or features that are basic for differentiating one class of objects from another. In this case description differentiates between the eccentricity of the particles in the image. The last stage in Figure 4.1 deals with recognition and interpretation. *Recognition* is the process that assigns a label to an object based on the information provided by its descriptors. *Interpretation* involves the assigning of meaning to a collection of recognised objects. In this case the recognition process decides whether a particle can be classified as a drop or not. The interpretation stage is not applicable in this case as it is used in more advanced applications where a certain amount of artificial intelligence is required. It should be noted from Figure 4.1 that there is an interaction between the *knowledge base* and the processing stages. Knowledge about a problem domain is coded into an image processing system in the form of a knowledge database. This knowledge may be as simple as detailing regions of the image where the information of interest is known to be located, or adapting the image acquisition process to highlight the information of interest.

It must finally be noted that image processing is characterized by specific solutions. Hence techniques that work well in one area can be totally inadequate in another. The availability of basic hardware and powerful image processing software provides a starting point much further advanced than was the case a decade ago. However, the actual solution of a particular problem still generally requires a certain amount of research and development.

Image processing software can be divided into two categories, namely high-level and low-level software. Low-level software provides basic image processing algorithms, enabling the user flexibility to use any combination of these algorithms to obtain a desired result. High-level software is designed for specific applications and uses a number of algorithms in a fixed combination to process an image. It is therefore not very flexible. Both low-level and high-level software can be combined, however, to develop an overall procedure for processing an image. This was also the case in this study. High-level software was available for the processing of photographic images of drops. This software was, however, limited in the type of photographic images that can be processed. Because of this, low-level software had to be employed to adapt the photographic images in a form suitable for processing by the high-level software.

4.2 IMAGE ENHANCEMENT

The principal objective of enhancement techniques is to process an image so that the result is more suitable than the original image for a specific application. As such it forms part of the preprocessing stage in image processing, but it is also used to enhance the results obtained from other processing techniques.

The approaches discussed in this section fall into two broad categories: spatial domain methods and frequency domain methods. The spatial domain refers to the image plane itself, and approaches in this category are based on direct manipulation of pixels in an image. Frequency domain processing techniques are based on modifying the Fourier transform of an image. Enhancement techniques based on various combinations of methods from these two categories are not unusual. This is also the case in the techniques employed in this study.

4.2.1 Background

A large number of image enhancement methods are based on either spatial or frequency domain techniques.

Spatial domain methods

The term spatial domain refers to the aggregate of pixels composing an image, and spatial domain methods are procedures that operate directly on these pixels. Image processing functions in the spatial domain may be expressed as

$$g(x,y) = T[f(x,y)] \tag{4.1}$$

where $f(x,y)$ is the input image, $g(x,y)$ is the processed image, and T is an operator on f,

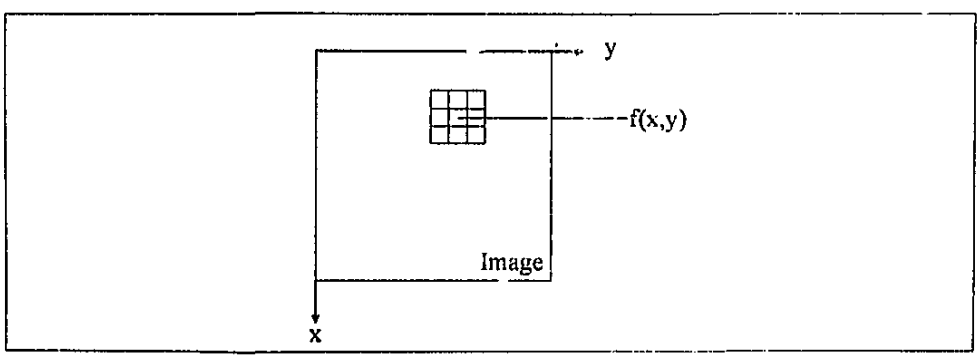

Figure 4.2 *A 3 x 3 neighborhood about a point (x,y) in an image.*

defined over some neighborhood of (x,y). The principal approach to defining a neighborhood about (x,y) is to use a square or rectangular subimage area centered at (x,y), as Figure 4.2 shows. The center of the subimage is moved from pixel to pixel and applying the operator at each location (x,y) to yield g at that location. The simplest form of T is when the neighborhood is (1×1). In this case, g depends only on the value of f at (x,y), and T becomes a gray-level transformation function. Because enhancement at any point in an image depends only on the gray level at that point, tecniques in this category are often referred to as *point processing*. Larger neighborhoods allow a variety of processing functions that go beyond just image enhancement. Regardless of the specific application, however, the general approach is to let the values of f in a predefined neighborhood of (x,y) determine the value of g at (x,y). One of the principal approaches in this formulation is based on the use of so-called masks (also referred to as templates, windows or filters). Basically, a mask is a small 2-D array, such as the one shown inFigure 4.2, in which the values of the coefficients determine he nature of the process, such as image sharpening. Enhancement tecniques based on this approach are often referred to as *spatial filtering*.

Frequency domain methods

The foundation of frequency domain techniques is the convolution theorem. Let $g(x,y)$ be an image formed by the convolution of an image $f(x,y)$ and a linear, position invariant operator $h(x,y)$., that is,

$$g(x,y) = h(x,y) f(x,y). \tag{4.2}$$

Then, from the convolution theorem, the following frequency domain relation holds :

$$G(u,v) = H(u,v).F(u,v) \tag{4.3}$$

where G,H and F are the Fourier transforms of g, h and f, respectively.

Numerous image enhancement problems can be expressed in the form of Equation (4.3). Equation (4.2) describes a spatial process that is anagolous to the use of the masks discussed in the previous section. For this reason, $h(x,y)$ is often referred to as a spatial convolution mask.

It must be noted that there is no general theory of image enhancement. When an image is being processed for visual interpretation, the viewer is the ultimate judge of how well a particular method works. This is, of course, highly subjective, making the definition of a 'good' image a difficult standard by which to compare algorithm performance. When an image is being processed for further machine evaluation, the evaluation task is *somewhat* easier. However,

even in situations when a clear-cut criterion of performance can be imposed on the problem, the analyst is still faced with a certain amount of trial and error before being able to settle on a particular image processing approach. This was also the case in this experimental study. The objective was to find a relatively simple, easy-to-use method as opposed to a more complex and elaborate approach, while still achieving acceptable results. Keeping this considerations in mind, an approach was developed which is based solely on a number of spatial filtering tecniques to produce acceptable results.

4.2.2 Spatial filtering

Spatial filters can be divided into two categories, namely linear and nonlinear spatial filters. The basic approach followed with linear filters is to sum products between the mask coefficients and the intensities of the pixels under the mask at a specific location in the image. Figure 4.11 shows a general 3 × 3 mask. Denoting the gray levels of the pixels under the mask at any location by $z_1, z_2, \ldots, z_9$, the response of the linear mask is

$$R = w_1z_1 + w_2z_2 + \ldots + w_9z_9 \tag{4.4}$$

Nonlinear spatial filters also operate on neighborhoods. In general, however, their operation is based directly on the values of the pixels in the neighborhood under consideration, and they do not explicitly use the coefficients in the manner described in Equation (4.4).

The method developed to enhance the images obtained through photography contains 2 nonlinear filters, namely median filtering and minimum filtering.

Median filtering

Median filtering are part of a family of smoothing filters. Smoothing filters are used for blurring and for noise reduction. It can be used for the removal of small details from an image prior to large object abstraction, and bridging of small gaps in lines or curves. A median filter is a nonlinear filter. In median filtering the gray level of each pixel is replaced by the *median* of the gray levels in a neighborhood of that pixel.

w_1	w_2	w_3
w_4	w_5	w_6
w_7	w_8	w_9

Figure 4.3 A 3 x 3 mask with arbitrary coefficients (weights).

Minimum filtering

Minimum filtering is also nonlinear and similar to median filtering. With minimum filtering the gray level of a pixel is replaced by the *minimum* value of the gray levels in a neighborhood of that pixel, instead of by the *median* value.

4.2.3 Frequency domain methods

In terms of the discussion in Section 4.2.1, enhancement in the frequency domain is relatively straightforward. The Fourier transform of the image to be enhanced is computed, the result is multiplied by a filter transfer function, and the inverse transform is computed to produce the enhanced image.

Highpass filtering

Highpass filters are used to sharpen an image. Because edges and other abrupt changes in gray levels are associated with high-frequency components, image sharpening can be achieved in the frequency domain by a highpass filtering process, which attenuates the low-frequency components without disturbing high-frequency information in the Fourier transform. Low-frequency components are responsible for the slowly varying characteristics of an image, such as overall contrast and average intensity. The net result of highpass filtering is a reduction of these features and a correspondingly apparent sharpening of edges and other sharp details.

A 2-D ideal highpass filter (IHFP) is one whose transfer function satisfies the relation

$$H(u,v) = \begin{cases} 1 & \text{if } D(u,v) > D_0, \\ 0 & \text{if } D(u,v) \le D_0 \end{cases} \tag{4.5}$$

where D_0 is a specified nonnegative quantity, and $D(u,v)$ is the distance from point (u,v) to the origin of the frequency plane; that is,

$$D(u,v) = (u^2 + v^2)^{1/2}. \tag{4.6}$$

This filter completely attenuates all frequencies inside a circle of radius D_0 while passing, without attenuation, all frequencies outside the circle.

It must be noted that spatial masks are used considerably more than the Fourier transform because of their simplicity of implementation and speed of operation. Both spatial filtering and frequency domain methods can produce similar results, such as sharpening or blurring an

image. However, there are problems that are not easily addressed by spatial techniques. In this case highpass spatial filters did not have the required effect and a highpass filter based on the frequency domain were used instead.

4.3 IMAGE SEGMENTATION

Segmentation subdivides an image into its constituent parts or objects. The level to which this subdivision is carried depends on the problem being solved. That is, segmentation should stop when the objects of interest in an application have been isolated. Segmentation algorithms for monochrome images are based on one of two basic properties of gray-level values: discontinuity and similarity. In the first category, the approach is to partition an image based on abrupt changes in gray level. The principal areas of interest in this category are detection of isolated points and detection of lines and edges in an image. The principal approach in the second category is based on thresholding, region growing, and region splitting and merging.

Two segmentation methods are used in this study to separate drops in an image from the background. They are edge detection and thresholding.

4.3.1 Edge detection

The idea underlying most edge detection techniques is the computation of a local derivative operator. Consider a gray-level transition shown in Figure 4.4. The first derivative of the gray-level profile is positive at the leading edge of a transition, negative at the trailing edge, and as expected, zero in areas of constant gray level. The second derivative is positive for that part of the transition associated with the dark side of the edge, negative for that part of the transition associated with light side of the edge, and zero in areas of constant gray level. Hence the magnitude of the first derivative can be used to detect the presence of an edge in an image, and the sign of the second derivative can be used to determine whether an edge pixel lies on the dark or light side of an edge. Note that the second derivative has a zero crossing at the midpoint of a transition in gray level. Because of this property second derivatives also provide a powerful approach for locating edges in an image. Although the preceding example was 1-D, a similar argument applies to an edge of any orientation in an image. The first derivative at any point in an image is obtained by using the magnitude of the gradient at that point. The second derivative is similarly obtained by using the Laplacian.

The Laplacian of a 2-D function $f(x,y)$ is a second-order derivative defined as

$$\nabla^2 f = \frac{\partial^2 f}{\partial x^2} + \frac{\partial^2 f}{\partial y^2}. \tag{4.7}$$

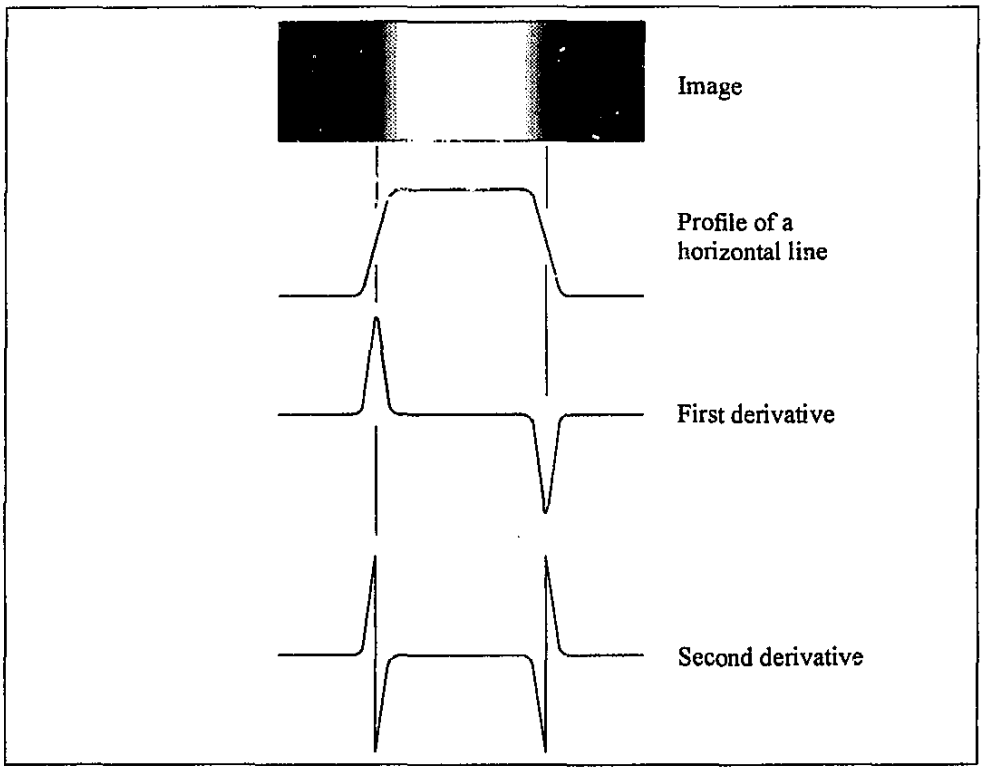

Figure 4.4 *Edge detection by derivative operators.*

Equation (4.7) may be implemented in digital form in various ways. For a 3 × 3 region, the form most frequently encountered in practice is

$$\nabla^2 f = 4z_5 - (z_2 + z_4 + z_6 + z_8) \tag{4.8}$$

where the z's have been defined already. The basic requirement in defining the digital Laplacian is that the coefficient associated with the center pixel be positive and the coefficient associated with the outer pixel be negative. Figure 4.5 shows a spatial mask that can be used to implement Equation (4.8).

0	-1	0
-1	4	-1
0	-1	0

Figure 4.5 *Mask used to implement the Laplacian.*

4.3.2 Thresholding

Thresholding is the other method employed in this study to separate drops in an image from the background.

Figure 4.6 shows the gray-level histogram corresponding to an image, $f(x,y)$, composed of dark objects on a light background in such a way that object and background pixels have gray levels grouped into two dominant modes. This is similar to the images found in this study after some enhancement and segmentation. One obvious way to extract the objects from the background are to select a threshold T that separates these modes. Then, any point (x,y) for which $f(x,y) < T$ is called an object point; otherwise, the point is called a background point. Based on this approach, thresholding may then be viewed as an operation that involves tests against a function T of the form

$$T = T[x,y,p(x,y),f(x,y)] \tag{4.9}$$

where $f(x,y)$ is the gray level of point (x,y), and $p(x,y)$ denotes some local property of this point. A thresholded image $g(x,y)$ is defined as

$$g(x,y) = \begin{cases} 1 & \text{if } f(x,y) > T, \\ 0 & \text{if } f(x,y) \leq T. \end{cases} \tag{4.10}$$

Thus pixels labeled 1 correspond to the background, whereas pixels labeled 0 correspond to

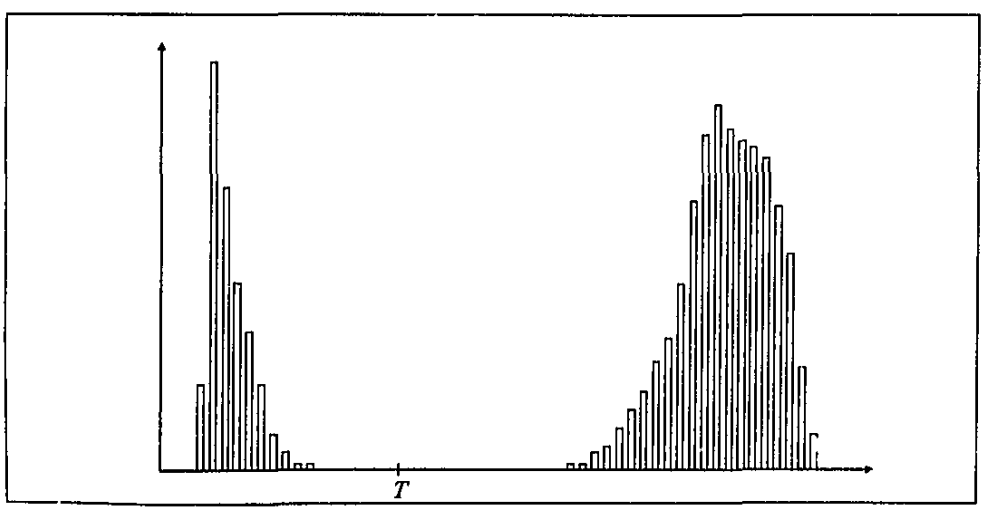

***Figure 4.6** Gray-level histogram that can be partitioned by a single threshold.*

objects.

When T depends only on $f(x,y)$, the threshold is called global. (Figure 4.4 shows an example of such a threshold.) If T depends on both $f(x,y)$ and $p(x,y)$, the threshold is called local. If, in addition, T depends on the spatial coordinates x and y, the threshold is called dynamic.

4.4 IMAGE PROCESSING SOFTWARE

As have been stated previously, both high-level and low-level software were used in the processing of photographic images in this study. A digital image processing computer program developed by Dreyer [93DR1], called PCX_EVAL, provided a high-level specific solution to the measurement of drop sizes from photographs. However, due to certain limitations, PCX_EVAL could not be applied directly to the images obtained. These limitations will be discussed shortly.

PCX_EVAL image processing software

The PCX_EVAL program in its present form takes as input an image consisting of 16 gray levels. This image is then segmented through thresholding into a binary image showing the drops as black and the background as white. The drops are then detected and filled, and the drop sizes are calculated from the number of black pixels making up each drop. However, the program is limited in its use because the input images have to be of a very high quality with good contrast. For the original purposes for which this program was developed this was quite possible because,

a) the drops photographed were in a single focusing plane (no sprays photographed),
b) the photographic conditions were easily controllable, resulting in even illumination, and,
c) the photographs were edited using a black pen and correction fluid.

Because of these factors the input images consisted only of in-focus drops with little or no background noise, simplifying the segmentation of the images considerably.

In this study, the input images were characterized by in-focus drops as well as out-of-focus drops. The images also had a fair amount of background noise. The photographs were furthermore scanned using 256 gray scales, resulting in images with high quality contrast making it easier to differentiate between in-focus and out-of-focus drops. Because of these factors, the segmentation part of PCX_EVAL was not quite suitable for the processing of images obtained in this study. The detection and drop sizing part of PCX_EVAL could, however, be used very successfully. The only problem remaining then was the enhancement and segmentation of the images into a form suitable for processing by PCX_EVAL. This was done with the iPhoto Plus picture editing program.

iPhoto Plus image processing software

The iPhoto Plus program is supplied with the DextraPalm handheld scanner used in this study. This program was used to scan and process the images and then save the images for use with PCX_EVAL. The program contains a variety of image processing algorithms that could be used to enhance and segment an image.

4.5 FINAL PROCESSING METHOD

The abstraction of the required drop size data from the photographs was done in two stages. The first stage included the scanning-in of the photographs and the application of certain image enhancement and segmentation algorithms. This stage was done using the iPhoto Plus picture editing program and the DextraPalm handheld scanner. The second stage comprises the counting and sizing of the drops using the PCX_EVAL software, and the calculation of the drop size distribution parameters.

Figure 4.7 shows a sample of a 256 grayscale image of the photographs taken of the spray in the test facility. As can be seen from Figure 4.7, the image consists of drops that are in focus, drops that are out of focus, as well as the background. The backround is made up mainly of low-frequency changes due to illumination irregularities, as well as drops that are very much out of focus and show up as smudges on the image.

The purpose of the image enhancement and segmentation techniques applied to this images is to separate the in-focus drops from the out-of-focus drops and the background. A number of techniques are applied sequentially to obtain the desired result. The following is a step by step description of the techniques and the effect it has on the original image.

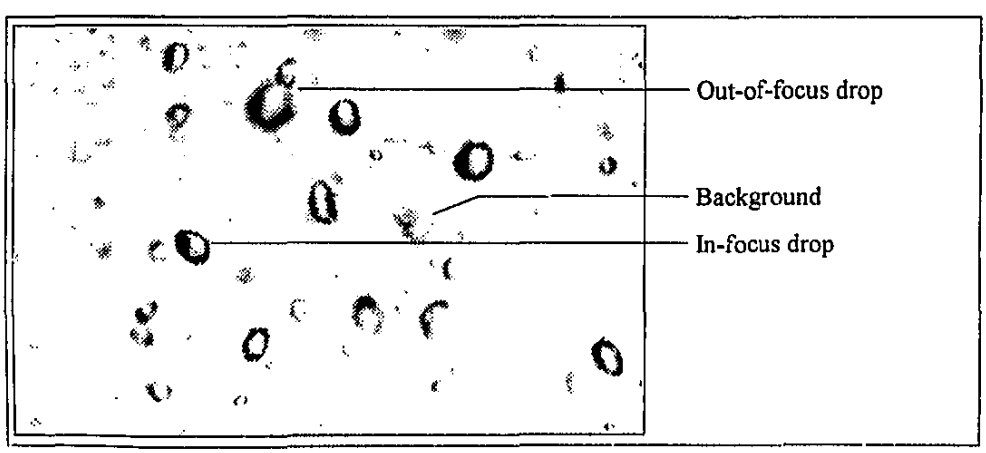

Figure 4.7 Sample image.

4.5.1 First stage

① Highpass filtering

Figure 4.8 shows the effect of a highpass filter applied to the original image. The low-

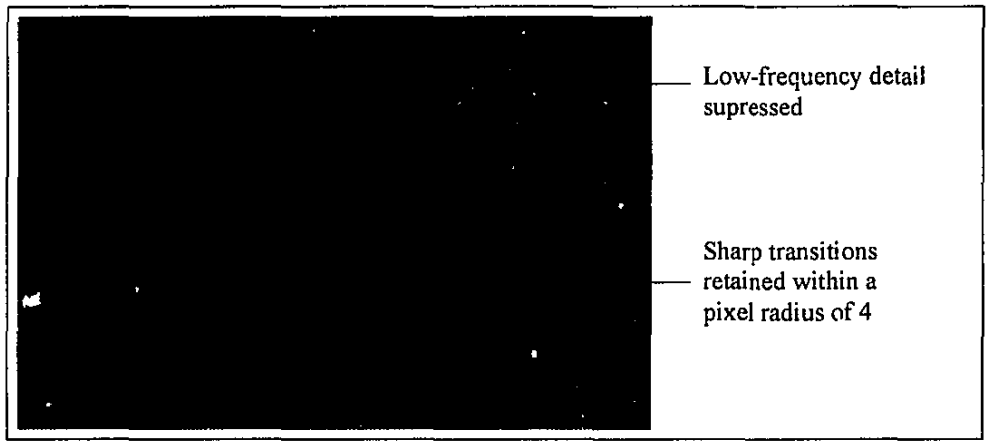

***Figure 4.8** Highpass filter applied to original image (Cutoff radius 4).*

frequency components of the image are attenuated, while the high-frequency detail is not influenced. The highpass filter used is based on the frequency domain method discussed earlier in this chapter. In the application of the filter one parameter has to be specified, namely the cutoff radius. This parameter specifies the radius of pixels around the image edges that the filter retains. A high value retains more of the pixels adjacent to the edge pixels, a low value retains only the edges themselves. The net effect of the filter is to retain, within the specified radius, sharp gray-level transitions, while suppressing the rest of the image. In this case a value of 4 for the cutoff radius gave the best results, i.e., the in-focus drops are retained and the rest of the image is suppressed.

② Edge detection

The next step in the processing was the detection of drop edges. The edge detection method is based on the Laplacian operator, which uses the zero crossings of the second derivative to detect the existence of edges. A mask similar to the one in Figure 4.5 is used. In this case a larger, 5×5 mask is used. The resultant image is then inverted (the gray levels of pixels are inverted, i.e., black becomes white and white becomes black. Figure 4.9 (next page) shows the effect of this filter. It can be seen that sharp transitions such as edges of in-focus drops are clearly outlined.

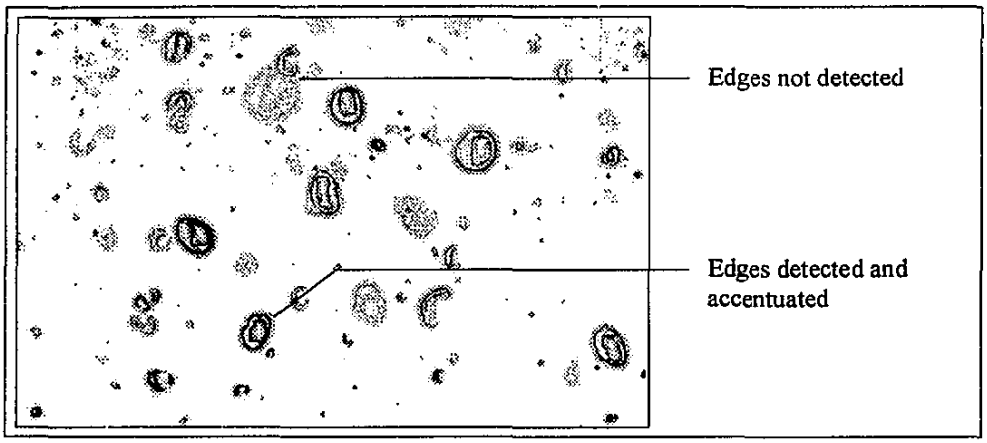

***Figure 4.9** Result of edge detection on Figure 4.8.*

③ Minimum filter

Figure 4.9 shows that, although the drops have been outlined, there are still small gaps in some of the outlines. This problem was addressed by the use of a minimum filter. Figure 4.10 shows the effect of this filter. The minimum filter bridges small gaps in the outlines of drops and strengthens these lines. With both the minimum and the median filters, a radius between 1 and 10 has to be specified. This radius specifies the size of the mask applied to the image. In this case circular masks are used. Operating one pixel at a time, the filter examines the gray-level values of the pixels within the radius specified, and replaces the gray-level value of the current pixel with the minimum gray-level value of the surrounding pixels. A radius of 1 gave good results, bridging small gaps, thus closing uncompleted outlines as well as amplifying smaller drops.

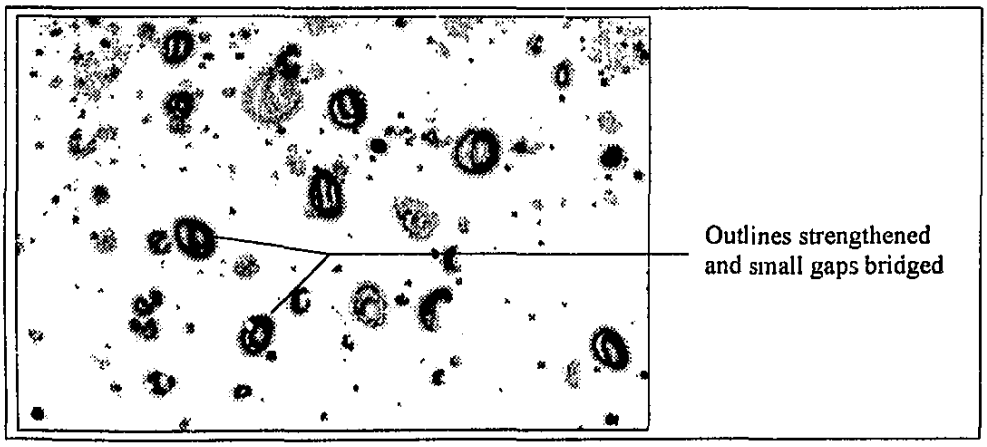

***Figure 4.10** Result of minimum filtering with radius 1 on Figure 4.9.*

④ Median filter

The median filter is used to blur the background noise. The median filter increases the average grey-level of the background. When the image is thresholded, unwanted specks and noise will then disappear because they have been, in effect, averaged out. A radius of 1 is also used with the median filter. This softens the background adequately without blurring the drop edges too much. Figure 4.11 shows the effect of this filter.

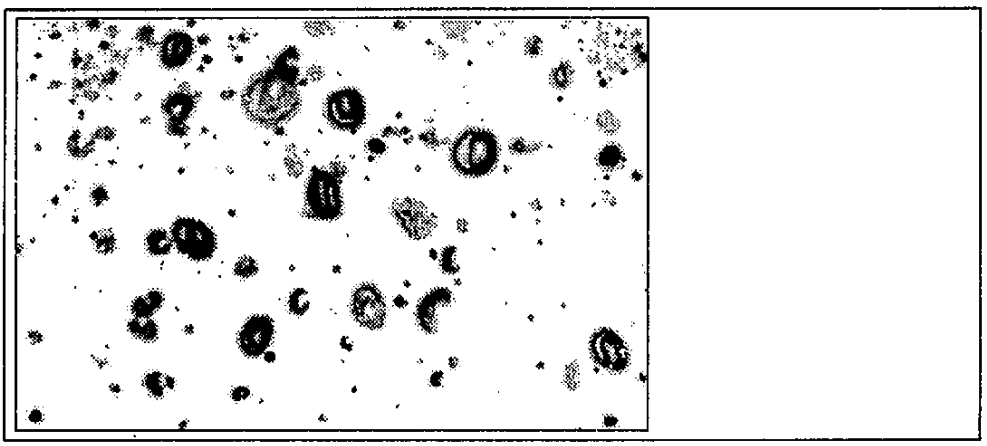

***Figure 4.11** Result of median filtering with radius 1 on Figure 4.10.*

⑤ Thresholding

The image is finally thresholded into a binary image consisting only of black pixels (drops) and white pixels (background). Figure 4.12 shows the effect of thresholding. A global

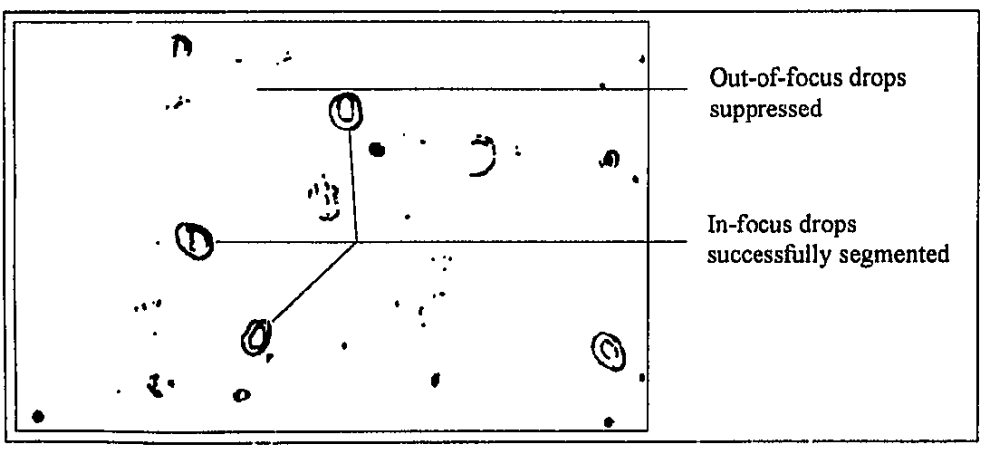

***Figure 4.12** Thresholding of Figure 4.11 with threshold value 76.*

threshold value of 76 was used in this case, giving acceptable results.

Discussion

Examination of Figures 4.7 through to 4.12 shows remarkable success in seperating the in-focus drops from the rest of the image. It was initially attempted to quantify the frequency of the edges of in-focus drops. This quantity would then be used to specify which drops should be classified as in-focus drops. However, this approach proved unnecessary. Rather, an approach based on visual inspection of the result of the various combinations of highpass filtering and edge detection on the images was favored. This method could be implemented using the available software, without resorting to more complex image processing software.

However, it can be seen that portions of some slightly out-of-focus drops still remain in the final segmented image (Figure 4.12). This problem was adressed in the next stage. The PCX_EVAL program not only detects and sizes the particles in an image, but also calculates the eccentricity of the particles. Because the remaining portions of the out-of-focus drops appear as lines, an eccentricity cutoff can be used to ignore the segments of the image.

4.5.2 Second stage

In the second stage the enhanced and segmented images was processed by the PCX_EVAL program. When using PCX_EVAL a number of parameters have to be specified. The most significant of these are the following:

- Minimum pixel area
- Eccentricity cutoff
- Test for large ellipsoids
- Eccentricity cutoff for large ellipsoidal particles
- Minimum size of large ellipsoids
- Enlargement ratio

Minimum pixel area

This parameter specifies the minimum number of pixels required before an object is considered to be a drop. Any objects consisting of fewer pixels than that specified by this parameter is not considered in further calculations. This option is usually set to 1. When an image contains a certain amount of background noise, a large number of very small objects could be counted if this parameter is set to low. In such cases the parameter should be set higher.

Eccentricity cutoff

As has been stated previously, the eccentricity of each particle is calculated by the program. A perfect circle has an eccentricity of 1 and a straight line has an eccentricity of 0. All objects less spherical than the eccentricity cutoff are discarded by the program. This allows the program to discriminate effectively against the counting of objects other than drops (i.e. lines and smudges). This parameter must be given a value between 0.5 and 0.95. It is usually set to 0.8.

Test for large ellipsoids

In some cases larger drops appear as large ellipsoids, which will normally be discarded when these drops exhibit eccentricities outside the allowable range specified by the eccentricity cutoff. Setting this option to "Yes" will force the program to measure the sizes of ellipsoidal objects falling outside the valid range specified by the cutoff, as well as that of spherical particles.

Eccentricity cutoff for large ellipsoidal particles

Specifying an eccentricity cutoff for large particles of less than the general cutoff, allows the program to take large ellipsoids into account but still discards smaller eccentric particles. This parameter must be given a value between 0.4 and 0.95.

Minimum size of large ellipsoids

A particle with an eccentricity smaller than the general eccentricity cutoff but larger than the eccentricity cutoff for large ellipsoids will be measured as a large ellipsoid only if the equivalent spherical drop size is larger than the size specified by this parameter. This effectively eliminates the possibility of very small ellipsoids being counted as drops. This parameter has to be larger than 1.0 *mm*.

Enlargement ratio

This is the ratio between the size of the image that was scanned to the size of the original image.

The following values for these parameters were used:

Minimum pixel area	10
Eccentricity cutoff	0.8
Eccentricity cutoff for large ellipsoidal particles	0.4
Minimum size of large ellipsoids	2.0
Enlargement ratio	0.488

A rather high number of pixels was specified for the minimum pixel area, because the segmented images still contained an amount of background noise consisting of particles larger than 1 pixel, which did not represent drops. The resolution of the images used is 400 dpi (dots per inch). This translates to 1 pixel representing 0.13 mm if the enlargement ratio is also taken into account. A group of 10 pixels will then represent a drop with an equivalent diameter of 0.469 *mm*. Because of this parameter setting, drop sizes smaller than 0.5 *mm* are not measured.

Visual inspection of the images showed that most of the larger drops were ellipsoidal in shape due to drop oscillation. Because of this the program was set to test for large ellipsoids.

4.6 CORRELATION OF METHOD

The results obtained were correlated with respect to size and number.

Size correlation

Some of the filters used in the enhancement of the images caused a slight thickening of the lines in the image. This resulted in the segmented drops being larger than the original drops, with the effect being more pronounced with the smaller drop sizes. To address this problem the sizing error had to be correlated in terms of the drop sizes. To this end a number of glass beads of different size was manufactured. This beads were photographed and processed through the usual method. The results of the drop sizing could then be compared to the actual sizes of the beads. The percentage oversize was calculated as follows

$$\% \text{ oversize} = (d_{calculated} - d_{actual}) / (d_{actual}) * 100 \qquad (4.12)$$

The data obtained was correlated with the following function

$$\% \text{ oversize} = 14.8921 - 1.3195 * d_c \,. \qquad (4.13)$$

Figure 4.13 shows the correlation between the measured and the predicted percentage difference in size. It can be seen that the accuracy of the processing method is quite high for larger drop diameters but decreases with smaller drop diameter to approximately 10 %.

Number correlation

The actual number of drops in each size class was also correlated with the number of drops calculated. A series of 8 photographs of the same operating condition were taken. These

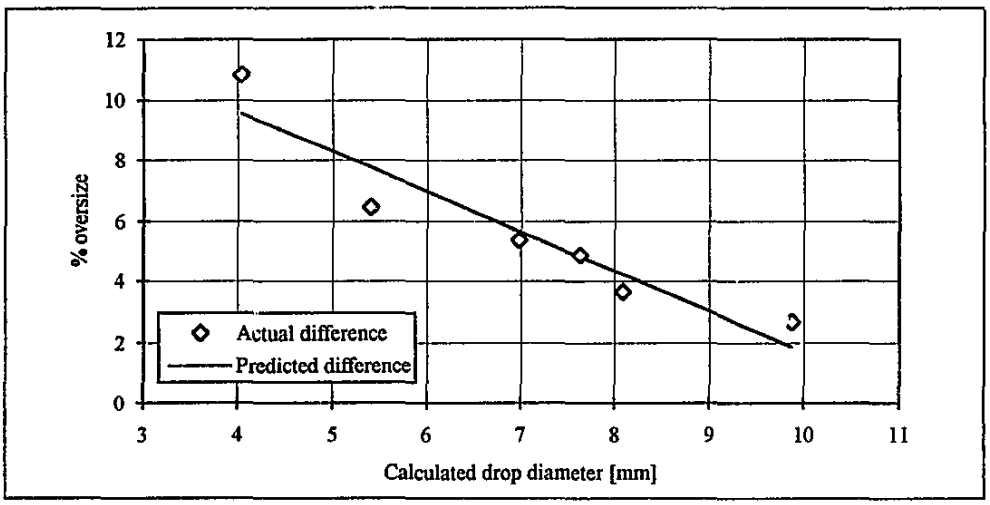

Figure 4.13 *Comparison between measured and predicted % oversize for drop diameters calculated with processing method.*

images were enlarged through photocopying and the drops were sized and counted manually. This was done with a transparent sizing grid and counting the number of squares of the sizing grid occupied by each drop. The smallest drops that could be counted with this method are drops with a diameter of 1.23 *mm*. The images were also processed by computer. The number of drops in each size class were added for all 8 samples and the averages calculated. The average number distribution for the manually processed images could then be compared with the distribution for the computer processed images. The difference fraction was calculated as follows

$$\text{fraction} = [(n_{i\ \text{calculated}} - n_{i\ \text{actual}}) / (n_{i\ \text{actual}})]/d \qquad (4.14)$$

The data obtained was correlated with the following function

$$\text{fraction} = [c_1 d + c_2 d^2 + c_3 e^d]/d \qquad \text{for } 0 < d \leq 5.0\ mm \qquad (4.15)$$

with

$c_1 = -0.07125$

$c_2 = -0.07508$

$c_3 = +0.02134$

and

$$\text{fraction} = 0.5/d \qquad \text{for } 5 < d < 10\ mm \qquad (4.16)$$

The larger drop diameters only represent a small number of drops (1 to 5) and hence difference fractions calculated at these diameters are amplified more than those calcultaed at the smaller drop diameters where much larger drop numbers occur. The difference fraction calculated by Equations 4.15 and 4.16 was therefore referred to the drop diameter by division in order to make the difference fractions more amenable for comparison.

Figure 4.14 shows the correlation between the measured and the predicted difference fractions. It can be seen that the computer processing method overpredicts the number of drops in the smaller drop diameters and overpredicts the number of drops in the larger drop diameters. The overprediction can be ascribed to background noise that was unsuccessfully segmented and the underprediction can be ascribed to large in-focus drops not being detected because of small discontinuities in the drop outlines.

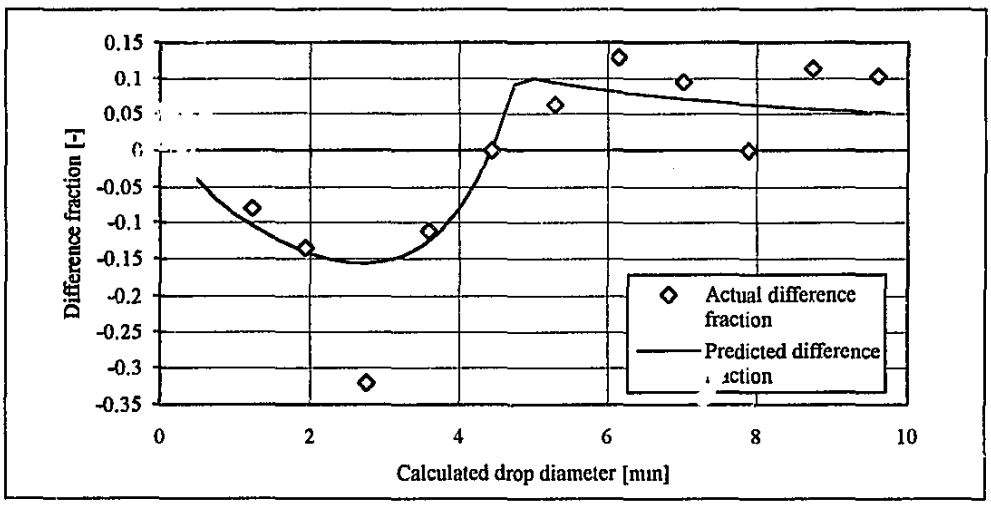

Figure 4.14 *Comparison between measured and predicted difference fraction in drop number distribution calculated with computer.*

Equation 4.14 was used to correct the size classes measured with PCX_EVAL and Equation 4.15 and 4.16 was used to correct the number distributions obtained.

CHAPTER 5

RESULTS OF EXPERIMENTAL STUDY

In Chapter 3 the apparatus and procedures that were used in the different components of the experimental work were described, while Chapter 4 explained the methods employed to abstract data from photographs obtained through one of these components. This chapter describes the objectives of the experimental study and presents the results of the experimental work done. The data is correlated and trends are pointed out and discussed.

5.1 SCOPE OF EXPERIMENTAL WORK

As stated earlier, the objective of this study is to investigate the possibility of reducing drop sizes in the rain zone beneath film packs and trickle packs. An obvious solution would be to position a few layers of splash grid beneath the packing, which, in theory, would then reduce the average drop size through splashing, without a significant increase in pressure drop. The experimental work was aimed at establishing the effect of such a layer of splash grid beneath trickle pack as well as determining the optimum position of the grids beneath the trickle pack. To this end, experiments were carried out to determine drop size distributions as well as transfer characteristic and pressure drop data.

Figure 5.1 (next page) shows the manner in which the trickle pack and the splash grids were placed in the cooling tower test section. At the top of the main section, just beneath the water distribution system, a 0.5 m thick layer of trickle pack was placed. At a distance z beneath this trickle pack, two layers of splash grid were placed 0.01 *m* apart, and at right angles to each other. Figure 5.2 (next page) shows the dimensions of these splash grids. Two basic configurations were tested. With Configuration A the cooling tower test section contained only the trickle pack, whereas with Configuration B the two layers of splash grid were added to the section and placed at 5 different positions beneath the trickle pack. Configuration A was tested twice, once to determine drop size distributions and once to determine transfer characteristics and pressure drops. Configuration B was tested 6 times, the first 5 times to determine the drop size distributions beneath the varying positions of the splash grids, and the last time to determine the transfer characteristic and pressure drop with the splash grids in the position which resulted in the smallest average drop sizes. For the purpose of this study, the distance between the splash grid and the trickle pack is labeled the drop fall distance, z_{sz}. (The subscript sz indicates that this distance is the spray zone distance if the trickle pack is subtracted from calculations.)

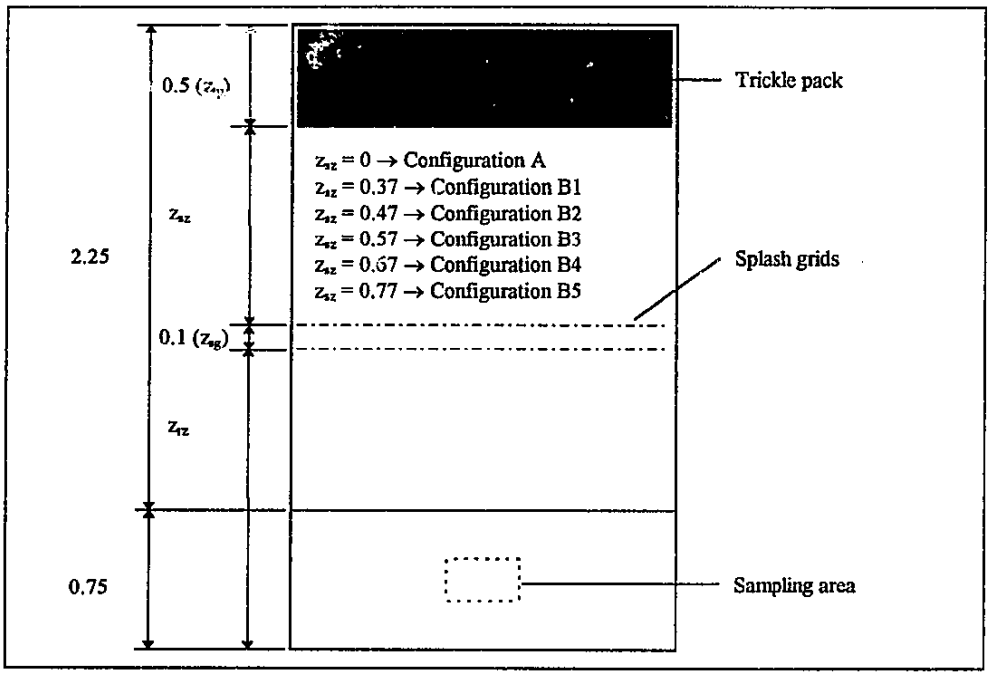

***Figure 5.1** Experimental setup.*

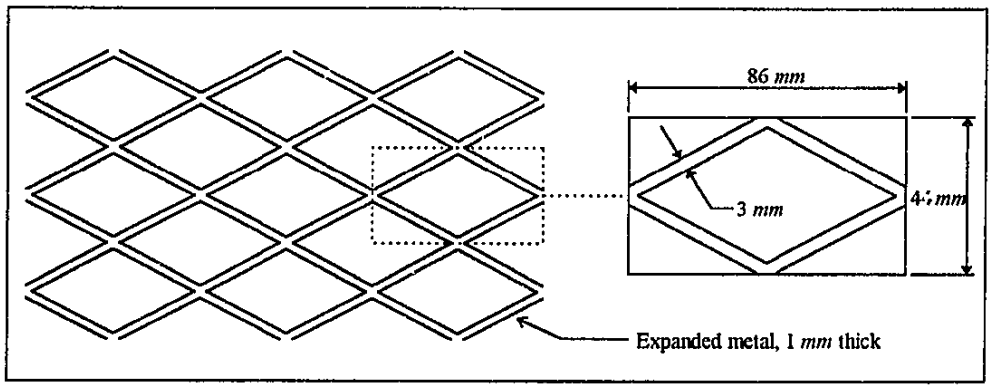

***Figure 5.2** Splash grid dimensions.*

5.2 DROP SIZE DISTRIBUTION

The determination of drop size distributions in the cooling tower test facility has a twofold objective :

1. To determine whether the splash grids do indeed break up the spray emerging from the trickle pack as predicted, resulting in a smaller mean diameter, and
2. the position beneath the trickle pack where the splash grids have a maximal effect.

5.2.1 Results

Configurations A and B were each tested at 6 different water/air mass flow ratios. The tests were done at three different water mass fluxes and two different air mass fluxes, similar to those found in industrial cooling towers. Four photographs were taken of each operating condition, resulting in 24 sets of drop number distribution data for each configuration. This data was used to calculate cumulative mass fraction distributions. The drop distribution data is tabulated in Appendix A and the averaged distribution curves for Configuration A and Configuration B4 is shown in Figure 5.3 and 5.4.

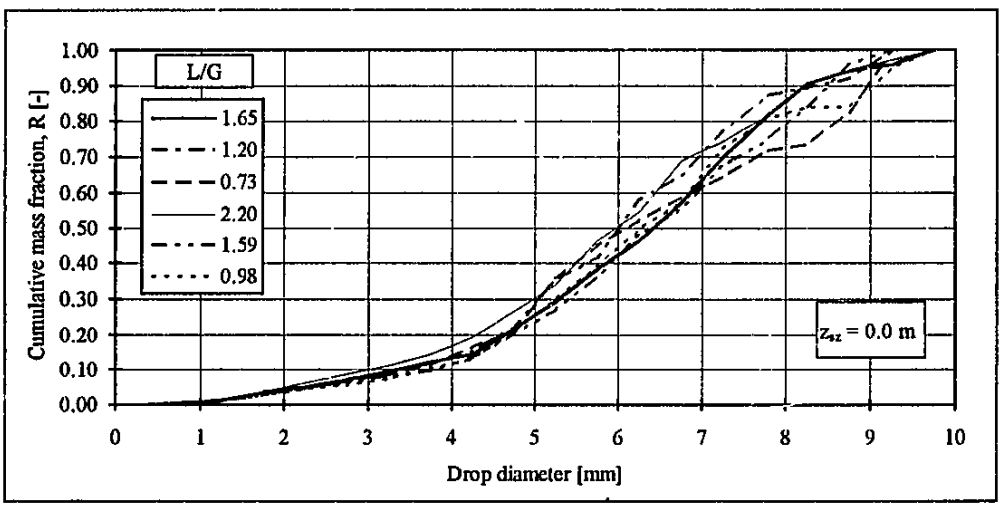

Figure 5.3 *Measured cumulative mass fraction for Configuration A.*

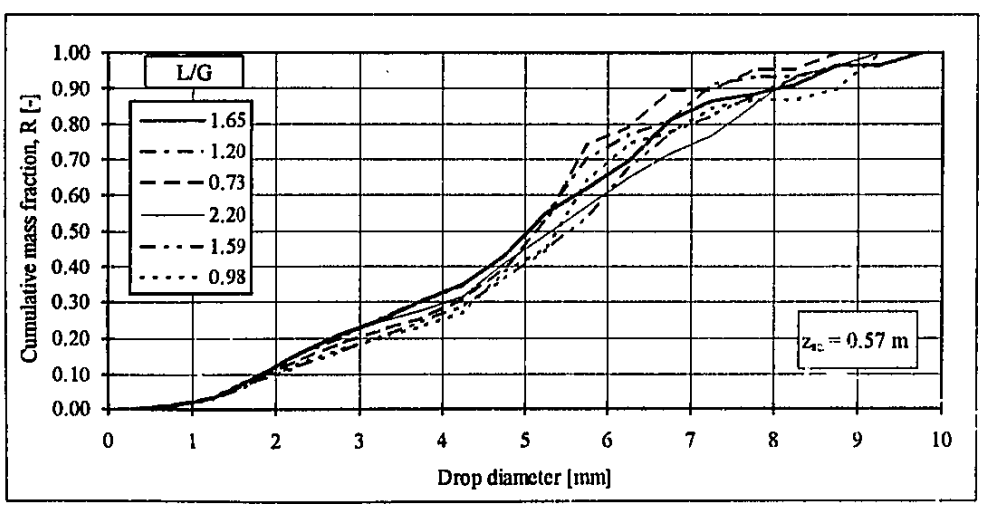

Figure 5.4 *Measured cumulative mass fraction for Configuration B4.*

The following quantities were calculated from the drop distributions for each test :

- Sauter mean diameter, d_{32}
- Mass mean diameter, d_{30}
- Total mass counted in sampling area

These quantities are plotted in Figures 5.5, 5.6 and 5.7.

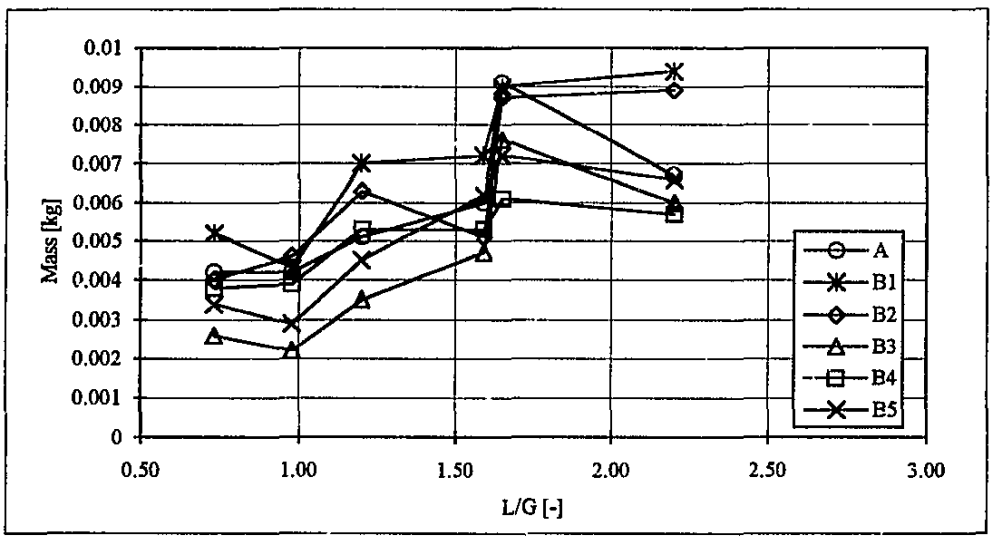

***Figure 5.5** Total mass counted for each configuration.*

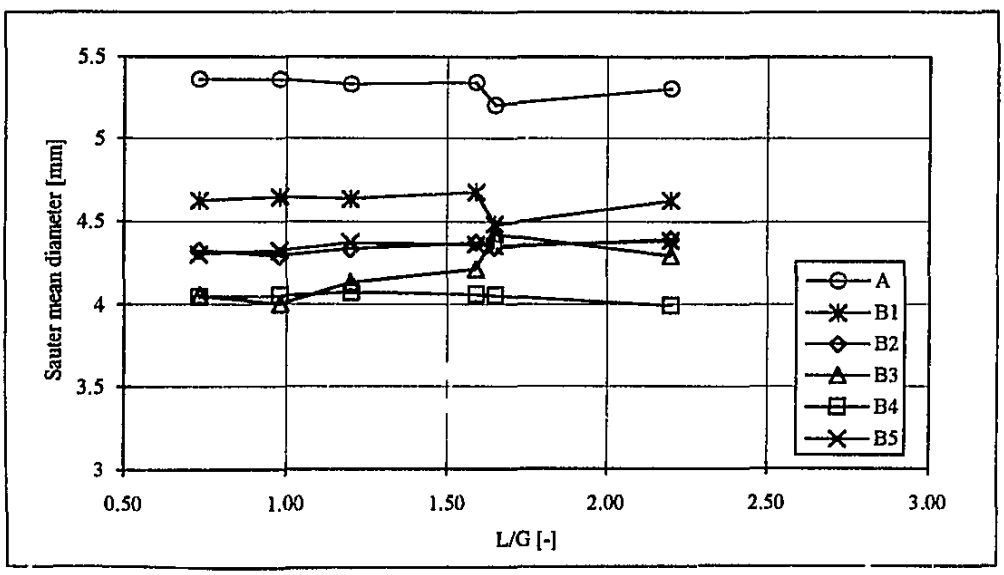

***Figure 5.6** Sauter mean diameter, d_{32}, calculated for each configuration.*

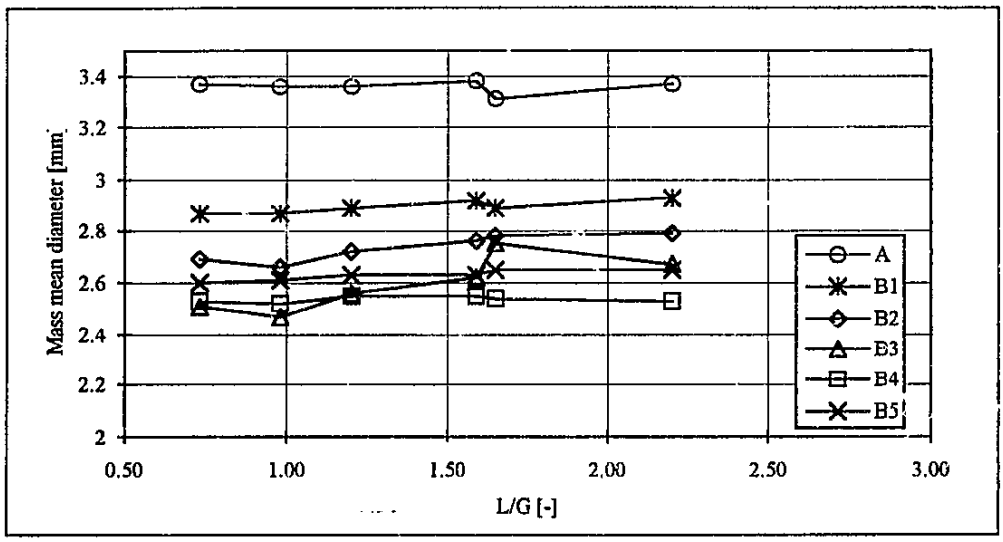

***Figure 5.7** Mass mean diameter, d_{30}, calculated for each configuration.*

Discussion

It is expected that variations in the distribution curves, as well as the mean diameters, will be dependent on the various configurations tested, as well as the different combination of mass flow rates. The addition of the splash grids should increase the number of smaller drops, thus shifting the distribution curves for Configuration B to the left of those of Configuration A. It is also expected that the difference in drop fall distance, z_{sz}, should effect the distribution curves of Configuration B. However, the measured cumulative mass fraction curves are quite difficult to analyze in terms of dependence on the above mentioned factors, due to their irregular form. In the next two sections the correlation of these curves is discussed, with the resultant distribution functions being much more amenable for the analysis of trends. Consequently, in this section the emphasis is placed on the mean diameter variations, with the variations of the distribution curves discussed in more detail in Section 5.2.3.

Distribution curves

From Figures 5.3 and 5.4 is can be seen that the distribution curves for Configuration B have moved to the left, when compared to Configuration A. This indicates that more mass is contained in the smaller diameters and a resultant decrease in mean diameter should be expected.

Mass counted

Figure 5.5 shows that the mass counted in the sampling area increases with increasing water/air mass flow ratio, which is the expected tendency. This confirms the consistency of the experimental method and data abstraction techniques.

Mean diameters

Figures 5.6 and 5.7 show that there is not a significant variation or identifiable trend in mean diameter with varying mass flow rates. The values for each configuration were consequently averaged and the percentage difference between the diameters of Configuration A and Configuration B calculated. These differences are tabulated in Table 5.1.

***Table 5.1** Percentage decrease in mean diameters.*

Configuration	d_{32} [*mm*]	% decrease (based on $d_{32,A}$)	d_{30} [*mm*]	% decrease (based on $d_{30,A}$)
A	5.31		3.36	
B1	4.62	13.09	2.90	13.80
B2	4.34	21.12	2.73	21.64
B3	4.18	26.05	2.60	27.89
B4	4.05	30.32	2.54	31.77
B5	4.35	23.92	2.63	28.84

Clearly there is a marked difference between the mean diameters of configurations A and B. There is also a definite variation in mean diameter within Configuration B, i.e. the diameters vary with the drop fall distance, z_{az}, as shown in Figure 5.1. This is to be expected because the fall distance influences the velocity of the drops striking the splash grids and should therefore have an effect on the amount of splashing on the grid. Figure 5.8 plots this variation against increase in drop fall distance. From this graph it would seem that the splash grids have a maximal effect at a distance of 0.67 *m*.

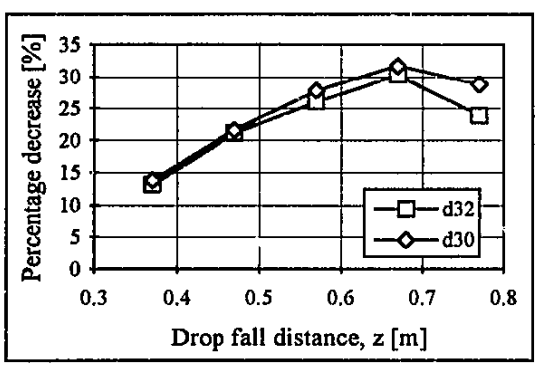

***Figure 5.8** Percentage decrease in mean diameters.*

5.2.2 Application of drop distributions functions

A series of ten photographs was initially taken of a single operating condition. The photographs were processed and the data abstracted in the manner described in the previous chapter. The data thus acquired was then used to determine the applicability of the available distribution functions on the actual distributions measured. Figure 5.9 shows the drop number

distribution obtained for the specific operating condition tested.

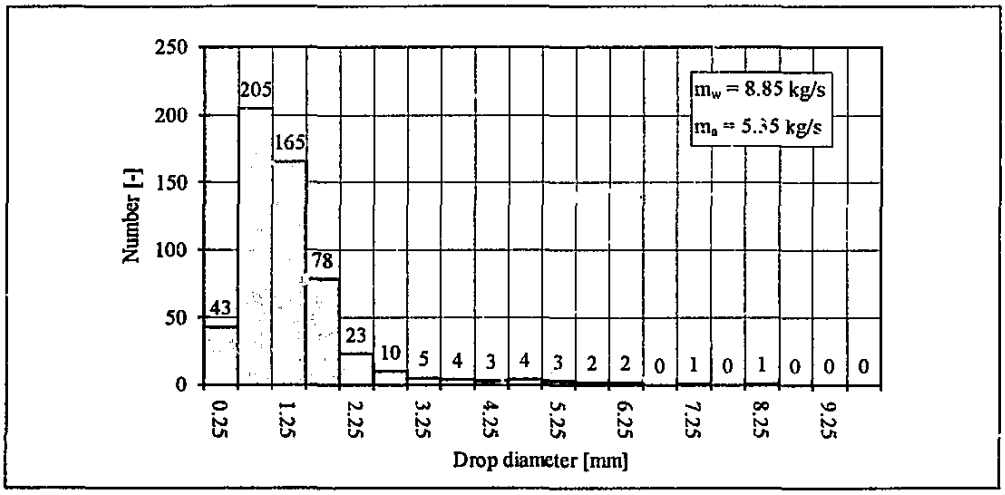

***Figure 5.9** Drop number distribution for test case (Average of 10 samples).*

As stated in Chapter 2, Section 2.2.2, the best known distribution functions are the log-normal and the Rosin-Rammler functions. The Rosin-Rammler distribution function, which is applied to the cumulative mass fraction distribution, was originally developed for broken coal, and has since been found to apply to many materials. The distribution obtained could be correlated reasonably well with the Rosin-Rammler function. This distribution function is generally given in the cumulative mass form :

$$1 - R = \exp\left(-\left(\frac{d}{d_{RR}}\right)^{n_{RR}}\right) \tag{5.1}$$

where $1 - R$ is the mass fraction of drop material occurring in drops of diameter greater than d, d_{RR} is a size parameter and n_{RR} is a distribution parameter. From Equation 5.1 a mass distribution equation can be derived

$$\frac{dR}{dd} = \frac{n_{RR} d^{n_{RR}-1}}{d_{RR}^{n_{RR}}} \exp\left(-\left(\frac{d}{d_{RR}}\right)^{n_{RR}}\right) \tag{5.2}$$

The numerical distribution function is obtained by dividing Equation 5.2 by d^3 and inserting a factor to make $\int_0^\infty \frac{dn}{dd} dd = 1$:

$$\frac{dn}{dd} = \frac{n_{RR} d^{n_{RR}-4}}{d_{RR}^{n_{RR}-3} \Gamma\left(1 - \frac{3}{n_{RR}}\right)} \exp\left(-\left(\frac{d}{d_{RR}}\right)\right) \tag{5.3}$$

The gamma function appearing in this equation is the generalized factorial. Its defining equation is

$$\Gamma(c) = \int_0^\infty U^{c-1} e^{-U} dU \tag{5.4}$$

From Mugele and Evans [51MU1] the general relation for a mean diameter is given by

$$\bar{d}_{qp}{}^{q-p} \int_{d_0}^{d_m} d^p \frac{dn}{dd} dd = \int_{d_0}^{d_m} d^q \frac{dn}{dd} dd \tag{5.5}$$

This expression for mean diameters becomes

$$\bar{d}_{qp}{}^{q-p} = d_{RR}{}^{q-p} \, \Gamma\left(\frac{q-3}{n_{RR}} + 1\right) \Big/ \Gamma\left(\frac{p-3}{n_{RR}} + 1\right) \tag{5.6}$$

In particular, the Sauter mean diameter is

$$d_{32} = d_{RR} / \Gamma\left(1 - \frac{1}{n_{RR}}\right) \tag{5.7}$$

and the mass mean diameter

$$d_{30} = \left(d_{RR}{}^3 / \Gamma\left(1 - \frac{3}{n_{RR}}\right)\right)^{1/3} \tag{5.8}$$

For application to data, Equation 5.1 is put into the form

$$\ln \ln\left(\frac{1}{1-R}\right) = n_{RR} (\ln d - \ln d_{RR}) \tag{5.9}$$

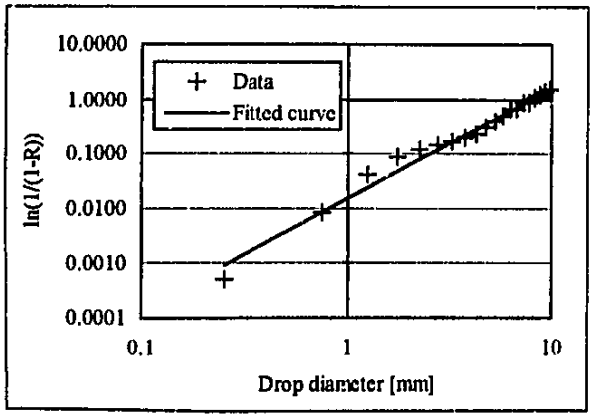

Figure 5.10 Rosin-Rammler function fitted to experimental data.

This represents ln ln (1/(1-R)) as a linear function of ln x. Figure 5.10 shows the experimental data and the fitted Rosin-Rammler function. With this approach, n_{RR} is the slope of the line and d_{RR} is the value of d where $1-R = e^{-1}$. A somewhat easier method to evaluate d_{30}, as compared to Equation (5.8), is to set R = 0.5 in Equation (5.9). This is, by definition, the value of R where d = d_{30}. With this manipulation, the equation for d_{30}

becomes

$$d_{30} = d_{RR}\left(0.6931^{(1/n_{RR})}\right) \tag{5.10}$$

However, the Rosin-Rammler equation is not very reliable for calculating mean diameters, even if a good fit to the experimental data can be obtained. This is mainly due to the assumption of an infinite range of x-values made in the derivation of the Rosin-Rammler equation. It is therefore better to calculate mean diameters directly from experimental data, and use mean diameters calculated from the Rosin-Rammler only for comparative purposes. The Rosin-Rammler parameters are very useful for predicting trends in drop distributions. Figure 5.11 shows the effect of varying values of n_{RR} and d_{RR} on the distribution curve.

It can be clearly seen from Figure 5.11 that a decrease in either the Rosin-Rammler parameters, or both, has the effect of moving the distribution curve to the left. This, in effect, means that there is more mass contained in small drops, resulting in more smaller drops in the distribution.

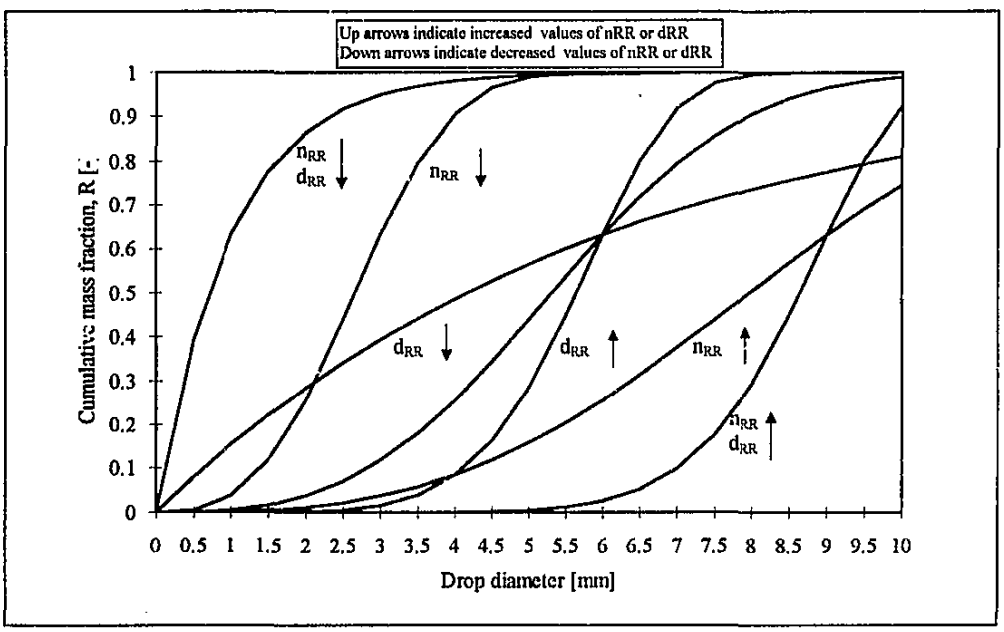

***Figure 5.11** Effect of varying values of n_{RR} and d_{RR} on Rosin-Rammler distribution curve.*

5.2.3 Correlation of drop distribution data

As stated in the previous section, the Rosin-Rammler function is useful for the correlation of data in order to accentuate and identify possible trends. The cumulative mass fraction curves

obtained from the drop distribution testing were correlated with the Rosin-Rammler function. The values of the Rosin-Rammler parameters, d_{RR} and n_{RR}, as well as the coefficient of correlation for each case, are tabulated in Appendix A. In Figure 5.12 these parameters are plotted for the various configurations as functions of water/air mass flow ratio.

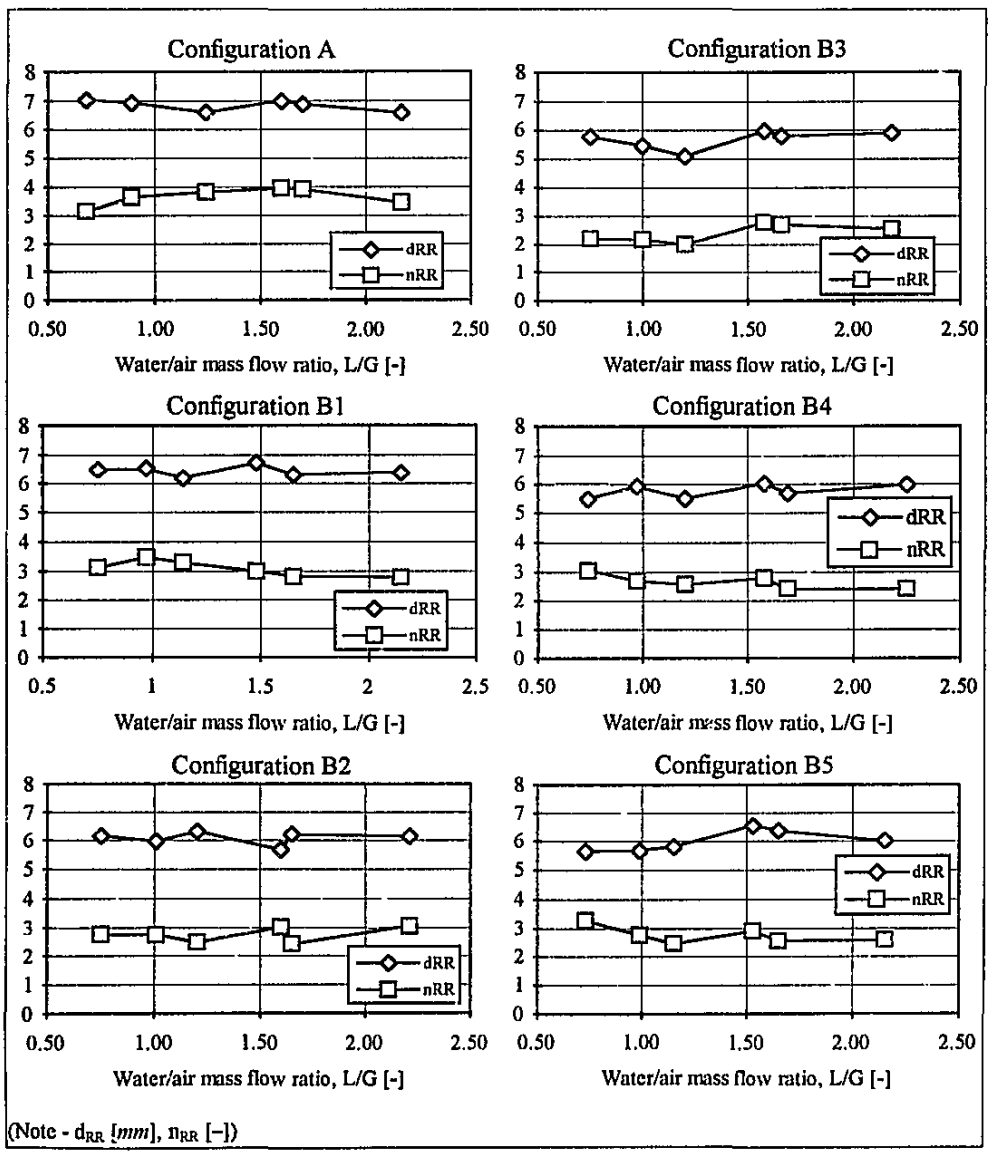

***Figure 5.12** Rosin-Rammler parameters describing drop distributions for each configuration.*

From Figure 5.12 it can be seen that there is no obvious relation between the parameters at different water/air mass flow ratios, although there is a definite decrease between the

parameters of Configuration A and Configuration B. Due to the nature of the Rosin-Rammler function, the parameters were consequently plotted in the form $x_{RR} = 1-\exp(-(1/d_{RR})^{n_{RR}})$, which is the cumulative mass fraction at a drop diameter of 1 *mm*. Figure 5.13 shows this value plotted against the water/air mass flow ratio and for the various drop fall distances of Configuration B.

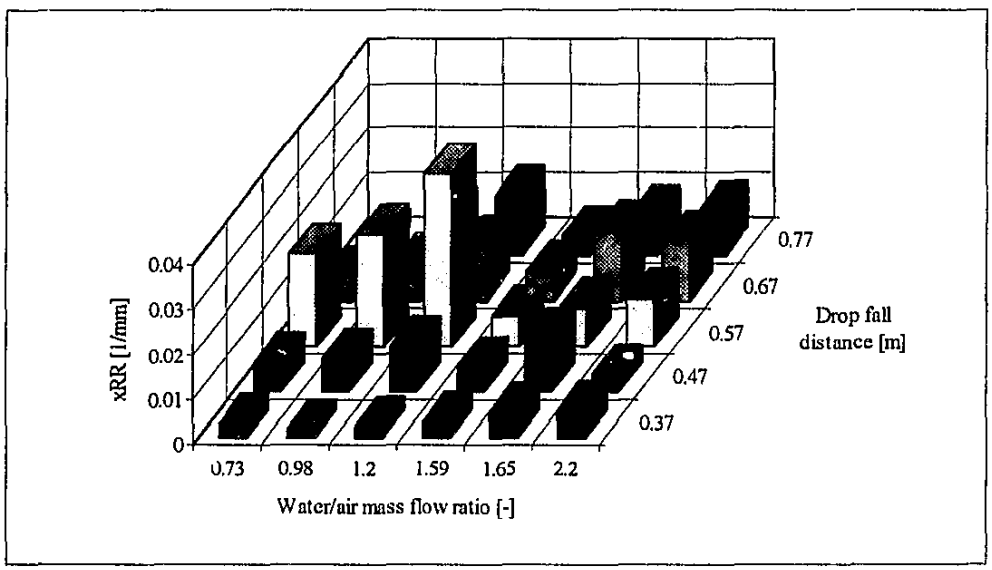

***Figure 5.13** Variation in Rosin-Rammler parameter x_{RR}.*

The x_{RR} data for Configuration B was correlated as a function of water/air mass flow rate and drop fall distance, z_{az}, yielding the following equation

$$x_{RR} = c_1 - c_2 z_{az} + c_3 z_{az}^2 \qquad \text{for } 0.35 < z_{az} < 0.8\ m \tag{5.11}$$

where

$$c_1 = 0.25 - 0.695(1/(L/G)) + 0.331(1/(L/G))^2 \qquad \text{for } 0.5 \le L/G \le 2.5 \tag{5.12}$$

$$c_2 = -0.95 + 2.655(1/(L/G)) - 1.259(1/(L/G))^2 \qquad \text{for } 0.5 \le L/G \le 2.5 \tag{5.13}$$

$$c_3 = 0.82 - 2.273(1/(L/G)) + 1.069(1/(L/G))^2 \qquad \text{for } 0.5 \le L/G \le 2.5 \tag{5.14}$$

This function is shown in Figure 5.14 (next page). From this plot it can be seen that the maximum value of x_{RR} occurs in the region of $z_{az} = 0.6\ m$ and L/G = 1.00. This finding agrees well with the maximal decrease in mean drop diameter also occurring between $z_{az} = 0.6\ m$ and $z_{az} = 0.7\ m$ (see Figure 5.8). It can therefore be concluded that the distance where the

cumulative mass contained in drops 1 *mm* in diameter and smaller reaches a maximum is an indication of the position where the largest decreases in mean drop diameter occur.

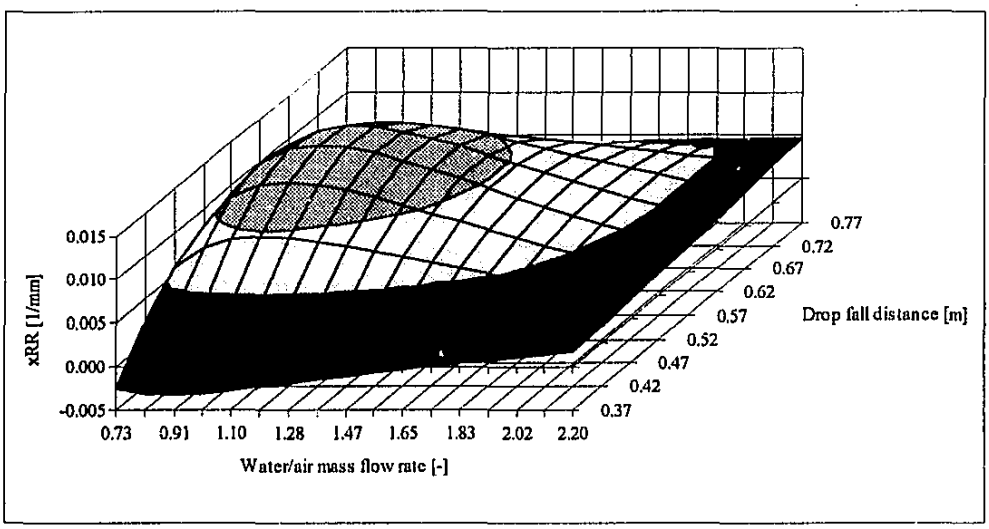

***Figure 5.14** Rosin-Rammler parameter function x_{RR}.*

5.3 TRANSFER CHARACTERISTIC AND PRESSURE DROP

Transfer characteristic

It was shown in the previous section that the splash grids have a maximal effect at a distance of approximately 0.65 *m*. The transfer characteristic was subsequently determined experimentally for two configurations : the one configuration without the splash grids and the other configuration with the splash grids at a distance of $z_{sz} = 0.57$ *m* beneath the trickle pack. In this position the effect of the splash grids is near to optimal, and the rainzone height beneath the grids is kept as large as possible, thus maximizing the amount of heat transfer that occurs in this region.

The objectives of the thermal testing are :

1. To determine whether the resultant decrease in mean diameters due to the addition of the splash grids to the cooling tower test facility does in fact improve the transfer characteristic accordingly, and
2. to quantify this improvement, if any.

Both configurations were tested at 16 different water/air mass flow ratios. The experimental data for these tests is tabulated in Appendix A. The data sets obtained were correlated with the following equations :

Configuration A (No splash grids)

$$\frac{KaV}{L} = 0.478\,L^{-0.470}G^{0.872} \tag{5.15}$$

$$\frac{KaV}{L} = 0.686\left(\frac{L}{G}\right)^{-0.676} \tag{5.16}$$

Configuration B (Splash grids placed 0.57 *m* beneath trickle pack)

$$\frac{KaV}{L} = 0.557\,L^{-0.526}G^{0.922} \tag{5.17}$$

$$\frac{KaV}{L} = 0.792\left(\frac{L}{G}\right)^{-0.650} \tag{5.18}$$

Equations 5.16 and 5.18 are plotted in Figure 5.15. It can be seen that there is a definite improvement in the transfer characteristic with the addition of the splash grids, with the increase in KaV/L at (L/G) = 1 approximately 0.11.

The transfer characteristics calculated represent the transfer for the whole cooling tower test section, which includes the trickle pack (z_{tp}), the region below the trickle pack (z_{az}) and the rain zone (z_{rz}) below the splash grids. For further analysis it would be advantageous to

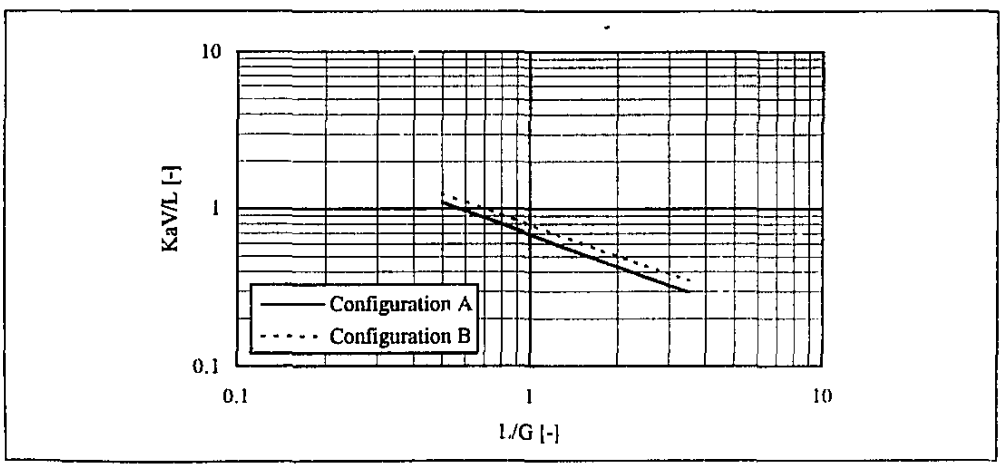

Figure 5.15 *Transfer characteristic correlations.*

determine the transfer characteristics of only the drop zone, thereby excluding the contribution of the trickle pack. However, the available correlation for the transfer characteristic of the trickle pack is not sufficiently accurate to allow subtraction of the trickle pack correlation data from the correlation data of Equations 5.16 and 5.18. This is because the errors incurred with the isolation of the drop zone transfer characteristic is of the same magnitude as the transfer characteristic of the drop zone itself. It can be reasoned that any increase in the transfer characteristic is due to the effect of the added splash grids, with the contribution of the trickle pack staying the same. Subsequent analysis is therefore concentrated on differences in the transfer characteristic, with the absolute values being of lesser importance. Figure 5.16 shows the increase in KaV/L calculated from Equations 5.16 and 5.18.

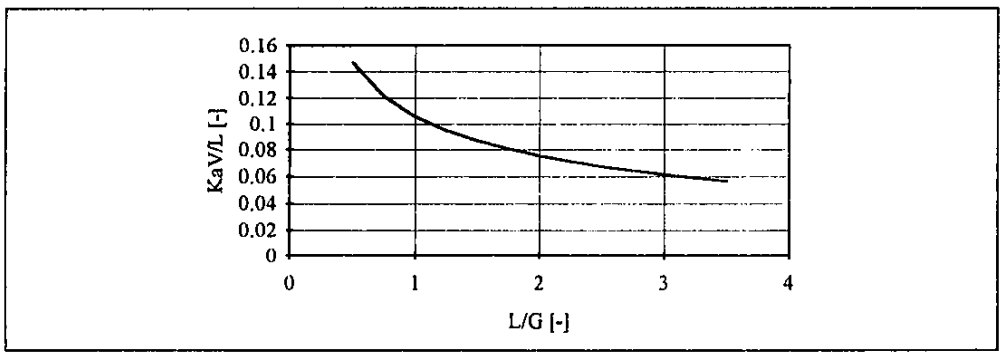

Figure 5.16 *Increase in transfer characteristic*

Pressure drop

The pressure drop measured during the thermal testing is tabulated in Appendix A. The resultant pressure loss coefficients were correlated with the following equations

Configuration A

$$N_p = 1.98 L^{0.984} G^{-0.668} \tag{5.19}$$

Configuration B

$$N_p = 2.29 L^{1.01} G^{-0.613} \tag{5.20}$$

The difference between these two equations is plotted in Figure 5.18. The differences for various air flow rates are approximately the same and were consequently averaged. It can be seen that the air flow resistance for Configuration B is indeed higher than that of Configuration

A, due to the added resistance of the splash grids and the smaller mean drop diameters caused by the grids.

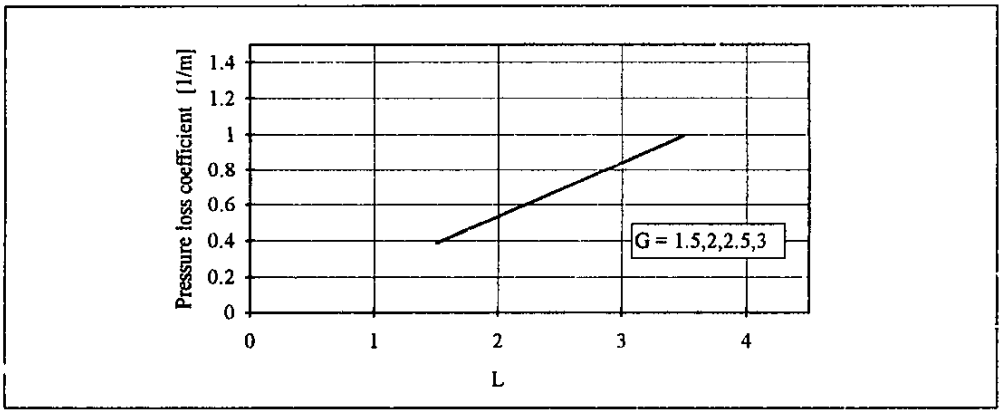

***Figure 5.17** Averaged increase in pressure loss coefficient.*

CHAPTER 6

COMPUTER SIMULATION

In his dissertation 'Modelling of cooling tower splash pack', Dreyer [94DR1], presented a computer program that may be used to analyze rain zone and packing performance. His study was aimed at developing a mathematical model to describe the performance of splash packing material using basic aerodynamic, hydrodynamic and heat/mass transfer information without depending on empirically determined data from cooling tower testing. This model can be used to optimize the layout of splash packing material, as well as studying the effect of different types of water distribution systems on the performance on a given packing. It can also be used to predict drop size distributions through the packing zone and therefore allows accurate prediction of the rain zone performance.

The program SPSIM (Splash Pack SIMulation) was used in this study as an additional tool to study the effect of the splash grids on the performance of the drop zone (the zone *beneath* the trickle pack). The comparison of data obtained in this experimental study with the data generated with the computer program is also part of an ongoing research effort, of which further verification of the validity and applicability of SPSIM is a component.

Dreyer [94DR1] also developed a computer simulation for natural draft wet cooling towers. The program NDCT (Natural Draft Cooling Tower) could be used determine the manner in which the placement of a layer of splash grid beneath normal packing influenced the performance of a typical cooling tower.

This chapter described the manner in which the computer program SPSIM was used to evalute the drop zone and the influence of the splash grid on the spray characteristics. The data generated with the program and the correlations obtained is presented and the simulation results is compared with the experimental results. Finally, the computer program NDCT is used to quantify the effect of the splash grid on cooling tower performance due to the change in mean drop diameters that will occur when the grids are placed beneath the normal cooling tower packing.

6.1 DROP ZONE EVALUATION

The simulation program was used to evaluate the drop zone, i.e. the zone beneath the trickle pack for two of the configurations that were tested during the experimental study. The basic operation of the program aand the conditions and available options are described in Appendix C. The two configurations that were tested are:

Configuration A – Cooling tower section with no splash grids.

Configuration B – Cooling tower section with 2 splash grids placed 0.57 m beneath the trickle pack.

The splash grid below the trickle pack (as shown in Figure 5.2) was approximated as a grid consisting of parallel slats, 0.003 m wide, and with a pitch of 0.0196 m. This produced an equivalent blockage factor for both the actual grid and the grid used in the program.

The program takes as input parameters the atmospheric pressure, the ambient dry- and wet-bulb temperatures, the inlet water temperature, the water mass flux and the air velocity. For the determination of the transfer characteris' and the pressure drop the values used for these parameters were those obtained during thermal testing, and are tabulated in Appendix A, tables A.2.1 and A.2.2. Similarly, for the determination of drop size distributions, the values used for the parameters were those obtained during the experimental measurement of the drop distributions.

6.1.1 Drop size distribution

Figure 6.1 shows the cumulative mass fraction distribution curves used as the initial drop

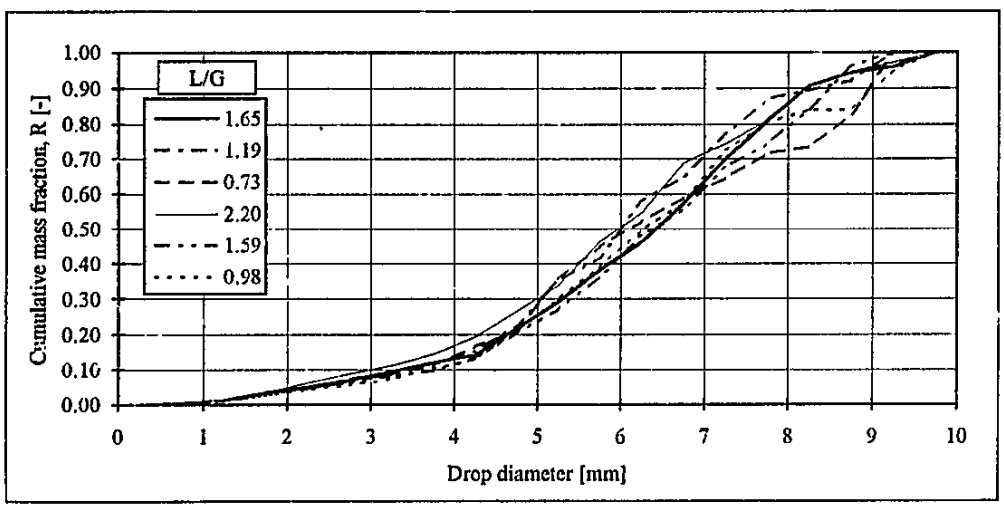

***Figure 6.1** Initial drop size distribution used in SPSIM.*

size distribution at the top of the drop zone in SPSIM. These distribution curves are also the final distribution curves for Configuration A, due to the absence of any splash grids in this configuration. The simulation program was subsequently used to predict the drop distribution curves for Configuration B resulting from the presence of the splash grids in the test section. The data is tabulated in Appendix B and the resulting curves are plotted in Figure 6.2.

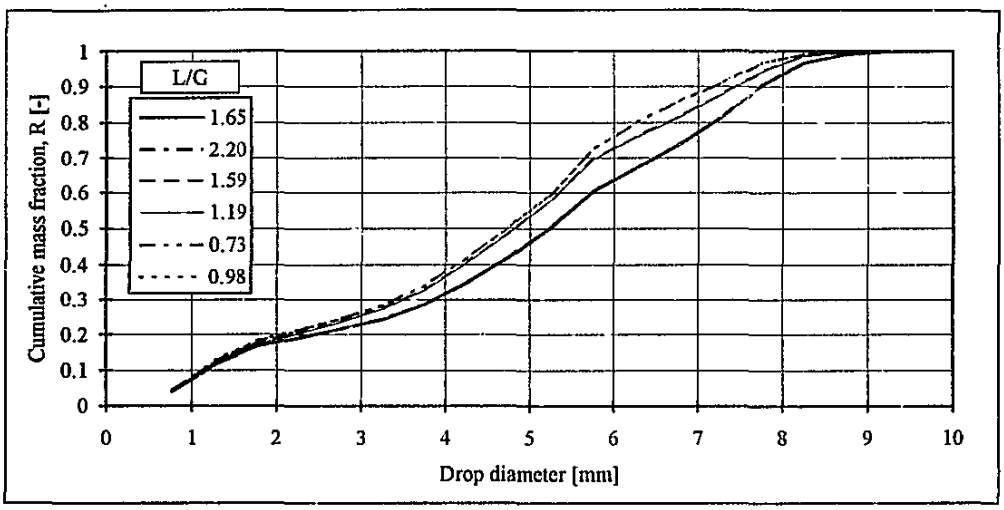

Figure 6.2. *Predicted cumulative mass fraction for Configuration B.*

It can be seen from Figures 6.1 and 6.2 that the distribution curves have shifted more to the left for Configuration B, indicating more mass contained in smaller drops and accordingly more smaller drops, which are the expected result.

Data correlation

The distribution curves shown in Figure 6.2 were correlated with the Rosin-Rammler function as discussed in the previous chapter. Table 6.1 compares the Rosin-Rammler parameters for Configuration B with those of Configuration A (which had been previously calculated).

Table 6.1 Comparison of Rosin-Rammler parameters for configurations A and B.

	d_{RR} , *mm*		n_{RR} , -	
L/G, -	A	B	A	B
0.73	7.037	5.191	3.159	2.289
0.98	6.939	5.181	3.651	2.279
1.19	6.994	5.335	3.942	2.248
1.59	6.593	5.340	3.821	2.256
1.65	6.881	5.792	3.903	2.337
2.20	6.581	5.780	3.453	2.324

It can be seen from Table 6.1 that there is a marked decrease in the Rosin-Rammler parameters for Configuration B. As shown in the previous chapter, a decrease in the Rosin-Rammler parameters results in a shift to the left of the distribution curves, which is indeed the case in this example, as can be seen from Figure 6.1 and 6.2.

6.1.2 Transfer characteristic and pressure drop

The simulation program was used to predict the transfer characteristic and pressure drop for both configurations at similar operating conditions as those of the experimental tests. The data obtained from this computer simulation is tabulated in Appendix B.

Transfer characteristic

The computer predicted transfer characteristics data obtained were correlated with the following equations :

Configuration A

$$\frac{KaV}{L} = 0.143\left(\frac{L}{G}\right)^{-0.254} \tag{6.1}$$

Configuration B

$$\frac{KaV}{L} = 0.259\left(\frac{L}{G}\right)^{-0.213} \tag{6.2}$$

Figure 6.3 shows the increase in transfer characteristic as predicted by Equations 6.1 and 6.2.

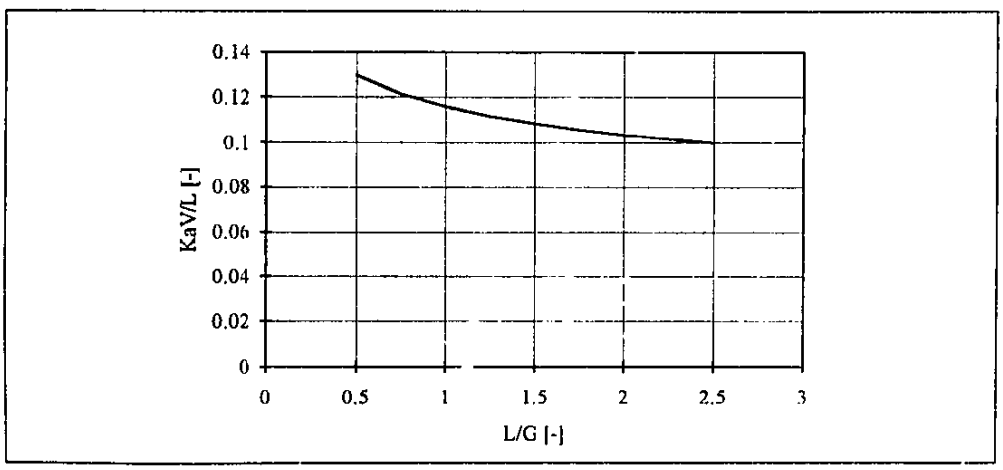

***Figure 6.3** Increase in transfer characteristic predicted by SPSIM.*

Pressure drop

The computer predicted pressure loss data obtained were correlated with the following equations :

Configuration A

$$N_p = 0.36 L^{0.873} G^{-1.337} \tag{6.3}$$

Configuration B

$$N_p = 5.309 L^{0.730} G^{-1.374} \tag{6.4}$$

The difference between these two equations is plotted in Figure 6.4.

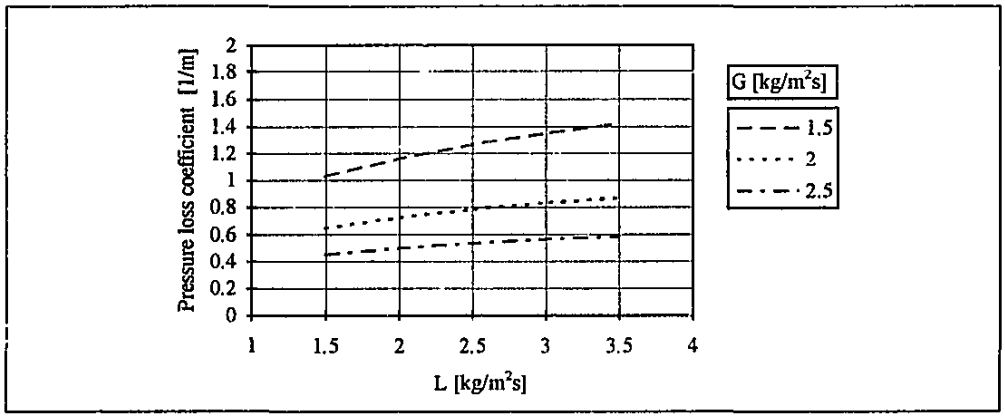

***Figure 6.4** Increase in pressure loss coefficient.*

6.2 COMPARISON AND DISCUSSION

In this section the drop size distribution, transfer characteristic and pressure drop data obtained with the simulation program SPSIM, is compared with the equivalent experimental results.

6.2.1 Drop size distribution

The measured drop size distribution for Configuration B3 (z_{sz} = 0.57 *m*) is compared to the drop distribution predicted by SPSIM in Figures 6.5 to 6.10.

It can be seen from these figures that the computer simulation generally over-predicts the number of drops, especially with drops smaller than 2 *mm*, shown as the uncharacteristic bulge at the beginning of the curves. It seems that the simulation is more accurate in the mid-range (2 to 6 *mm*) of the distribution curves.

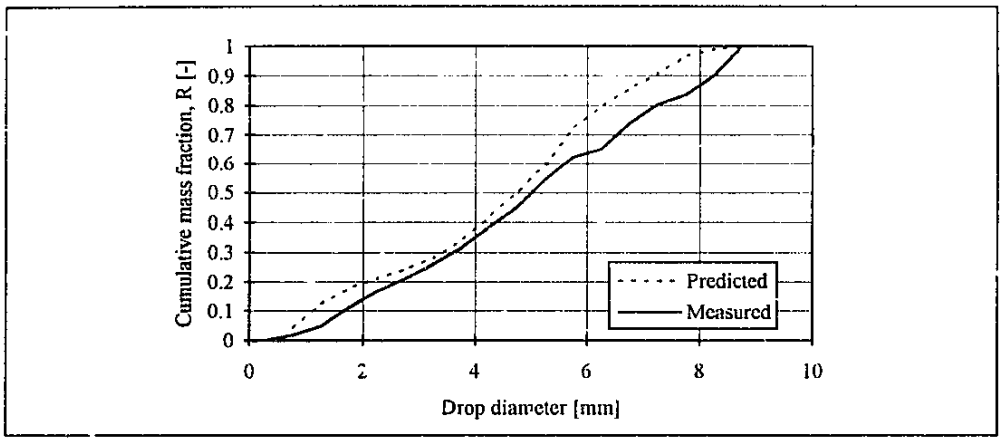

Figure 6.5 *Comparison of drop size distribution for $m_w \approx 4$ kg/s and $m_a \approx 5.45$ kg/s*

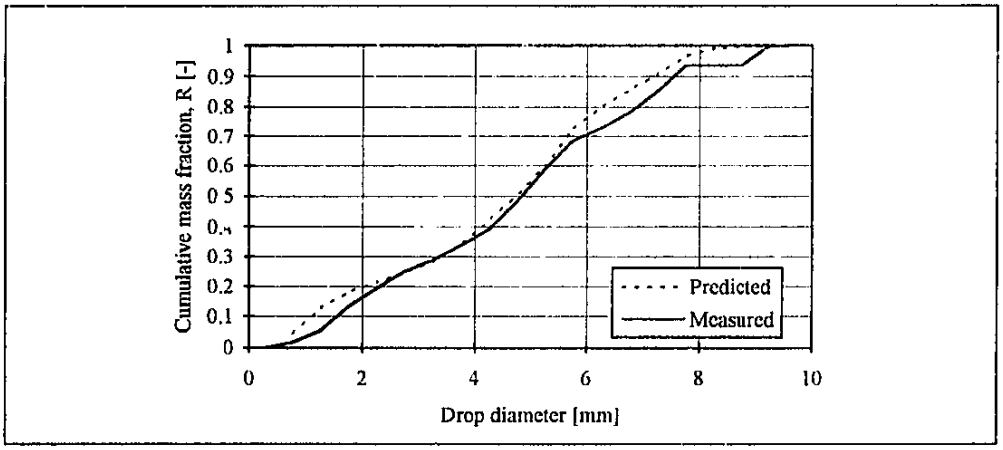

Figure 6.6 *Comparison of drop size distribution for $m_w \approx 4$ kg/s and $m_a \approx 4.09$ kg/s*

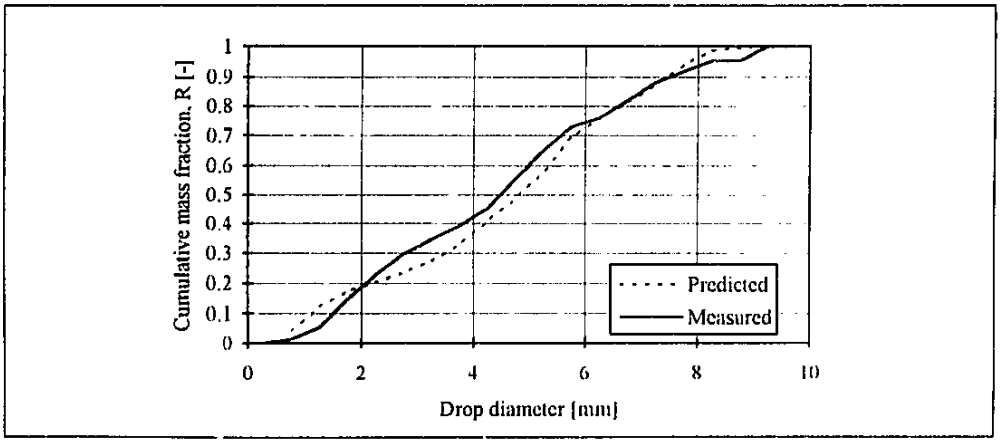

Figure 6.7 *Comparison of drop size distribution for $m_w \approx 6.5$ kg/s and $m_a \approx 5.45$ kg s*

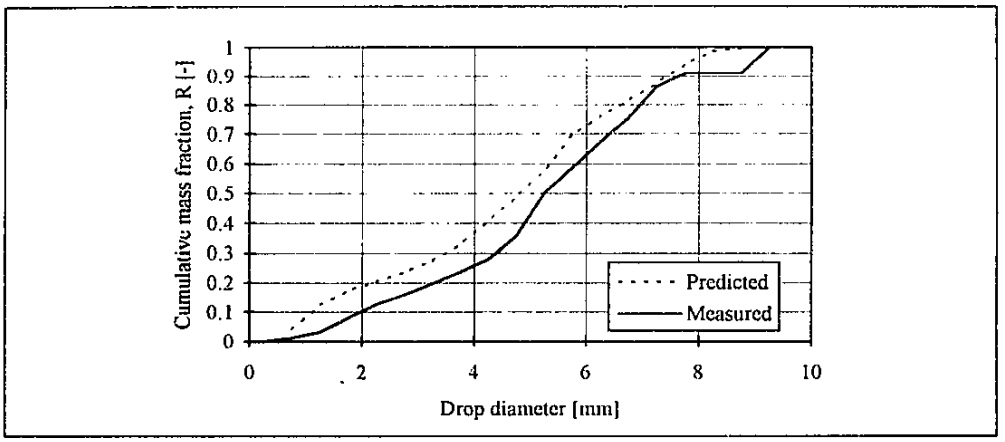

***Figure 6.8** Comparison of drop size distribution for $m_w \approx 6.5$ kg/s and $m_a \approx 4.09$ kg/s*

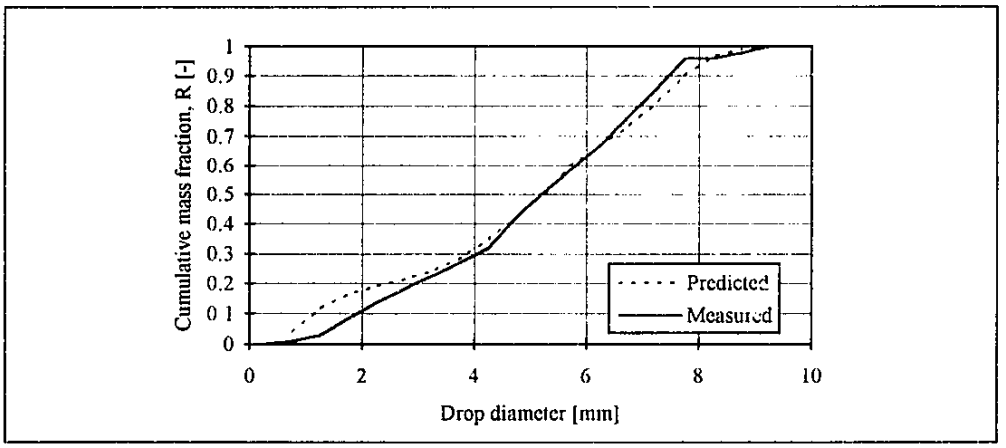

***Figure 6.9** Comparison of drop size distribution for $m_w \approx 9$ kg/s and $m_a \approx 5.45$ kg/s*

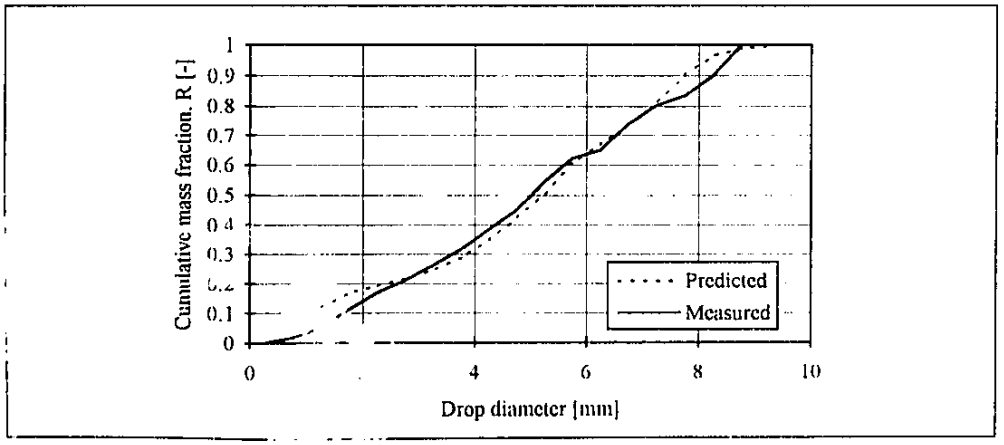

***Figure 6.10** Comparison of drop size distribution for $m_w \approx 9$ kg/s and $m_a \approx 4.09$ kg/s*

One of the shortcomings of SPSIM is the failure to account for the interaction between adjacent splash crowns that form when drops strike the grid, which results in the over-prediction of drops formed by splashing. In his dissertation, Dreyer [94DR1], showed that the average time between drop impacts at a given point is of the same order of magnitude as the crown lifetimes, i.e. the interference factor is of the order unity. This implies that, on average, a splash crown will not have disappeared before the next drop impact in the direct proximity of the original splash crown. Dreyer suggested that the splash mass fractions in SPSIM be artificially reduced by 50 % due to this crown interference effects.

The drop distribution curves shown in Figures 6.5 to 6.10 were in fact generated with the splash fraction reduced by 50 %, with the resulting curves approximating the experimentally determined curves much more closely than would have been the case if the splash fraction had not been reduced.

6.2.2 Transfer characteristic and pressure drop

Transfer characteristic

Figure 6.11 compares the predicted and the measured increases in transfer characteristic, and shows that there is good agreement at the higher air flow rates (i.e. at low water/air mass flow ratios) with over-prediction at the lower air flow rates.

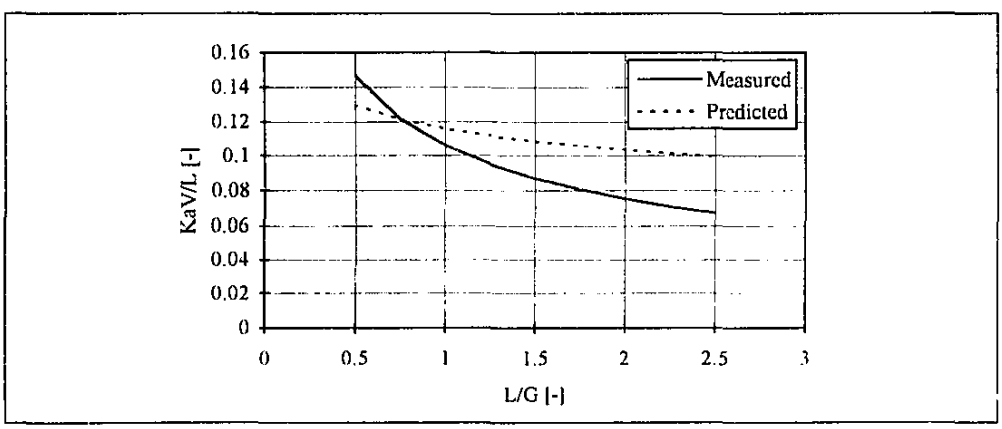

Figure 6.11 *Comparison of measured and predicted increases in transfer characteristic.*

Pressure drop

Figure 6.12 compares the predicted and the measured increases in pressure loss coefficient, and shows that the simulation program predicts a definite variation in pressure loss with air flow rate, which was not the case with the experimental results. The pressure loss is over-predicted at the lower air flow rates while at higher air flow rates there is a variation with water mass

flow rate, with over-prediction at lower water flow rate and under-prediction at higher water flow rates.

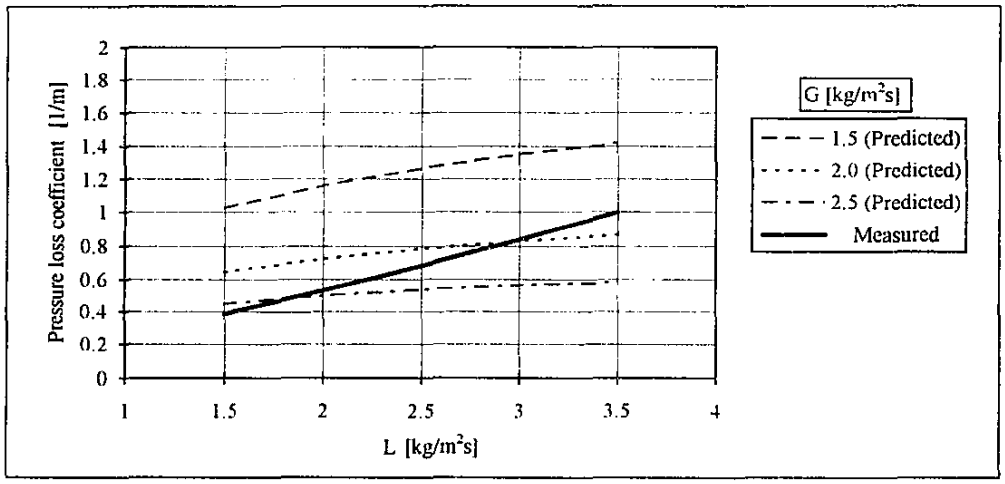

Figure 6.12 *Comparison of measured and predicted increase in pressure loss coefficients.*

The previous two sections presented and briefly discussed the differences between measured and predicted quantities. (See Dreyer [94DR1] for detailed explanation of the possible reasons for the discrepancies).The results obtained in this study are consistent with the results obtained by Dreyer [94DR1] in his comparison of the simulation program results with measured transfer characteristic and as such substantiates the findings obtained by him.

6.3 COOLING TOWER PERFORMANCE PREDICTION

Dreyer [94DR1] used the most recent correlations for pressure drop and the most recent developements for the derivation of the draft equation to calculate the operating point of natural draft wet cooling towers with the computer program NDCT. The program allows considerable flexibility in the specification of cooling tower layout and operating conditions. It was used in this study to quantify the effect of the splash grid on cooling tower performance due to the change in mean drop diameters that will occur when the grids is placed beneath the normal cooling tower packing.

Computer programs used for the analysis of cooling tower performance prediction usually use the Sauter mean diameter to represent the characteristics of the spray in the rain zone. The transfer characteristic and pressure drop for the rain zone based on this mean diameter can then be calculated. A more accurate approach would be to calculate the transfer characteristic and

pressure drop for the rain zone based on the actual drop size distribution. With normal cooling tower performance prediction programs this is not possible because the drop size distributions is usually not known and analysis based on a drop distributions would be to time-consuming.

This problem may be overcome with the use of the program SPSIM. SPSIM can be used to generate transfer characteristic and pressure drop data for large drop zones based on user-specified drop size distributions. The data obtained can then be correlated and used to specify the transfer and pressure drop correlations for the rain zone in the cooling tower analysed by NDCT.

Following this approach, the program SPSIM was used to generate transfer characteristic and pressure drop data for a rain zone for the drop size distributions measured for configurations A and B. This values could then be implemented in the program NDCT.

The physical dimensions and other relevant parameters of the cooling tower which was analyzed is given in Table 6.2. This tower is similar to the towers used in the power generation industry.

Table 6.2 *Cooling tower information*

Tower dimensions	
Tower height	147.0 *m*
Tower diameter at inlet	104.5 *m*
Tower diameter at top	60.85 *m*
Tower inlet height	8.0 *m*
Frontal area of fill	8300 m^2
Other	
Fill correlations	$KaV/L = 1.233\ L^{-0.515}\ G^{0.847}$ $N_p = 8.134\ L^{0.200}\ G^{-0.022}$
Water inlet mass flow rate	12500 *kg/s*
Water inlet temperature	40.00 °C

Cooling tower evaluation based on specified Sauter mean diameter

As shown in Figure 5.8 the splash grids reduced the Sauter mean diameter of the spray beneath the packing by up to 30 %. The values obtained for the Sauter mean diameter for Configuration A and B4 were subsequently implemented in NDCT. Table 6.3 shows the results of the analysis.

Table 6.3 *Results of comparative cooling tower evaluation based on specified Sauter mean diameter in rain zone.*

		Cooling capacity			
T_{aidb}	T_{aiwb}	d_{32} = 5.31 *mm*	d_{32} = 4.05 *mm*	Increase	
℃	℃	*MW*	*MW*	*MW*	*%*
15.00	10.76	986.68	1000.62	13.94	1.41
17.50	11.70	947.98	962.64	14.66	1.55
20.00	12.62	908.89	924.34	15.45	1.70
22.50	13.50	869.69	886.06	16.37	1.88
25.00	14.36	829.86	847.23	17.37	2.09
27.50	15.19	789.45	807.88	18.43	2.33
30.00	15.99	748.17	767.81	19.64	2.63

(Patm = 84100 Pa, w = 0.008)

Cooling tower evaluation based on specified drop size distribution

Using the simulation program SPSIM, two sets of transfer characteristic and pressure loss correlations could be obtained for the rain zone of the cooling tower tested. They are

1) Correlations based on drop size distribution measured for Configuration A :

$$Ka/L = 0.522\ L^{-0.013}\ G^{0.238}$$

$$N_p = 1.037\ L^{1.033}\ G^{-1.622}$$

2) Correlations based on drop size distribution meassured for Configuration B4 :

$$Ka/L = 0.837\ L^{-0.009}\ G^{0.235}$$

$$N_p = 1.032\ L^{0.913}\ G^{-2.254}$$

These correlation were subsequently implemented in the program NDCT and the results are shown in Table 6.4.

Discussion

It can be seen from both Table 6.3 and Table 6.4 that the addition of the splash grids improved the cooling capacity of the cooling tower over a range of inlet air temperatures. The cooling capacity calculated with the Sauter mean diameter is smaller than that calculated with the

Table 6.4 *Results of comparative cooling tower evaluation based on specified drop size distribution in rain zone.*

		Cooling capacity			
T_{aidb}	T_{aiwb}	d_{32} = 5.31 *mm*	d_{32} = 4.05 *mm*	Increase	
℃	*℃*	*MW*	*MW*	*MW*	*%*
15.00	10.76	1038.56	1082.38	43.82	4.22
17.50	11.70	996.74	1039.87	43.13	4.33
20.00	12.62	954.25	996.66	42.41	4.44
22.50	13.50	911.34	953.04	41.70	4.58
25.00	14.36	867.34	908.24	40.90	4.72
27.50	15.19	822.17	862.15	39.98	4.86
30.00	15.99	775.42	814.28	38.86	5.01

(Patm = 84100 Pa, w = 0.008)

correlations determined with SPSIM, and the percentage increases predicted is also smaller. However, the calculations based on the measured drop size correlation should be the most accurate approach and it can therefore be assumed that the cooling capacity of the tower is increased by between 4 and 5 %.

CHAPTER 7

CONCLUSION AND RECOMMENDATION

Conclusions

The original idea of improving rain zone performance beneath trickle pack by placing a layer of splash grid beneath the pack has been investigated and shown to have definite effect on the performance of the rain zone.

Experimental results have shown a decrease of approximately 20 % in the mean diameters of the spray beneath the added splash grids, resulting in an increase of transfer characteristic of approximately 0.11 at a water/air mass flow ratio of 1. The smaller mean diameters of the sprays also resulted in increases in the pressure loss coefficients between 0.4 and 1.

The experimental results were corroborated by computer simulation [94DR1]. The simulation program predicted the drop size distributions remarkably well, although there was a marked over-prediction at the small drop diameters ($d \leq 2$ *mm*). However, it was explained that the results were influenced by certain approximating parameters and could be adjusted to deliver better results. The increases in transfer characteristic and pressure loss coefficient were also predicted with reasonable accuracy. The discrepancy between the measured and predicted values can be ascribed to both theoretical assumptions and experimental inaccuracy. Although considerable effort was made to ensure accurate measurement, the increases in transfer characteristic were relatively small since the additional transfer occurred in a rain zone of height 1.7 *m*, thus amplifying errors in measurement.

A computer program developed by Dreyer [94DR1] to determine the cooling capacity of natural draft wet cooling towers was used to determine what effect the placement of the splash grids would have on the performance of the tower. The program showed that the decrease in Sauter mean diameter of the drops in the rain zone resulted in an increase of up to 5 % in the cooling capacity of the cooling tower.

The semi-automated procedure developed for the abstraction of data from photographs proved to be relatively uncomplicated and easy to implement, while still giving satisfactory results. The decreases in mean diameters measured by the method was well corroborated by the accompanying increases in transfer characteristic.

Recommendations

The image processing method employed in the data abstraction failed to detect and segment large, irregular shaped drops due to discontinuities in the outlines of the drops. The implementation of Hough's method [92GO1] to detect the drop outlines should be able to rectify this problem, although it would be at the expense of simplicity and speed of operation.

In this study only one splash grid arrangement was tested, namely 2 layers of expanded metal grids, spaced at 0.1 *m*, at different distances beneath the trickle pack. Future investigation may be aimed at investigating variations in this arrangement, such as the number of layers and grid spacing. The effectiveness of other types of splash grid in breaking up drop sprays can also be investigated.

In conclusion, it is recommended that the method used to decrease the mean drop diameter in the rain zone presented in this study be implemented in a full-size natural draft wet cooling tower in order to obtain actual performance data.

REFERENCES

[26ME1] Merkel, F., **Verdunstungskühlung**, VDI-Zeitschrift, Vol. 70, No. 4, pp. 123-128,January , 26

[33RO1] Rosin, P.P., and Rammler, E., **Laws governing the fineness of powdered coal**, Journal of the Institute of Fuel, Vol. 7, pp. S-14-S-15, 1939.

[38FR1] Frössling, N., **Uber die Verdunstung Fallender Tropfen**, Gerlands Beitrage Zur Geophysik, Vol. 52, pp. 170-216, 1938.

[40NO1] Nottage, H.B., and Boelter, L.M.K., **Dynamic and thermal behaviour of water drops in evaporative cooling processes**, ASHVE, Research Report, No. 1146, 10EEE, pp. 41-82, 1940.

[41NI1] Niederman, H.H., Howe, E.D., Longwell, J.P., Seban, R.A., and Boelter, L.M.K., **Performance characteristics of a forced draft, counterflow spray cooling tower**, Heating, Piping and Air Conditioning, pp. 591-597, September 1941.

[49GU1] Gunn, R., and Kinzer, G.D., **The terminal velocity of fall for water droplets in stagnant air, Journal of Meteorology**, Vol. 6, pp. 243-248, August 1949.

[49MI1] Mickley, H.S., **Design of forced draft air conditioning equipment**, Chemical Engineering Progress, Vol. 45, No. 12, pp. 739-745, 1949.

[51MU1] Mugele, R.A., and Evans, H.D., **Droplet size distribution in sprays**, Industrial and Engineering Chemistry, Vol. 43, pp. 1317-1324, 1951.

[52BA1] Baker, D.R., and Mart, L.T., **Cooling tower characteristics as determined by the unit-volume coefficient**, Refrigerating Engineering, pp. 965-971, September 1952.

[52BA1] Baker, D.R., and Mart, L.T., **Cooling tower characteristics as determined by the unit-volume coefficient**, Refrigeration Engineering, pp. 965-971, 1952.

[52RA1] Ranz, W.E., and Marshall Jr, W.R., **Evaporation from drops**, Part I, Chemical Engineering Progress, Vol. 48, No. 3, pp. 141-146, March 1952.

[56KE1] Kelly, N.W., and Swenson, L.K., **Comparative performance of cooling tower packing arrangements**, Chemical Engineering Progress, Vol. 52, No. 7, pp. 263-268, 1956

[57FU1] Fuller, A.L., Kohl, A.L., and Butcher, E., **A new plastic packing for cooling towers**, Chemical Engineering Progress, Vol. 53, No. 10, pp. 501-505, 1957.

[59C .1] Cribb, G., **Liquid phase resistance in water cooling**, British Chemical Engineering, Vol. 4, pp. 264-266, 1959.

[59Mc1] McKelvey, K.K., and Brooke, M., **The Industrial Cooling Tower**, Elsevier Publishing Company, Amsterdam, 1959.

[61BA2] Baker, D.R., and Shryock, H.A., **A comprehensive approach to the analysis of cooling tower performance**, ASME Journal of Heat Transfer, pp. 339-350, 1961.

[61MU1] Munters, C., and Lindqvist, L., **A new concept of cooling tower design**, Proceedings of the Institute of Refrigeration, pp. 89-114, February 1961

[62LO1] Lowe, H.J., and Christie, D.G., **Heat transfer and pressure drop on cooling tower packings, and model studies of the resistance of natural draft towers to airflow**, Proceedings of the 2nd International Heat Transfer Conference Boulder Colorado Part V, Paper 113, pp 933-950 1962.

[62RE1] Renzi, P.N., and Kosowski, N., **Compact mass transfer packings**, International Institute of Refrigeration, pp. 255-271, August 1962.

[66DU1] Dutkiewicz, R.K., **Natural-draught spray-cooling towers**, International Conference on Heat Transfer, Vol. 1, pp. 331-338, 1966.

[68RA1] Ramshaw, C., **A technique for drop-size measurement by direct photography and electronic image size analysis**, Journal of the Institute of Fuel, Vol. 41, pp. 288-292, July 1968.

[70PR1] Pruppacher, H.R., and Beard, K.V., **A wind tunnel investigation of the internal circulation and shape of water drops falling at terminal velocity in air**, Quarterly Journal of the Royal Meteorological Society, Vol. 96, pp. 247-256, 1970.

[71PR1] Pruppacher, H.R., and Pitter, R.L., **A semi-empirical determination of the shape of cloud and rain drops**, Journal of the Atmospheric Sciences, Vol. 23, pp. 86-94, 1971.

[73TE1] Tezuka, S., **Performance of aqueous-film-type packing of cooling tower**, Heat Transfer- Japanese Research, Vol. 2-3, pp. 40-52, 1973.

[74HO1] Hollands, K.G.T., **An analysis of a counterflow spray cooling tower**, International Journal of Heat and Mass Transfer, Vol. 17, pp. 1227-1239, 1974.

[74NA1] Nahavandi, A.N., Kershah, R.M., and Serico, B.J., **The effect of cooling tower evaporation losses in the analysis of counterflow cooling towers**, Nuclear Engineering and Design, Vol. 32, pp. 29-36, 1975.

[74YA1] Yao, S.C., **Investigation on falling drop heat-mass transfer and drift elimination in wet cooling systems**, Ph.D. dissertation, University of California, Berkeley, 1974.

[75TE1] Tezuka, S., and Nakamura, T., **Performance of multitubular-type cooling tower packing, Transactions of the Society of Heating, Air-Conditioning and Sanitary Engineers of Japan**, Vol. 13, pp. 44-52, 1975

[76BE1] Beard, K.V., **Terminal velocity and shape of cloud and precipitation drops aloft**, Journal of the Atmospheric Sciences, Vol. 33, pp. 851-864, May 1976

[76YA1] Yao, S.C., and Shrock, V.E., **Heat and mass transfer from freely falling drops**, ASME Journal of Heat Transfer, pp. 120-126, February 1976

[76OT1] Otsu, N., **A threshold selection method from gray-level histograms**, IEEE Transactions on System, Man and Cybernetics, Vol SMC-9, No. 1, pp 62-66, 1975.

[77CH1] Chen, K.C., and Trezek, G.J., **The effect of heat transfer coefficient, local wet bulb temperature and droplet size distribution function on the thermal performance of sprays**, ASME Journal of Heat and Mass Transfer, Vol 99, pp 381-385, 1977.

[77SI1] Simmons, H.C., **The correlation of drop-size distributions in fuel nozzle sprays**, Journal of Engineering for Power, pp. 309-319, July 1977.

[77ST1] Stockham, J.D., and Fochtman, E.G., **Particle Size Analysis**, Ann Arbor Science Publishers Inc., Michigan, 1977.

[77TI1] Tishkoff, J.M., and Law, C.K., **Application of a class of distribution functions to drop-size data by logarithmic least-squares technique**, Journal of Engineering for Power, pp. 684-688, October 1977.

[78AZ1] Azzopardi, B.J., **Measurement of drop sizes**, International Journal of Heat and Mass Transfer, Vol. 22, pp. 1245-1279, 1978.

[78CL1] Clift, R., Grace, J.R., and Weber, M.E., **Bubbles, drops and particles**, Academic Press, New York, 1978.

[81AL1] Allen, T., **Particle Size Measurement**, Chapman and Hall, New York, 1981.

[81SC1] Schrodt, V.N., and Saunders, A.M., **Interactive image processing in research**, Computers in Chemical Engineering, Vol. 5, pp. 299-305, 1981.

[81SI1] Srikrishna, M., Sivaji, K., and Narasimhamurty, G.S.R., **Mechanics of liquid drops in air**, Chemical Engineering Journal. Vol. 24, pp. 27-34, 1982.

[82PA1] Pavlidis, T., **Algorithms for Graphics and Image Processing**, Computer Science Press, Orlando, Florida, 1982.

[83BO1] Bourillot, C., TEFERI, **Numerical model for calculating the performance of an evaporative cooling tower**, EPRI Special Report CS-3212-SR, August 1983 (Translated by J.A. Bartz).

[83CA1] Cale, S.A., **Developement of evaporative cooling packing**, Commission of European Communities, Report EUR 7709 EN, 1982.

[83CH1] Chigier, N., **Drop size and velocity instrumentation**, Progress in Energy Combustion Sciences, Vol. 9, pp. 155-177, 1983.

[83SI1] Singham, J.R., **Heat Exchanger Design Handbook**, Ch. 3.12, Cooling Towers, Hemisphere Publishing Company, 1983.

[83SU1] Sutherland, J.W., **Analysis of mechanical-draught counterflow air/water cooling towers**, ASME Journal of Heat Transfer, Vol. 105, pp. 576-583, August 1983.

[83WA1] Warrington, R.O., and Musselman, R.L., **Analysis of liquid/gas direct contact heat exchanger concept**, Journal of Energy, Vol. 7, No. 6, pp 732-734, 1983

[84LE1] Lefevre, M.R., **"Eliminating the Merkel theory approximations -- can it replace the empirical 'temperature correction factor'?"**, Paper No TP-84-18, CTI 1984 Annual Meeting, Houston, Texas.

[84PO1] Poppe, M. and Rögener, H., **Evaporative cooling systems**. VDI-Wärmeatlas, Section Mh, 1984.

[85KA1] Kapur, J.N., Sahoo, P.K., and Wong, A.K.C., **A new method for gray-level picture thresholding using the entropy of the histogram**, Computer Vision, Graphics and Image Processing, Vol. 29, pp 273-285, 1985

[85LE1] Lefevre, M.R., **Influence of air and water temperature on fill characteristic curve**, Cooling Tower Institute Annual Meeting, Paper No TP-85-8, 1985

[85MI1] Missimer, J.R., and Brackett, C.A, **Model tests of the rain zone of a counterflow natural draft cooling tower**, TVA Report No. WR28-1-85, May 1985.

[86BE1] Benton, D.J., and Rehberg, R.L., **Mass transfer and pressure drop in sprays falling in a freestream at various angles**, Proceedings of the 5th IAHR Cooling Tower Workshop, Monterey, California, September 1986.

[86BE1] Benocci, C., Buchlin, J-M., and Weinacht, P., **Prediction of the air-droplet interaction in the inlet section of a natural draught cooling tower**, Proceedings of the 5th IAHR Cooling Tower Workshop, Monterey, California, September 1986.

[86FU1] Fujita, T. and Tezuka, S., **Calculations on thermal performance of mechanical draft cooling towers**, ASHRAE Transactions No. 2952, pp. 274-287, 986.

[86TU1] Turton, R., and Levenspiel, O., **A short note on the drag correlation for spheres**, Powder Technology, Vol. 47, pp. 83-86, 1986.

[87BE1] Beard, K.V., and Chuang, C., **A new model for the equilibrium shape of raindrops**, Journal of the Atmospheric Sciences, Vol. 44, No. 11, pp. 1509-1524, 1987.

[87BE1] Beukman, J., **Elektroniese evaluasie van die druppel spektrum op bespuite blare** (Electronic evaluation of the drop (size) spectrum on sprayed leaves), B.Eng. project, University of Stellenbosch, Stellenbosch, South Africa, 1987.

[87HO1] Horn, B.K.P., **Robot Vision**, 3rd printing, The MIT Press, Cambridge, Massachusetts, 1987.

[87KA1] Kametani, S., Fujita, T. and Tezuka, S., **Enthalpy-transfer coefficients in mechanical-draft counterflow cooling/heating tower**, Preprint of 17th ICR, Vienna, Austria, 1987.

[87KA1] Kamel, A.H., Akashah, S.A., Leeri, F.A., and Fahim, M.A., **Particle size distribution in oil water dispersions using image processing**, Computers in Chemical Engineering, Vol. 11, pp. 435-439, 1987.

[88CH1] Chandrasekar, V., Cooper, W.A., and Bringi, V.I., **Axis ratios and oscillations of raindrops**, Journal of the Atmospheric Sciences, Vol. 45, pp. 1323-1333, 1988.

[88DR1] Dreyer, A.A., **Analysis of evaporative coolers and condensors**, M.Eng. Thesis, University of Stellenbosch, Stellenbosch, South Africa, 1988

[88GO1] Gösi, P., and Bergmann, G., **Operational experience and further developement of plastic packing**, Proceedings of the International Cooling Tower Conference, Pisa, Italy, October 1988.

[88PO1] Popplewell, L.M., Campanella, O.H., Normand, M.D., and Peleg, M., **Description of normal, log-normal and Rosin-Rammler particle populations by a modified version of the beta distribution function**, Powder Technology, Vol. 54, pp. 119-125, 1988.

[88WE1] Webb, R.L., **A critical evaluation of cooling tower design methodology**, Heat Transfer Equipment Design, Eds. R.K. Shah, E.C. Subbarao and R.F. Mashelkar,

Hemisphere Publishing Corporation, New York, pp. 547-558, 1988.

[88WI1] Winter, R.J., **CEGB research on the effects of fouling of plastic packings on natural draught cooling tower performance**, Proceedings of the International Cooling Tower Conference, Pisa, Italy, October 1988.

[90FA1] Fantini, E., Tognotti, L., and Tonazzini, A, **Drop size distribution in sprays by image processing**, Computers in Chemical Engineering, Vol. 14, No. 11, pp. 1201-1211, 1990.

[90GL1] Glassner, A.S., ed., **Graphics Gems**, Academic Press, New York, 1990.

[90HO1] Hoffmann, J.E., and Kröger, D.G., **Analysis of heat, mass and momentum transfer in the rain zone of a natural draft counterflow cooling tower**, Paper 19-EN-19, Proceedings of the 9th International Heat Transfer Conference, Jerusalem, pp. 227-231, August 1990.

[90JO1] Johnson, B.M. and Bartz, J.A., **Comparative performance characteristic of selected crossflow and counterflow cooling tower fills in an engineering-scale test facilty**, 7th Cooling Tower and Spraying Pond Symposium, Leningrad, 1990.

[90PA1] Rumpf, H., **Particle Technology**, Chapman and Hall, New York, 1990.

[90SC1] Schultz, T. and Erens, P.J., **Measurement of cooling tower fill material performance at low temperatures**, Article to be submitted for publication, University of Stellenbosch, Stellenbosch, South Africa, 1990.

[90YU1] Yu, A.B., and Standish, N., A **study of particle size distributions**, Powder Technology, Vol. 62, pp. 101-118, 1990.

[91FE1] Feltzin, A.E., and Benton D.J., A **more nearly exact representation of cooling tower theory**, Cooling Tower Institute Journal, Vol. 12, No. 2, pp. 8-26, 1991.

[91MA1] Marseille, T.J., Schliesing, J.S., Bell, D.M., and Johnson, B.M., **Extending cooling tower thermal performance prediction using a liquid-side film resistance model**, Heat Transfer Engineering, Vol. 12, No. 3, pp. 19-30, 1991.

[92BR1] Brink, A.D., **Thresholding of digital images using a correlation measure**, Proceedings of the First South African Workshop on Patterns Recognition, pp. 125-127, 1992.

[92GO1] Gonzalez, R.C., and Woods, R.E., **Digital Image Processing**, Addison-Wesley Publishing Company, New York, 1992.

[92NI1] Ninic, N., and Vehauc, A., **The effect of the choice of enthalpy zero point on cooling tower design and packing data processing**, Wärme- und Stoffübertragung, Vol. 27, pp. 305-310, 1992.

[92RE1] Rennie, E.J., and Hay, N, **A 2-D model for natural-draught counter-flow cooling towers**, Proceedings of the 8th Cooling Tower and Spraying Pond Symposium, Karlsruhe, Germany, October 1992.

[92SE1] Sedina, M., **Heat and mass transfer and pressure drop in the rain zone of the cooling towers**, Proceedings of the 8th Cooling Tower and Spraying Pond Symposium, Karlsruhe, Germany, October 1992.

[93CO1] Conradie, C.F.G., **Die verkoelingsvermoë van nat koeltorings en droë/nat stelsels by kragstasies** (The cooling capacity of wet cooling towers and dry/wet

systems at power stations), M.Eng. Thesis, University of Stellenbosch, Stellenbosch, South Africa, 1993.

[93DR1] Dreyer, A.A., **Digital image processing software for the measurement of drop sizes from photographs**, Stellenbosch, South Africa, December 1993.

[93LI1] Lin, C.L., and Miller, J.D., **The developement of a PC, image-based, on-line particle-size analyzer**, Minerals and Metallurgical Processing, pp. 29-35, February 1993.

[93ME1] Mercker, J.H., **Heat and mass transfer from accelerating water drops**, M.Eng. thesis, University of Stellenbosch, Stellenbosch, 1993.

[93YA1] Yamashita, Y., Kuwashima, M., Nonaka, T., and Suzuki, M., **On-line measurement of cell size distribution and concentration of yeast by image processing**, Journal of Chemical Engineering of Japan, Vol. 26, No. 6, pp. 615-619, 1993.

[94BA1] Basson, T., **Die herontwerp van 'n koeltoring-toetsfasiliteit om wandeffekte uit te skakel** (The re-design of a cooling tower test facility in order to eliminate wall effects), B.Eng. project, University of Stellenbosch, Stellenbosch, South Africa, 1994.

[94DR1] Dreyer, A.A., **Modelling of cooling tower splash pack**, PhD.Eng dissertation, University of Stellenbosch, Stellenbosch, South Africa, 1993.

[94DR2] Dreyer, A.A., **Simulation of a natural draft cooling tower**, Stellenbosch, South Africa, 1994.

APPENDIX A

RESULTS OF EXPERIMENTAL STUDY

A.1 RESULTS OF DROP DISTRIBUTION TESTING

Table A.1.1 Drop size distribution for configuration A (no splash grids)

m_w, *kg/s*	9.09	9.09	9.09	9.09	9.04	9.04	9.04	9.04
m_a, *kg/s*	5.34	5.34	5.34	5.34	4.17	4.17	4.17	4.17
d, *mm*	R, -	R, -	R, -	R, -	R, -	R, -	R, -	R, -
0.25	0.0000	0.0000	0.0000	0.0000	0.0000	0.0000	0.0000	0.0000
0.75	0.0044	0.0030	0.0033	0.0019	0.0053	0.0045	0.0039	0.0039
1.25	0.0131	0.0209	0.0102	0.0073	0.0185	0.0144	0.0128	0.0132
1.75	0.0355	0.0494	0.0259	0.0188	0.0431	0.0402	0.0288	0.0291
2.25	0.0530	0.0738	0.0463	0.0267	0.0746	0.0697	0.0478	0.0546
2.75	0.0696	0.1126	0.0596	0.0367	0.1001	0.1136	0.0672	0.0697
3.25	0.0970	0.1410	0.0859	0.0502	0.1211	0.1466	0.0885	0.0900
3.75	0.1197	0.1847	0.1129	0.0686	0.1750	0.1719	0.1147	0.1178
4.25	0.1480	0.2006	0.1276	0.0954	0.2142	0.2383	0.1623	0.1633
4.75	0.2072	0.3043	0.1893	0.1702	0.2909	0.3618	0.2222	0.1916
5.25	0.2783	0.4042	0.2633	0.2208	0.4092	0.3896	0.3120	0.2488
5.75	0.4184	0.4568	0.3362	0.3203	0.6035	0.4991	0.4064	0.3490
6.25	0.4784	0.6254	0.3674	0.3843	0.6534	0.5929	0.4367	0.5098
6.75	0.6295	0.7528	0.4461	0.4648	0.9049	0.7111	0.5512	0.5909
7.25	0.8167	0.8581	0.5922	0.5313	0.9049	0.7843	0.6458	0.6411
7.75	0.9310	0.9224	0.7708	0.6126	1.0000	0.7843	0.7025	0.7637
8.25	1.0000	1.0000	0.9143	0.7106	1.0000	1.0000	0.7036	0.9117
8.75	1.0000	1.0000	1.0000	0.7691	1.0000	1.0000	0.7867	1.0000
9.25	1.0000	1.0000	1.0000	0.8382	1.0000	1.0000	0.8850	1.0000
9.75	1.0000	1.0000	1.0000	1.0000	1.0000	1.0000	1.0000	1.0000

Table A.1.2 Drop size distribution for configuration A (no splash grids)

m_w, *kg/s*	6.70	6.70	6.70	6.70	6.70	6.70	6.70	6.70
m_a, *kg/s*	4.19	4.19	4.19	4.19	5.42	5.42	5.42	5.42
d, *mm*	R, -	R, -	R, -	R, -	R, -	R, -	R, -	R, -
0.25	0.0000	0.0000	0.0000	0.0000	0.0000	0.0000	0.0000	0.0000
0.75	0.0037	0.0031	0.0051	0.0038	0.0056	0.0042	0.0033	0.0039
1.25	0.0118	0.0124	0.0152	0.0101	0.0162	0.0110	0.0147	0.0103
1.75	0.0256	0.0268	0.0325	0.0241	0.0376	0.0322	0.0374	0.0292
2.25	0.0482	0.0449	0.0578	0.0382	0.0617	0.0489	0.0495	0.0423
2.75	0.0668	0.0573	0.0693	0.0582	0.0802	0.0698	0.0789	0.0607
3.25	0.0838	0.0846	0.0820	0.0795	0.0992	0.0884	0.0971	0.0910
3.75	0.0890	0.1003	0.0966	0.1013	0.1168	0.1169	0.1157	0.1236
4.25	0.1194	0.1384	0.1392	0.1382	0.1765	0.1347	0.1564	0.1507
4.75	0.1937	0.2662	0.1392	0.2193	0.2241	0.2092	0.2322	0.2359
5.25	0.2797	0.3525	0.1926	0.2591	0.4170	0.3434	0.3856	0.2615
5.75	0.3551	0.5037	0.2278	0.3637	0.4593	0.4610	0.3856	0.3622
6.25	0.4518	0.5522	0.3180	0.5988	0.5677	0.5742	0.7307	0.4485
6.75	0.5128	0.6744	0.3180	0.7258	0.6361	0.6217	0.7307	0.6115
7.25	0.6638	0.7502	0.4588	0.8306	0.7207	0.6806	1.0000	0.6788
7.75	0.7560	0.8427	0.5449	0.8306	0.8242	0.8965	1.0000	0.7610
8.25	0.8673	0.8427	0.7524	0.9078	0.8242	0.8965	1.0000	0.8602
8.75	1.0000	0.8427	1.0000	1.0000	0.8242	1.0000	1.0000	0.8602
9.25	1.0000	1.0000	1.0000	1.0000	1.0000	1.0000	1 0000	1.0000
9.75	1.0000	1.0000	1.0000	1.0000	1.0000	1.0000	1.0000	1.0000

Table A.1.3 Drop size distribution for configuration A (no [illegible] grids)

m_w, *kg/s*	3.76	3.76	3.76	3.76	3.76	3.76	3.76	3.76
m_a, *kg/s*	5.55	5.55	5.55	5.55	4.22	4.22	4.22	4.22
d, *mm*	**R, -**	**R, -**	**R, -**	**R, -**	**R, -**	**R, -**	**R, -**	**R, -**
0.25	0.0000	0.0000	0.0001	0.0000	0.0000	0.0000	0.0000	0.0000
0.75	0.0032	0.0050	0.0085	0.0045	0.0047	0.0051	0.0066	0.0050
1.25	0.0105	0.0116	0.0194	0.0109	0.0107	0.0122	0.0140	0.0120
1.75	0.0242	0.0300	0.0447	0.0310	0.0259	0.0232	0.0318	0.0238
2.25	0.0376	0.0409	0.0626	0.0440	0.0390	0.0375	0.0583	0.0418
2.75	0.0519	0.0637	0.0905	0.0644	0.0524	0.0517	0.0687	0.0527
3.25	0.0638	0.0731	0.1290	0.0812	0.0701	0.0634	0.1086	0.0563
3.75	0.0929	0.1093	0.1409	0.1070	0.1040	0.0755	0.1612	0.0729
4.25	0.1354	0.1934	0.1925	0.1446	0.1336	0.0929	0.1994	0.0972
4.75	0.1724	0.2522	0.2406	0.1795	0.1887	0.2394	0.2706	0.1535
5.25	0.2924	0.3315	0.4353	0.3684	0.3003	0.3713	0.3187	0.2144
5.75	0.3449	0.3315	0.6911	0.4305	0.3003	0.5012	0.5082	0.2543
6.25	0.4799	0.3315	0.6911	0.5898	0.3630	0.5568	0.5082	0.5624
6.75	0.5224	0.4158	0.8291	0.5898	0.4421	0.6269	0.6104	0.6271
7.25	0.5750	0.4158	1.0000	0.5898	0.7360	0.7137	0.7370	0.7072
7.75	0.7037	0.4158	1.0000	0.7417	0.8556	0.8197	0.7370	0.8051
8.25	0.7813	0.4158	1.0000	0.7417	1.0000	0.8197	0.7370	0.8051
8.75	0.7813	0.7831	1.0000	0.7417	1.0000	0.8197	0.7370	0.8051
9.25	1.0000	1.0000	1.0000	1.0000	1.0000	1.0000	1.0000	0.8051
9.75	1.0000	1.0000	1.0000	1.0000	1.0000	1.0000	1.0000	1.0000

Table A.1.4 Drop size distribution for configuration B1 (z = 0.37 *m*)

m_w, *kg/s*	9.18	9.18	9.18	9.18	9.15	9.15	9.15	9.15
m_a, *kg/s*	5.55	5.55	5.55	5.55	4.25	4.25	4.25	4.25
d, *mm*	**R, -**	**R, -**	**R, -**	**R, -**	**R, -**	**R, -**	**R, -**	**R, -**
0.25	0.0000	0.0000	0.0001	0.0000	0.0000	0.0001	0.0000	0.0000
0.75	0.0053	0.0054	0.0066	0.0042	0.0039	0.0074	0.0057	0.0058
1.25	0.0201	0.0208	0.0215	0.0178	0.0180	0.0274	0.0190	0.0232
1.75	0.0624	0.0562	0.0670	0.0515	0.0547	0.0766	0.0531	0.0645
2.25	0.1043	0.0982	0.0991	0.0827	0.0857	0.1207	0.0973	0.1084
2.75	0.1412	0.1444	0.1310	0.1073	0.1237	0.1633	0.1297	0.1473
3.25	0.1818	0.1886	0.1698	0.1349	0.1587	0.2127	0.1456	0.1775
3.75	0.2095	0.2164	0.2124	0.1705	0.1834	0.2807	0.1822	0.2297
4.25	0.2549	0.2792	0.2558	0.1867	0.2324	0.3040	0.2177	0.2761
4.75	0.3887	0.3482	0.3509	0.2727	0.2825	0.4341	0.2425	0.3705
5.25	0.5218	0.4329	0.4444	0.3338	0.3809	0.6097	0.2928	0.4023
5.75	0.6218	0.5663	0.5671	0.3820	0.4617	0.7251	0.3807	0.4860
6.25	0.6538	0.6806	0.7248	0.4439	0.5240	0.7992	0.5502	0.5666
6.75	0.7347	0.7525	0.7248	0.5737	0.5763	0.7992	0.6569	0.6004
7.25	0.8348	0.8417	0.9094	0.6703	0.7059	0.9148	0.7010	0.7262
7.75	0.8960	0.8417	0.9094	0.6703	0.8642	0.9148	0.7010	0.7774
8.25	0.8960	0.9074	1.0000	0.7651	0.8642	1.0000	0.8309	0.8392
8.75	0.8960	0.9074	1.0000	0.7651	0.9212	1.0000	0.9084	0.9129
9.25	1.0000	1.0000	1.0000	0.7651	0.9212	1.0000	1.0000	1.0000
9.75	1.0000	1.0000	1.0000	1.0000	1.0000	1.0000	1.0000	1.0000

Table A.1.5 Drop size distribution for configuration B1 (z = 0.37 *m*)

m_w, *kg/s*	6.32	6.32	6.32	6.32	6.32	6.32	6.32	6.32
m_a, *kg/s*	4.28	4.28	4.28	4.28	5.55	5.55	5.55	5.55
d, *mm*	R, -	R, -	R, -	R, -	R, -	R, -	R, -	R, -
0.25	0.0000	0.0000	0.0001	0.0000	0.0001	0.0000	0.0000	0.0000
0.75	0.0045	0.0069	0.0084	0.0061	0.0083	0.0065	0.0072	0.0062
1.25	0.0164	0.0237	0.0282	0.0187	0.0278	0.0209	0.0251	0.0222
1.75	0.0432	0.0610	0.0664	0.0519	0.0686	0.0591	0.0709	0.0586
2.25	0.0672	0.0897	0.1080	0.0818	0.1060	0.0936	0.1068	0.0905
2.75	0.0949	0.1204	0.1592	0.1066	0.1401	0.1299	0.1452	0.1299
3.25	0.1097	0.1352	0.1874	0.1312	0.1786	0.1585	0.1954	0.1659
3.75	0.1323	0.1676	0.2500	0.1564	0.2297	0.1865	0.2198	0.1807
4.25	0.1763	0.2102	0.3061	0.2296	0.2870	0.2389	0.2671	0.2130
4.75	0.1967	0.2431	0.3257	0.3447	0.3590	0.3364	0.3001	0.2956
5.25	0.2520	0.2965	0.4578	0.4828	0.4454	0.4022	0.4115	0.3766
5.75	0.3427	0.3667	0.4925	0.5735	0.5873	0.5176	0.4700	0.4299
6.25	0.3660	0.3968	0.5371	0.5735	0.5873	0.5916	0.6203	0.5667
6.75	0.5420	0.6617	0.7056	0.7203	0.8168	0.6849	0.6677	0.6960
7.25	0.5420	0.6617	0.7751	0.8112	0.9305	0.7427	0.7859	0.8561
7.75	0.6753	0.8335	0.7751	0.8112	1.0000	0.8133	1.0000	0.9213
8.25	0.8360	0.9026	0.8777	0.8112	1.0000	0.8984	1.0000	1.0000
8.75	0.8360	0.9026	1.0000	0.8112	1.0000	1.0000	1.0000	1.0000
9.25	0.9116	1.0000	1.0000	1.0000	1.0000	1.0000	1.0000	1.0000
9.75	1.0000	1.0000	1.0000	1.0000	1.0000	1.0000	1.0000	1.0000

Table A.1.6 Drop size distribution for configuration B1 (z = 0.37 *m*)

m_w, *kg/s*	4.10	4.10	4.10	4.10	4.09	4.09	4.09	4.09
m_a, *kg/s*	5.47	5.47	5.47	5.47	4.22	4.22	4.22	4.22
d, *mm*	R, -	R, -	R, -	R, -	R, -	R, -	R, -	R, -
0.25	0.0000	0.0001	0.0001	0.0001	0.0000	0.0000	0.0000	0.0000
0.75	0.0075	0.0091	0.0065	0.0088	0.0109	0.0060	0.0056	0.0077
1.25	0.0249	0.0294	0.0205	0.0303	0.0285	0.0139	0.0141	0.0227
1.75	0.0597	0.0753	0.0523	0.0785	0.0726	0.0374	0.0507	0.0572
2.25	0.0886	0.1143	0.0769	0.1226	0.1149	0.0496	0.0761	0.0821
2.75	0.1086	0.1416	0.0926	0.1486	0.1508	0.0659	0.1051	0.1048
3.25	0.1297	0.1623	0.1152	0.2000	0.1918	0.0860	0.1194	0.1299
3.75	0.1759	0.2048	0.1251	0.2264	0.2338	0.1117	0.1635	0.1683
4.25	0.2297	0.2513	0.1468	0.2647	0.2745	0.1192	0.2063	0.2336
4.75	0.2766	0.2945	0.1670	0.3585	0.3314	0.1715	0.2661	0.3508
5.25	0.4288	0.3528	0.3304	0.5031	0.4466	0.3127	0.3064	0.4211
5.75	0.6286	0.4295	0.4020	0.5981	0.5475	0.3498	0.4124	0.5135
6.25	0.7142	0.4787	0.4020	0.5981	0.5475	0.3498	0.5485	0.5728
6.75	0.7681	0.5407	0.4599	0.5981	0.5475	0.4699	0.6342	0.7222
7.25	0.9016	0.7711	0.5316	0.8837	0.8510	0.6186	0.7405	1.0000
7.75	0.9016	0.8650	0.6192	1.0000	0.8510	0.7095	1.0000	1.0000
8.25	1.0000	0.8650	0.7249	1.0000	1.0000	0.8191	1.0000	1.0000
8.75	1.0000	1.0000	0.8510	1.0000	1.0000	0.8191	1.0000	1.0000
9.25	1.0000	1.0000	1.0000	1.0000	1.0000	0.8191	1.0000	1.0000
9.75	1.0000	1.0000	1.0000	1.0000	1.0000	1.0000	1.0000	1.0000

Table A.1.7 Drop size distribution for configuration B2 (z = 0.47 *m*)

m_w, *kg/s*	9.05	9.05	9.05	9.05	9.05	9.05	9.05	9.05
m_a, *kg/s*	5.47	5.47	5.47	5.47	4.09	4.09	4.09	4.09
d, *mm*	R, -	R, -	R, -	R, -	R, -	R, -	R, -	R, -
0.25	0.0001	0.0000	0.0000	0.0001	0.0001	0.0000	0.0000	0.0000
0.75	0.0062	0.0055	0.0059	0.0071	0.0069	0.0049	0.0076	0.0060
1.25	0.0248	0.0208	0.0221	0.0306	0.0224	0.0177	0.0308	0.0203
1.75	0.0695	0.0645	0.0673	0.0838	0.0693	0.0559	0.0781	0.0601
2.25	0.1216	0.1085	0.1107	0.1363	0.1157	0.0867	0.1214	0.1039
2.75	0.1656	0.1457	0.1543	0.2019	0.1581	0.1187	0.1697	0.1371
3.25	0.2172	0.1772	0.1922	0.2547	0.2070	0.1357	0.2070	0.1635
3.75	0.2748	0.2052	0.2213	0.2912	0.2428	0.1619	0.2397	0.1867
4.25	0.3378	0.2533	0.2637	0.3561	0.2636	0.1757	0.3111	0.2416
4.75	0.4256	0.3361	0.3997	0.4303	0.3655	0.2966	0.4024	0.2711
5.25	0.4849	0.4758	0.4795	0.4748	0.4637	0.4533	0.4922	0.3029
5.75	0.5888	0.6043	0.5215	0.5917	0.6444	0.5219	0.5216	0.3866
6.25	0.6221	0.6750	0.5754	0.6292	0.7106	0.6321	0.7865	0.4403
6.75	0.6641	0.7641	0.6093	0.6765	0.7941	0.6876	0.8819	0.6771
7.25	0.7682	0.8009	0.6514	0.7351	0.8459	0.7907	1.0000	0.8028
7.75	0.8318	0.8458	0.7028	0.8783	0.9091	0.8327	1.0000	0.8028
8.25	0.9085	0.8458	0.7648	0.8783	0.9091	0.8327	1.0000	0.9263
8.75	1.0000	0.9105	0.9126	0.8783	1.0000	0.8327	1.0000	1.0000
9.25	1.0000	0.9105	1.0000	1.0000	1.0000	0.8327	1.0000	1.0000
9.75	1.0000	1.0000	1.0000	1.0000	1.0000	1.0000	1.0000	1.0000

Table A.1.8 Drop size distribution for configuration B2 (z = 0.47 *m*)

m_w, *kg/s*	6.58	6.58	6.58	6.58	6.58	6.58	6.58	6.58
m_a, *kg/s*	4.11	4.11	4.11	4.11	5.50	5.50	5.50	5.50
d, *mm*	R, -	R, -	R, -	R, -	R, -	R, -	R, -	R, -
0.25	0.0001	0.0001	0.0001	0.0001	0.0001	0.0000	0.0000	0.0001
0.75	0.0111	0.0075	0.0111	0.0131	0.0099	0.0057	0.0062	0.0110
1.25	0.0380	0.0257	0.0334	0.0459	0.0425	0.0188	0.0267	0.0436
1.75	0.0876	0.0708	0.0856	0.1234	0.1148	0.0525	0.0757	0.1027
2.25	0.1374	0.1071	0.1393	0.1902	0.1769	0.0764	0.1090	0.1577
2.75	0.1871	0.1411	0.1734	0.2416	0.2182	0.1037	0.1441	0.2145
3.25	0.2264	0.1635	0.2073	0.2908	0.2931	0.1262	0.1784	0.2650
3.75	0.2868	0.2066	0.2362	0.3458	0.3350	0.1469	0.1946	0.3038
4.25	0.3267	0.2506	0.3034	0.3858	0.3807	0.2174	0.2476	0.3521
4.75	0.3825	0.2944	0.3621	0.4835	0.5083	0.2806	0.3217	0.3747
5.25	0.4427	0.4600	0.4573	0.5589	0.5657	0.3376	0.4106	0.4659
5.75	0.5614	0.6775	0.5406	0.7570	0.6411	0.3625	0.4690	0.5857
6.25	0.6630	0.8371	0.6475	0.8206	0.6896	0.4265	0.5065	0.6882
6.75	0.7270	0.9377	0.6475	0.9007	0.7506	0.5475	0.5065	0.8820
7.25	0.8063	1.0000	0.8980	1.0000	0.7506	0.7473	0.5650	0.8820
7.75	1.0000	1.0000	1.0000	1.0000	0.8430	0.8084	0.7080	0.8820
8.25	1.0000	1.0000	1.0000	1.0000	0.8430	0.8084	0.7942	1.0000
8.75	1.0000	1.0000	1.0000	1.0000	0.8430	0.8962	1.0000	1.0000
9.25	1.0000	1.0000	1.0000	1.0000	1.0000	1.0000	1.0000	1.0000
9.75	1.0000	1.0000	1.0000	1.0000	1.0000	1.0000	1.0000	1.0000

Table A.1.9 Drop size distribution for configuration B2 (z = 0.47 *m*)

m_w, *kg/s*	4.12	4.12	4.12	4.12	4.15	4.15	4.15	4.15
m_a, *kg/s*	5.50	5.50	5.50	5.50	4.11	4.11	4.11	4.11
d, *mm*	**R**, -	**R**, -	**R**, -	**R**, -	**R**, -	**R**, -	**R**, -	**R**, -
0.25	0.0001	0.0001	0.0001	0.0001	0.0001	0.0000	0.0001	0.0000
0.75	0.0083	0.0142	0.0117	0.0103	0.0142	0.0089	0.0144	0.0082
1.25	0.0262	0.0492	0.0385	0.0394	0.0483	0.0348	0.0461	0.0245
1.75	0.0610	0.1183	0.1003	0.0873	0.1157	0.0771	0.1227	0.0674
2.25	0.0885	0.1722	0.1510	0.1340	0.1711	0.1167	0.1716	0.0942
2.75	0.1202	0.2020	0.1919	0.1649	0.2217	0.1332	0.2179	0.1231
3.25	0.1377	0.2315	0.2324	0.2033	0.2511	0.1630	0.2343	0.1414
3.75	0.1712	0.2693	0.2738	0.2425	0.3039	0.2088	0.2678	0.1752
4.25	0.2005	0.3133	0.3241	0.3092	0.3588	0.2270	0.2800	0.1916
4.75	0.2277	0.3747	0.3802	0.4688	0.4354	0.3032	0.4334	0.2946
5.25	0.3381	0.3747	0.4560	0.5766	0.5182	0.3946	0.6634	0.3873
5.75	0.4348	0.4836	0.5058	0.5766	0.5725	0.4847	0.8447	0.4279
6.25	0.5590	0.5536	0.6977	0.6372	0.7820	0.6390	1.0000	0.4800
6.75	0.5590	0.7299	0.7782	0.7899	0.7820	0.6876	1.0000	0.4800
7.25	0.6559	0.8391	0.8781	0.8845	1.0000	0.7478	1.0000	0.5614
7.75	0.6559	0.8391	1.0000	1.0000	1.0000	0.7478	1.0000	0.7602
8.25	0.7987	1.0000	1.0000	1.0000	1.0000	0.7478	1.0000	1.0000
8.75	0.7987	1.0000	1.0000	1.0000	1.0000	0.8536	1.0000	1.0000
9.25	1.0000	1.0000	1.0000	1.0000	1.0000	0.8536	1.0000	1.0000
9.75	1.0000	1.0000	1.0000	1.0000	1.0000	1.0000	1.0000	1.0000

Table A.1.10 Drop size distribution for configuration B3 (z = 0.57 *m*)

m_w, *kg/s*	9.03	9.03	9.03	9.03	9.04	9.04	9.04	9.04
m_a, *kg/s*	5.45	5.45	5.45	5.45	4.14	4.14	4.14	4.14
d, *mm*	**R**, -	**R**, -	**R**, -	**R**, -	**R**, -	**R**, -	**R**, -	**R**, -
0.25	0.0001	0.0000	0.0001	0.0001	0.0001	0.0001	0.0001	0.0001
0.75	0.0093	0.0065	0.0079	0.0083	0.0077	0.0084	0.0078	0.0107
1.25	0.0360	0.0232	0.0274	0.0263	0.0266	0.0308	0.0238	0.0347
1.75	0.1031	0.0604	0.0787	0.0849	0.0732	0.0772	0.0671	0.1001
2.25	0.1749	0.0989	0.1301	0.1333	0.1176	0.1225	0.1055	0.1572
2.75	0.2339	0.1335	0.1694	0.1892	0.1404	0.1623	0.1497	0.2070
3.25	0.2916	0.1610	0.2203	0.2279	0.1945	0.2095	0.1799	0.2536
3.75	0.3193	0.2094	0.2629	0.2874	0.2414	0.2539	0.2224	0.3196
4.25	0.4080	0.2490	0.3198	0.2940	0.2782	0.3303	0.2562	0.3997
4.75	0.5432	0.3165	0.3848	0.4428	0.3295	0.4204	0.3505	0.5226
5.25	0.6040	0.4160	0.4433	0.5683	0.3890	0.5754	0.3929	0.7037
5.75	0.7239	0.5032	0.4946	0.6343	0.5191	0.6045	0.4766	0.7831
6.25	0.7752	0.5592	0.6262	0.7190	0.5860	0.6792	0.6198	0.9358
6.75	0.8398	0.7354	0.7091	0.7724	0.6281	0.7263	0.7100	1.0000
7.25	1.0000	0.7791	0.8118	0.8385	0.7325	0.8429	0.7658	1.0000
7.75	1.0000	0.8325	1.0000	1.0000	0.7962	0.9141	0.7658	1.0000
8.25	1.0000	0.8325	1.0000	1.0000	0.8731	1.0000	0.7658	1.0000
8.75	1.0000	0.9093	1.0000	1.0000	0.8731	1.0000	0.8641	1.0000
9.25	1.0000	1.0000	1.0000	1.0000	0.8731	1.0000	0.8641	1.0000
9.75	1.0000	1.0000	1.0000	1.0000	1.0000	1.0000	1.0000	1.0000

Table A.1.11 Drop size distribution for configuration B3 (z = 0.57 *m*)

m_w, *kg/s*	6.57	6.57	6.57	6.57	6.55	6.55	6.55	6.55
m_a, *kg/s*	4.17	4.17	4.17	4.17	5.47	5.47	5.47	5.47
d, *mm*	R, -	R, -	R, -	R, -	R, -	R, -	R, -	R, -
0.25	0.0001	0.0001	0.0000	0.0001	0.0001	0.0001	0.0001	0.0001
0.75	0.0125	0.0113	0.0111	0.0074	0.0106	0.0162	0.0127	0.0146
1.25	0.0378	0.0373	0.0328	0.0218	0.0448	0.0610	0.0525	0.0521
1.75	0.0935	0.0897	0.0770	0.0536	0.1189	0.1694	0.1450	0.1442
2.25	0.1533	0.1447	0.1216	0.0878	0.1903	0.2644	0.2258	0.2219
2.75	0.1956	0.1908	0.1414	0.1080	0.2419	0.3345	0.2977	0.3034
3.25	0.2324	0.2310	0.1777	0.1480	0.2906	0.3895	0.3569	0.3381
3.75	0.2775	0.2723	0.2112	0.1838	0.3031	0.4403	0.4379	0.3780
4.25	0.3104	0.3224	0.2518	0.2285	0.3666	0.5019	0.5115	0.4265
4.75	0.3678	0.4202	0.3539	0.2805	0.4300	0.6910	0.6143	0.4807
5.25	0.5848	0.4957	0.5070	0.4208	0.5326	0.6910	0.7808	0.5904
5.75	0.6663	0.5948	0.5874	0.4946	0.6674	0.7520	0.8538	0.6384
6.25	0.7709	0.5948	0.6907	0.6367	0.6674	0.7520	0.8538	0.7618
6.75	0.8367	0.5948	0.8209	0.7561	0.8129	0.8507	0.8538	0.7618
7.25	1.0000	0.7936	0.9015	0.7561	0.8129	0.8507	1.0000	0.8581
7.75	1.0000	0.7936	1.0000	0.8464	0.8129	1.0000	1.0000	0.8581
8.25	1.0000	0.7936	1.0000	0.8464	0.8129	1.0000	1.0000	1.0000
8.75	1.0000	0.7936	1.0000	0.8464	0.8129	1.0000	1.0000	1.0000
9.25	1.0000	1.0000	1.0000	1.0000	1.0000	1.0000	1.0000	1.0000
9.75	1.0000	1.0000	1.0000	1.0000	1.0000	1.0000	1.0000	1.0000

Table A.1.12 Drop size distribution for configuration B3 (z = 0.57 *m*)

m_w, *kg/s*	4.10	4.10	4.10	4.10	4.10	4.10	4.10	4.10
m_a, *kg/s*	5.47	5.47	5.47	5.47	4.11	4.11	4.11	4.11
d, *mm*	R, -	R, -	R, -	R, -	R, -	R, -	R, -	R, -
0.25	0.0001	0.0001	0.0001	0.0002	0.0001	0.0001	0.0001	0.0001
0.75	0.0139	0.0148	0.0133	0.0237	0.0175	0.0186	0.0178	0.0163
1.25	0.0360	0.0483	0.0318	0.0703	0.0480	0.0557	0.0642	0.0437
1.75	0.0897	0.1191	0.0728	0.1629	0.1247	0.1411	0.1431	0.1122
2.25	0.1283	0.1613	0.1174	0.2580	0.1950	0.1985	0.2057	0.1682
2.75	0.1605	0.1902	0.1580	0.3262	0.2626	0.2683	0.2465	0.2213
3.25	0.1945	0.2698	0.2139	0.3671	0.2961	0.2972	0.2937	0.2651
3.75	0.2466	0.3187	0.2483	0.4457	0.3475	0.3149	0.3558	0.3325
4.25	0.2899	0.3721	0.3608	0.5143	0.3850	0.3922	0.4161	0.3745
4.75	0.3655	0.4714	0.4481	0.5143	0.4721	0.4822	0.4582	0.5113
5.25	0.4472	0.5385	0.5896	0.6006	0.5191	0.5308	0.5718	0.7224
5.75	0.6082	0.6266	0.6515	0.6006	0.6427	0.6584	0.5718	0.8610
6.25	0.6082	0.7397	0.6515	0.6006	0.6427	0.7404	0.6676	0.8610
6.75	0.8686	0.7397	0.7517	0.6006	0.7427	0.8437	0.6676	0.8610
7.25	0.8686	0.7397	1.0000	0.6006	0.7427	0.8437	0.8172	1.0000
7.75	1.0000	0.7397	1.0000	0.6006	0.7427	1.0000	1.0000	1.0000
8.25	1.0000	1.0000	1.0000	0.6006	0.7427	1.0000	1.0000	1.0000
8.75	1.0000	1.0000	1.0000	1.0000	0.7427	1.0000	1.0000	1.0000
9.25	1.0000	1.0000	1.0000	1.0000	1.0000	1.0000	1.0000	1.0000
9.75	1.0000	1.0000	1.0000	1.0000	1.0000	1.0000	1.0000	1.0000

Table A.1.13 Drop size distribution for configuration B4 (z = 0.67 *m*)

m_w, *kg/s*	9.20	9.20	9.20	9.20	9.20	9.20	9.20	9.20
m_a, *kg/s*	5.45	5.45	5.45	5.45	4.09	4.09	4.09	4.09
d, *mm*	R_i -	R_i -	R_i -	R_i -	R_i -	R_i -	R_i -	R_i -
0.25	0.0001	0.0001	0.0001	0.0001	0.0001	0.0001	0.0001	0.0001
0.75	0.0080	0.0101	0.0086	0.0077	0.0078	0.0102	0.0079	0.0098
1.25	0.0283	0.0362	0.0357	0.0278	0.0305	0.0361	0.0291	0.0362
1.75	0.0834	0.0915	0.0944	0.0932	0.0875	0.0958	0.0934	0.1046
2.25	0.1403	0.1555	0.1643	0.1631	0.1344	0.1441	0.1541	0.1701
2.75	0.1953	0.2015	0.2168	0.2201	0.1809	0.1958	0.2077	0.2329
3.25	0.2281	0.2427	0.2573	0.2688	0.2208	0.2369	0.2413	0.2797
3.75	0.2668	0.2961	0.3150	0.3286	0.2585	0.2855	0.2600	0.3003
4.25	0.2894	0.3598	0.3796	0.3649	0.3203	0.2996	0.3078	0.3302
4.75	0.3760	0.4092	0.5058	0.4358	0.3682	0.4082	0.4411	0.4242
5.25	0.4823	0.4626	0.6276	0.6272	0.4717	0.4615	0.5183	0.5088
5.75	0.5940	0.5326	0.7236	0.6272	0.6077	0.5315	0.5521	0.5829
6.25	0.6299	0.6226	0.8058	0.7195	0.7386	0.5315	0.5955	0.7256
6.75	0.7654	0.7360	0.8575	0.8939	0.8486	0.5315	0.7595	0.7256
7.25	0.7654	0.8765	0.9217	0.8939	0.9168	0.6017	0.7595	0.7999
7.75	0.7654	0.8765	1.0000	0.8939	1.0000	0.7732	0.7595	0.8906
8.25	0.7654	0.8765	1.0000	1.0000	1.0000	0.8766	0.8593	1.0000
8.75	0.8638	1.0000	1.0000	1.0000	1.0000	1.0000	0.8593	1.0000
9.25	0.8638	1.0000	1.0000	1.0000	1.0000	1.0000	1.0000	1.0000
9.75	1.0000	1.0000	1.0000	1.0000	1.0000	1.0000	1.0000	1.0000

Table A.1.14 Drop size distribution for configuration B4 (z = 0.67 *m*)

m_w, *kg/s*	6.55	6.55	6.55	6.55	6.52	6.52	6.52	6.52
m_a, *kg/s*	4.14	4.14	4.14	4.14	5.45	5.45	5.45	5.45
d, *mm*	R_i -	R_i -	R_i -	R_i -	R_i -	R_i -	R_i -	R_i -
0.25	0.0001	0.0001	0.0000	0.0001	0.0001	0.0001	0.0001	0.0001
0.75	0.0065	0.0097	0.0116	0.0088	0.0088	0.0118	0.0101	0.0128
1.25	0.0217	0.0301	0.0370	0.0263	0.0260	0.0359	0.0360	0.0465
1.75	0.0581	0.0800	0.0963	0.0754	0.0774	0.0923	0.0945	0.1123
2.25	0.0954	0.1252	0.1413	0.1225	0.1235	0.1390	0.1603	0.1859
2.75	0.1337	0.1726	0.1851	0.1552	0.1575	0.1925	0.2023	0.2439
3.25	0.1639	0.2032	0.2483	0.1958	0.1977	0.2407	0.2527	0.3134
3.75	0.1892	0.2555	0.2969	0.2373	0.2305	0.3148	0.2817	0.3869
4.25	0.2567	0.2783	0.3474	0.2675	0.2544	0.3417	0.3028	0.4744
4.75	0.3595	0.3739	0.4180	0.3097	0.3296	0.4045	0.3716	0.6238
5.25	0.4521	0.4600	0.5703	0.3097	0.3972	0.6754	0.4247	0.6971
5.75	0.5129	0.5354	0.6204	0.4968	0.6342	0.7644	0.5642	0.8416
6.25	0.5909	0.5838	0.8775	0.6410	0.7483	0.8216	0.6090	0.9035
6.75	0.6401	0.8887	0.8775	0.7015	0.7962	0.8216	0.7218	0.9035
7.25	0.7620	0.8887	0.8775	0.7765	0.8556	1.0000	0.7917	1.0000
7.75	0.7620	0.8887	1.0000	0.8681	0.8556	1.0000	0.8771	1.0000
8.25	0.8518	1.0000	1.0000	0.8681	0.8556	1.0000	0.8771	1.0000
.75	0.8518	1.0000	1.0000	1.0000	0.8556	1.0000	1.0000	1.0000
9.25	0.8518	1.0000	1.0000	1.0000	0.8556	1.0000	1.0000	1.0000
9.75	1.0000	1.0000	1.0000	1.0000	1.0000	1.0000	1.0000	1.0000

Table A.1.15 Drop size distribution for configuration B4 (z = 0.67 *m*)

m_w, *kg/s*	4.05	4.05	4.05	4.05	4.05	4.05	4.05	4.05
m_a, *kg/s*	5.47	5.47	5.47	5.47	4.17	4.17	4.17	4.17
d, *mm*	**R**, -	**R**, -	**R**, -	**R**, -	**R**, -	**R**, -	**R**, -	**R**, -
0.25	0.0001	0.0001	0.0001	0.0001	0.0001	0.0001	0.0001	0.0001
0.75	0.0132	0.0097	0.0139	0.0119	0.0113	0.0082	0.0125	0.0139
1.25	0.0338	0.0266	0.0410	0.0338	0.0320	0.0265	0.0312	0.0376
1.75	0.0814	0.0645	0.1163	0.1023	0.0855	0.0642	0.0934	0.0872
2.25	0.1203	0.1016	0.1715	0.1586	0.1285	0.1016	0.1488	0.1341
2.75	0.1573	0.1366	0.2219	0.2161	0.1539	0.1257	0.1945	0.1941
3.25	0.1808	0.1790	0.2718	0.2510	0.1999	0.1422	0.2430	0.2153
3.75	0.2168	0.2027	0.3144	0.2816	0.2384	0.1626	0.2678	0.2587
4.25	0.2588	0.2285	0.4012	0.3374	0.2758	0.1848	0.3160	0.3061
4.75	0.3614	0.3368	0.4358	0.4465	0.3280	0.2365	0.4673	0.5046
5.25	0.4406	0.5318	0.5761	0.5727	0.4689	0.2645	0.5127	0.5642
5.75	0.6485	0.7025	0.8218	0.7937	0.7467	0.3745	0.6320	0.7990
6.25	0.6485	0.7574	0.9006	0.8647	0.9251	0.4217	0.6320	1.0000
6.75	0.8168	0.8955	1.0000	0.8647	1.0000	0.4810	0.6320	1.0000
7.25	0.8168	0.8955	1.0000	0.8647	1.0000	0.6281	0.7516	1.0000
7.75	0.8168	1.0000	1.0000	1.0000	1.0000	0.7179	0.7516	1.0000
8.25	0.8168	1.0000	1.0000	1.0000	1.0000	0.7179	0.7516	1.0000
8.75	1.0000	1.0000	1.0000	1.0000	1.0000	0.8472	0.7516	1.0000
9.25	1.0000	1.0000	1.0000	1.0000	1.0000	1.0000	1.0000	1.0000
9.75	1.0000	1.0000	1.0000	1.0000	1.0000	1.0000	1.0000	1.0000

Table A.1.16 Drop size distribution for configuration B5 (z = 0.77 *m*)

m_w, *kg/s*	9.00	9.00	9.00	9.00	9.00	9.00	9.00	9.00
m_a, *kg/s*	5.45	5.45	5.45	5.45	4.19	4.19	4.19	4.19
d, *mm*	**R**, -	**R**, -	**R**, -	**R**, -	**R**, -	**R**, -	**R**, -	**R**, -
0.25	0.0001	0.0001	0.0001	0.0001	0.0001	0.0001	0.0001	0.0001
0.75	0.0073	0.0084	0.0081	0.0064	0.0063	0.0138	0.0085	0.0074
1.25	0.0250	0.0333	0.0322	0.0242	0.0234	0.0514	0.0300	0.0274
1.75	0.0743	0.0855	0.0876	0.0648	0.0616	0.1246	0.0824	0.0730
2.25	0.1183	0.1426	0.1427	0.1035	0.0970	0.1991	0.1278	0.1128
2.75	0.1562	0.1900	0.1843	0.1313	0.1244	0.2671	0.1710	0.1522
3.25	0.1996	0.2275	0.2301	0.1733	0.1531	0.3020	0.2007	0.1835
3.75	0.2403	0.2659	0.2652	0.2027	0.1942	0.3138	0.2372	0.2235
4.25	0.2511	0.3009	0.3100	0.2454	0.2171	0.3658	0.2705	0.2410
4.75	0.3188	0.4082	0.4172	0.3170	0.2749	0.5592	0.3354	0.3305
5.25	0.3595	0.5400	0.4414	0.3975	0.3268	0.6897	0.3855	0.4404
5.75	0.4929	0.5747	0.5681	0.4398	0.3723	0.8613	0.5830	0.6135
6.25	0.4929	0.6636	0.6495	0.4942	0.4016	0.8613	0.6676	0.8359
6.75	0.6225	0.7757	0.6495	0.5284	0.5120	1.0000	0.7208	0.9293
7.25	0.7295	0.7757	0.7766	0.6557	0.6032	1.0000	0.7868	0.9293
7.75	0.7948	0.7757	0.7766	0.8629	0.6032	1.0000	0.7868	1.0000
8.25	0.7948	0.8780	0.7766	0.9254	0.6032	1.0000	0.8840	1.0000
8.75	0.8889	1.0000	1.0000	1.0000	0.6834	1.0000	1.0000	1.0000
9.25	1.0000	1.0000	1.0000	1.0000	0.7781	1.0000	1.0000	1.0000
9.75	1.0000	1.0000	1.0000	1.0000	1.0000	1.0000	1.0000	1.0000

Table A.1.17 Drop size distribution for configuration B5 (z = 0.77 *m*)

m_w, *kg/s*	6.41	6.41	6.41	6.41	6.42	6.42	6.42	6.42
m_a, *kg/s*	4.19	4.19	4.19	4.19	5.58	5.58	5.58	5.58
d, *mm*	R, -	R, -	R, -	R, -	R, -	R, -	R, -	R, -
0.25	0.0001	0.0001	0.0001	0.0001	0.0000	0.0001	0.0001	0.0001
0.75	0.0088	0.0098	0.0083	0.0094	0.0061	0.0099	0.0120	0.0141
1.25	0.0272	0.0326	0.0261	0.0297	0.0210	0.0328	0.0379	0.0466
1.75	0.0765	0.0745	0.0659	0.0786	0.0590	0.0877	0.1083	0.1271
2.25	0.1256	0.1194	0.0998	0.1289	0.0999	0.1398	0.1830	0.2043
2.75	0.1506	0.1491	0.1300	0.1574	0.1338	0.1732	0.2216	0.2655
3.25	0.1835	0.1952	0.1632	0.1743	0.1478	0.2241	0.2853	0.3211
3.75	0.2004	0.2395	0.1973	0.2001	0.1650	0.2566	0.3304	0.3677
4.25	0.2249	0.2782	0.2468	0.2077	0.2025	0.2946	0.3852	0.4130
4.75	0.2677	0.3772	0.2540	0.2497	0.2986	0.3607	0.4463	0.5550
5.25	0.3834	0.4501	0.3340	0.3065	0.3222	0.4680	0.5289	0.7255
5.75	0.5049	0.5459	0.3953	0.4556	0.3841	0.5619	0.6917	0.8375
6.25	0.5049	0.6279	0.5528	0.5035	0.4239	0.6825	0.6917	0.9094
6.75	0.5049	0.7312	0.5528	0.6845	0.4741	0.8345	0.8672	1.0000
7.25	0.6877	0.7312	0.6143	0.9087	0.5362	0.8345	0.8672	1.0000
7.75	0.7621	0.8875	0.7644	1.0000	0.6879	0.8345	1.0000	1.0000
8.25	0.8518	0.8875	0.7644	1.0000	0.8710	0.8345	1.0000	1.0000
8.75	0.8518	1.0000	0.8724	1.0000	0.8710	1.0000	1.0000	1.0000
9.25	0.8518	1.0000	1.0000	1.0000	1.0000	1.0000	1.0000	1.0000
9.75	1.0000	1.0000	1.0000	1.0000	1.0000	1.0000	1.0000	1.0000

Table A.1.18 Drop size distribution for configuration B5 (z = 0.77 *m*)

m_w, *kg/s*	4.08	4.08	4.08	4.08	4.05	4.05	4.05	4.05
m_a, *kg/s*	5.58	5.58	5.58	5.58	4.09	4.09	4.09	4.09
d, *mm*	R, -	R, -	R, -	R, -	R, -	R, -	R, -	R, -
0.25	0.0001	0.0001	0.0001	0.0000	0.0001	0.0000	0.0001	0.0001
0.75	0.0155	0.0163	0.0107	0.0070	0.0149	0.0078	0.0077	0.0102
1.25	0.0381	0.0421	0.0275	0.0182	0.0407	0.0228	0.0200	0.0263
1.75	0.0914	0.1072	0.0627	0.0492	0.1049	0.0686	0.0520	0.1018
2.25	0.1353	0.1690	0.1069	0.0747	0.1606	0.1005	0.0784	0.1409
2.75	0.1775	0.2141	0.1349	0.1039	0.2166	0.1403	0.1012	0.1837
3.25	0.1984	0.2513	0.1523	0.1231	0.2418	0.1656	0.1221	0.2427
3.75	0.2198	0.2970	0.1878	0.1330	0.2934	0.1967	0.1414	0.2970
4.25	0.2977	0.3470	0.2655	0.1545	0.3685	0.2646	0.1695	0.4552
4.75	0.4934	0.5096	0.3377	0.2046	0.4996	0.4067	0.2609	0.6024
5.25	0.6695	0.5724	0.5329	0.2857	0.5704	0.4920	0.3667	0.7018
5.75	0.9009	0.6548	0.7892	0.3212	0.8495	0.6041	0.4130	0.8323
6.25	1.0000	0.8666	0.8715	0.4580	0.8495	0.6761	0.5320	1.0000
6.75	1.0000	1.0000	0.8715	0.6304	1.0000	0.7667	0.6070	1.0000
7.25	1.0000	1.0000	1.0000	0.7016	1.0000	0.7667	0.6999	1.0000
7.75	1.0000	1.0000	1.0000	0.7016	1.0000	0.7667	0.6999	1.0000
8.25	1.0000	1.0000	1.0000	0.7016	1.0000	0 7667	0.8367	1.0000
8.75	1.0000	1.0000	1.0000	0.8268	1.0000	0.7667	1.0000	1.0000
9.25	1.0000	1.0000	1.0000	0.8268	1.0000	1.0000	1.0000	1.0000
9.75	1.0000	1.0000	1.0000	1.0000	1.0000	1.0000	1.0000	1.0000

Table A.1.19 Drop size distribution implemented in SPSim (z = 0.57 *m*)

m_w, *kg/s*	9.06	9.06	9.06	9.06	8.06	8.06	8.06	8.06
m_a, *kg/s*	0.00	0.00	0.00	0.00	0.00	0.00	0.00	0.00
d, *mm*	R, -	R, -	R, -	R, -	R, -	R, -	R, -	R, -
0.25	0.0000	0.0000	0.0000	0.0000	0.0000	0.0000	0.0000	0.0000
0.75	0.0028	0.0025	0.0029	0.0026	0.0027	0.0048	0.0033	0.0029
1.25	0.0091	0.0094	0.0095	0.0100	0.0099	0.0185	0.0125	0.0083
1.75	0.0252	0.0260	0.0269	0.0271	0.0293	0.0453	0.0386	0.0208
2.25	0.0384	0.0434	0.0438	0.0459	0.0474	0.0785	0.0574	0.0350
2.75	0.0537	0.0641	0.0561	0.0618	0.0620	0.1059	0.0878	0.0527
3.25	0.0705	0.0767	0.0704	0.0801	0.0816	0.1285	0.1146	0.0702
3.75	0.0898	0.0878	0.0891	0.0925	0.0950	0.1682	0.1506	0.0882
4.25	0.1086	0.1241	0.1073	0.1333	0.1243	0.1898	0.1880	0.1317
4.75	0.1545	0.2422	0.2090	0.2218	0.1993	0.2100	0.3028	0.1864
5.25	0.2606	0.3030	0.2776	0.3754	0.2545	0.4005	0.3592	0.2849
5.75	0.3536	0.4227	0.4128	0.5100	0.4720	0.6509	0.5445	0.3712
6.25	0.4432	0.4996	0.4707	0.5388	0.6273	0.7887	0.5445	0.3712
6.75	0.4808	0.6288	0.6165	0.6114	0.6664	0.7887	0.6643	0.5107
7.25	0.5740	0.7488	0.6617	0.7013	0.6664	0.7887	0.6643	0.5972
7.75	0.5740	0.8466	0.7169	0.9210	0.7256	0.7887	0.8458	0.6500
8.25	0.6426	0.8466	0.7169	0.9210	0.7970	1.0000	0.8458	0.7137
8.75	0.8064	0.9169	0.7963	1.0000	0.8821	1.0000	0.8458	0.7897
9.25	1.0000	1.0000	0.8901	1.0000	0.8821	1.0000	1.0000	0.7897
9.75	1.0000	1.0000	1.0000	1.0000	1.0000	1.0000	1.0000	1.0000

Table A.1.20 Drop size distribution implemented in SPSim (z = 0.57 *m*)

m_w, *kg/s*	7.05	7.05	7.05	7.05	5.96	5.96	5.96	5.96
m_a, *kg/s*	0.00	0.00	0.00	0.00	0.00	0.00	0.00	0.00
d, *mm*	R, -	R, -	R, -	R, -	R, -	R, -	R, -	R, -
0.25	0.0000	0.0000	0.0000	0.0000	0.0000	0.0000	0.0000	0.0000
0.75	0.0027	0.0037	0.0044	0.0033	0.0017	0.0020	0.0017	0.0027
1.25	0.0108	0.0136	0.0154	0.0155	0.0060	0.0063	0.0074	0.0097
1.75	0.0340	0.0378	0.0476	0.0399	0.0216	0.0237	0.0184	0.0238
2.25	0.0622	0.0583	0.0783	0.0562	0.0354	0.0411	0.0317	0.0371
2.75	0.0939	0.0795	0.0939	0.0833	0.0540	0.0570	0.0424	0.0612
3.25	0.1086	0.1143	0.1234	0.1146	0.0790	0.0767	0.0599	0.0866
3.75	0.1339	0.1501	0.1631	0.1695	0.1003	0.1019	0.0754	0.1089
4.25	0.1769	0.1847	0.2292	0.2294	0.1563	0.1239	0.1146	0.1656
4.75	0.2799	0.3541	0.3674	0.3828	0.3126	0.2674	0.1852	0.1656
5.25	0.3262	0.4521	0.4919	0.4204	0.4767	0.3227	0.4179	0.3491
5.75	0.4480	0.4521	0.5737	0.5194	0.5383	0.4317	0.6403	0.5499
6.25	0.5652	0.6725	0.7312	0.6465	0.6965	0.5250	0.6760	0.7562
6.75	0.7129	0.7419	0.7973	0.7265	0.6965	0.6426	0.7659	0.8212
7.25	0.7129	1.0000	0.8793	0.8257	0.7582	0.7155	0.7659	0.9017
7.75	0.7129	1.0000	0.8793	0.8257	0.9090	0.7155	0.9020	1.0000
8.25	0.8927	1.0000	1.0000	0.8257	1.0000	0.8228	0.9020	1.0000
8.75	1.0000	1.0000	1.0000	1.0000	1.0000	0.8228	1.0000	1.0000
9.25	1.0000	1.0000	1.0000	1.0000	1.0000	0.8228	1.0000	1.0000
9.75	1.0000	1.0000	1.0000	1.0000	1.0000	1.0000	1.0000	1.0000

Table A.1.21 Drop size distribution implemented in SPSim (z = 0.57 *m*)

m_w, *kg/s*	5.05	5.05	5.05	5.05	4.06	4.06	4.06	4.06
m_a, *kg/s*	0.00	0.00	0.00	0.00	0.00	0.00	0.00	0.00
d, *mm*	**R, -**	**R, -**	**R, -**	**R, -**	**R, -**	**R, -**	**R, -**	**R, -**
0.25	0.0000	0.0000	0.0000	0.0000	0.0001	0.0000	0.0000	0.0000
0.75	0.0038	0.0027	0.0035	0.0023	0.0037	0.0032	0.0031	0.0028
1.25	0.0143	0.0105	0.0127	0.0069	0.0199	0.0102	0.0113	0.0108
1.75	0.0441	0.0286	0.0328	0.0196	0.0519	0.0347	0.0318	0.0302
2.25	0.0678	0.0413	0.0506	0.0378	0.1005	0.0530	0.0535	0.0585
2.75	0.0786	0.0614	0.0563	0.0588	0.1272	0.0735	0.0765	0.0844
3.25	0.1084	0.0779	0.0657	0.0675	0.1491	0.0947	0.0937	0.0972
3.75	0.1176	0.1117	0.0850	0.0763	0.2054	0.1338	0.1202	0.1365
4.25	0.1842	0.1486	0.1061	0.0957	0.3200	0.1906	0.1433	0.2224
4.75	0.2586	0.3033	0.1943	0.1318	0.4115	0.3097	0.2723	0.3157
5.25	0.4596	0.4426	0.2738	0.2536	0.5350	0.4169	0.3304	0.4597
5.75	0.7237	0.5645	0.3086	0.3817	0.6972	0.4638	0.4831	0.5543
6.25	0.8932	0.8778	0.4426	0.5461	0.8014	0.5241	0.6301	0.6757
6.75	1.0000	0.8778	0.5551	0.7014	0.8014	0.6760	0.7536	0.9052
7.25	1.0000	1.0000	0.6249	0.7656	0.8014	0.7701	0.9066	1.0000
7.75	1.0000	1.0000	0.6249	0.8439	1.0000	1.0000	1.0000	1.0000
8.25	1.0000	1.0000	0.8304	0.8439	1.0000	1.0000	1.0000	1.0000
8.75	1.0000	1.0000	0.8304	0.8439	1.0000	1.0000	1.0000	1.0000
9.25	1.0000	1.0000	0.8304	0.8439	1.0000	1.0000	1.0000	1.0000
9.75	1.0000	1.0000	1.0000	1.0000	1.0000	1.0000	1.0000	1.0000

Table A.1.22 Pressure drop data obtained during drop distribution testing

m_w, *kg/s*	4.00	4.00	6.50	6.50	9.00	9.00
m_a, *kg/s*	5.45	4.10	5.45	4.10	5.45	4.10
Configuration	**Δp, *Pa***	**Δp, *Pa***	**Δp, *Pa***	**Δp, *Pa***	**Δp, *Pa***	**Δp, *Pa***
A	14.0	9.0	19.5	13.5	25.0	18.0
B1	18.0	14.0	23.0	20.0	31.0	24.0
B2	14.0	10.0	18.0	13.0	32.0	22.0
B3	16.0	10.0	23.0	15.0	30.0	22.0
B4	18.0	11.0	24.0	15.0	34.0	26.0
B5	18.0	10.0	24.0	15.0	31.0	22.0

(Note-The mass flow rates indicated are approximate values - the exact values are given in Tables A.1.1 - A.1.18)

Table A.1.23 Total mass counted for each configuration [kg]

m_w , *kg/s*	4.00	4.00	6.50	6.50	9.00	9.00
m_a , *kg/s*	5.45	4.10	5.45	4.10	5.45	4.10
m_w/m_a	0.73	0.98	1.20	1.59	1.65	2.20
A	0.0042	0.0042	0.0051	0.0060	0.0091	0.0067
B1	0.0052	0.0043	0.0070	0.0072	0.0090	0.0094
B2	0.0040	0.0046	0.0063	0.0051	0.0087	0.0089
B3	0.0026	0.0022	0.0035	0.0047	0.0076	0.0060
B4	0.0038	0.0039	0.0053	0.0053	0.0061	0.0057
B5	0.0034	0.0029	0.0045	0.0062	0.0072	0.0066

(Note-The mass flow rates indicated are approximate values - the exact values are given in Tables A.1.1 - A.1.18)

Table A.1.24 Sauter mean diameter for each configuration [mm]

m_w , *kg/s*	4.00	4.00	6.50	6.50	9.00	9.00
m_a , *kg/s*	5.45	4.10	5.45	4.10	5.45	4.10
m_w/m_a	0.73	0.98	1.20	1.59	1.65	2.20
A	5.30	5.20	5.34	5.33	5.36	5.36
B1	4.63	4.48	4.68	4.64	4.65	4.63
B2	4.39	4.34	4.37	4.33	4.29	4.32
B3	4.29	4.42	4.21	4.13	4.00	4.05
B4	3.99	4.05	4.06	4.07	4.05	4.04
B5	4.38	4.35	4.36	4.37	4.32	4.30

(Note-The mass flow rates indicated are approximate values - the exact values are given in Tables A.1.1 - A.1.18)

Table A.1.25 Mass mean diameter for each configuration [mm]

m_w , *kg/s*	4.00	4.00	6.50	6.50	9.00	9.00
m_a , *kg/s*	5.45	4.10	5.45	4.10	5.45	4.10
m_w/m_a	0.73	0.98	1.20	1.59	1.65	2.20
A	3.37	3.31	3.38	3.36	3.36	3.37
B1	2.93	2.89	2.92	2.89	2.87	2.87
B2	2.79	2.78	2.76	2.72	2.66	2.69
B3	2.67	2.75	2.62	2.56	2.47	2.51
B4	2.53	2.54	2.55	2.55	2.52	2.53
B5	2.65	2.65	2.63	2.63	2.61	2.60

(Note-The mass flow rates indicated are approximate values - the exact values are given in Tables A.1.1 - A.1.18)

Table A.1.26 Rosin-Rammler parameters and correlation coefficients

A				**B1**				**B2**			
L/G	d_{RR}	n_{RR}	R^2	L/G	d_{RR}	n_{RR}	R^2	L/G	d_{RR}	n_{RR}	R^2
0.68	7.04	3.16	0.99411	0.75	6.50	3.13	0.99431	0.75	6.16	2.77	0.99371
0.89	6.94	3.65	0.99807	0.97	6.53	346	0.99394	1.01	5.96	2.74	0.99534
1.24	6.59	3.82	0.99835	1.14	6.19	3.29	0.99449	1.20	6.33	2.49	0.99458
1.60	6.99	3.94	0.99764	1.48	6.75	3.00	0.99529	1.60	5.66	3.01	0.99284
1.70	6.88	3.90	0.99787	1.65	6.31	2.81	0.99782	1.65	6.22	2.41	0.99725
2.17	6.58	3.45	0.99854	2.15	6.38	2.78	0.99717	2.21	6.14	3.06	0.99621
B3				**B4**				**B5**			
L/G	d_{RR}	n_{RR}	R^2	L/G	d_{RR}	n_{RR}	R^2	L/G	d_{RR}	n_{RR}	R^2
0.75	5.77	2.21	0.99535	0.74	5.50	3.06	0.99407	0.73	5.65	3.27	0.99493
1.00	5.45	2.17	0.99595	0.97	5.94	2.70	0.99427	0.99	5.68	2.76	0.99674
1.20	5.10	1.99	0.99721	1.20	5.52	2.57	0.99613	1.15	5.81	2.47	0.99591
58	5.97	2.79	0.99608	1.58	6.03	2.79	0.99632	1.53	6.56	2.91	0.99372
1.66	5.80	2.70	0.99567	1.69	5.69	2.40	0.99694	1.65	6.37	2.56	0.99351
2.18	5.90	2.55	0.99817	2.25	5.99	2.42	0.99454	2.15	6.01	2.59	0.99540

A.2 RESULTS OF THERMAL TESTING

Table A.2.1 Thermal test data (Configuration A - no splash grid)

Test	T_{aidb}	T_{aiwb}	T_{wi}	T_{wo}	G	L	Δp
	℃	℃	℃	℃	kg/m^2s	kg/m^2s	*Pa*
1	21.05	19.94	50.86	43.07	1.214	4.250	15.0
2	20.14	18.81	50.18	39.91	1.735	4.212	21.0
3	19.51	17.89	49.60	37.21	2.347	4.200	29.0
4	19.13	17.37	49.07	34.95	2.931	4.194	39.0
5	19.22	17.28	47.91	33.49	2.945	3.589	34.0
6	19.51	17.54	47.46	35.11	2.396	3.579	25.0
7	20.04	18.22	46.84	37.01	1.795	3.582	17.0
8	20.35	18.78	46.34	39.17	1.246	3.579	12.0
9	19.95	18.41	45.51	37.58	1.261	2.944	8.5
10	19.65	17.94	45.37	35.25	1.763	2.944	13.5
11	19.71	17.68	45.10	33.17	2.358	2.936	21.0
12	20.00	17.71	44.81	31.33	2.972	2.944	28.0
13	20.44	17.90	44.24	29.41	2.995	1.861	21.0
14	20.46	18.00	43.84	30.77	2.400	1.788	15.0
15	20.60	18.19	43.63	32.54	1.820	1.798	9.0
16	20.61	18.46	43.36	34.61	1.246	1.789	5.0

(P_{atm} = 100634 Pa, T_{atm} = 23.5 °C)

Table A.2.2 Thermal test data (Configuration B - splash grids at distance 0.57 m beneath trickle pack)

Test	T_{aidb}	T_{aiwb}	T_{wi}	T_{wo}	G	L	Δp
	℃	℃	℃	℃	kg/m^2s	kg/m^2s	*Pa*
1	21.72	19.66	50.24	42.33	1.187	4.090	17.0
2	21.21	19.12	49.42	38.95	1.726	4.084	24.5
3	20.99	18.71	49.02	36.03	2.367	4.078	35.5
4	20.92	18.56	48.62	33.82	2.953	4.063	47.0
5	21.18	18.63	47.2	32.15	2.970	3.312	39.5
6	21.17	18.73	46.96	33.98	2.357	3.305	30.0
7	21.34	19.01	46.49	36.24	1.744	3.310	19.0
8	21.35	19.27	46.03	38.62	1.196	3.304	12.0
9	21.22	19.17	45.56	36.98	1.206	2.615	9.0
10	21.31	19.03	45.33	34.27	1.760	2.614	14.5
11	21.27	18.78	45.02	32.07	2.374	2.615	23.0
12	21.54	18.79	44.81	30.14	2.968	2.590	34.0
13	21.54	18.77	44.44	29.11	2.972	2.008	29.0
14	21.42	18.76	44.21	30.72	2.387	2.006	19.0
15	21.52	18.99	43.98	32.88	1.723	2.003	11.0
16	21.53	19.19	43.72	34.84	1.227	1.998	7.0

(P_{atm} = 100526 Pa, T_{atm} = 24.0 °C)

Table A.2.3 Calculated transfer characteristic and pressure loss coefficients

	Configuration A				Configuration B			
Test	**L**	**G**	**KaV/L**	**N_p**	**L**	**G**	**KaV/L**	**N_p**
	kg/m^2s	*kg/m^2s*	-	*1/m*	*kg/m^2s*	*kg/m^2s*	-	*1/m*
1	4.250	1.214	0.265	8.523	4.090	1.187	0.286	10.134
2	4.212	1.735	0.387	5.829	4.084	1.726	0.432	6.960
3	4.200	2.347	0.504	4.565	4.078	2.367	0.594	5.291
4	4.194	2.931	0.623	3.802	4.063	2.953	0.741	4.594
5	3.589	2.945	0.684	3.360	3.312	2.970	0.823	3.741
6	3.579	2.396	0.566	3.695	3.305	2.357	0.672	4.545
7	3.582	1.795	0.445	4.416	3.310	1.744	0.503	5.195
8	3.579	1.246	0.314	6.417	3.304	1.196	0.344	7.038
9	2.944	1.261	0.368	4.545	2.615	1.206	0.421	5.114
10	2.944	1.763	0.500	3.691	2.614	1.760	0.595	3.935
11	2.936	2.358	0.627	3.195	2.615	2.374	0.750	3.428
12	2.944	2.972	0.767	2.679	2.590	2.968	0.931	3.254
13	1.861	2.995	0.887	1.958	2.008	2.972	0.995	2.790
14	1.788	2.400	0.747	2.182	2.006	2.387	0.818	2.797
15	1.798	1.820	0.602	2.305	2.003	1.723	0.631	3.101
16	1.789	1.246	0.455	2.755	1.998	1.227	0.484	3.916

APPENDIX B

RESULTS OF COMPUTER SIMULATION

Table B.1 Drop size distribution for Configuration B

L/G, –	2.00	2.67	3.25	4.33	4.50	6.00
d, *mm*	R, –	R, –	R, –	R, –	R, –	R, –
0.77	0.04330	0.04442	0.04246	0.04346	0.04060	0.04143
1.27	0.12546	0.12753	0.12295	0.12478	0.11720	0.11878
1.77	0.17975	0.18164	0.17371	0.17539	0.16557	0.16710
2.27	0.21189	0.21365	0.20287	0.20444	0.19034	0.19188
2.77	0.24414	0.24584	0.23537	0.23688	0.21560	0.21718
3.27	0.28280	0.28444	0.27357	0.27503	0.24336	0.24505
3.77	0.34211	0.34368	0.32865	0.33005	0.28657	0.28819
4.26	0.42068	0.42219	0.40795	0.40931	0.34926	0.35076
4.76	0.50403	0.50553	0.48964	0.49099	0.42403	0.42579
5.26	0.59724	0.59875	0.57949	0.58084	0.50405	0.50633
5.76	0.72422	0.72573	0.69556	0.69692	0.60425	0.60632
6.26	0.79804	0.79950	0.75900	0.76033	0.66934	0.67096
6.76	0.85613	0.85745	0.81322	0.81443	0.73550	0.73675
7.26	0.90620	0.90719	0.87394	0.87486	0.81091	0.81172
7.76	0.96577	0.96615	0.94075	0.94113	0.90275	0.90291
8.25	0.99103	0.99113	0.98671	0.98676	0.96562	0.96556
8.75	0.99945	0.99945	0.99815	0.99815	0.99019	0.99009
9.25	0.99976	0.99976	0.99918	0.99918	0.99840	0.99832
9.75	1.00000	1.00000	1.00000	1.00000	1.00000	1.00000

Table B.2 Simulation transfer characteristic and pressure loss coefficients (Configuration A - no splash grid)

Test	T_{aidb}	T_{aiwb}	T_{wi}	T_{wo}	L/G	KaV/L	N_p
	℃	℃	℃	℃	–	–	*1/m*
1	21.05	19.94	50.86	43.07	3.501	0.1003	9.577
2	20.14	18.81	50.18	39.91	2.428	0.1098	5.428
3	19.51	17.89	49.60	37.21	1.789	0.1171	3.916
4	19.13	17.37	49.07	34.95	1.431	0.1233	2.990
5	19.22	17.28	47.91	33.49	1.219	0.1381	2.709
6	19.51	17.54	47.46	35.11	1.494	0.1323	3.750
7	20.04	18.22	46.84	37.01	1.996	0.1203	4.720
8	20.35	18.78	46.34	39.17	2.872	0.1140	8.436
9	19.95	18.41	45.51	37.58	2.334	0.1221	7.085
10	19.65	17.94	45.37	35.25	1.670	0.1287	4.118
11	19.71	17.68	45.10	33.17	1.245	0.1360	2.945
12	20.00	17.71	44.81	31.33	0.991	0.1513	2.235
13	20.44	17.90	44.24	29.41	0.622	0.1618	1.492
14	20.46	18.00	43.84	30.77	0.745	0.1495	1.961
15	20.60	18.19	43.63	32.54	0.988	0.1407	2.544
16	20.61	18.46	43.36	34.61	1.436	0.1344	4.641

(P_{atm} = 100634 Pa, T_{atm} = 23.5 °C)

Table B.3 Simulation transfer characteristic and pressure loss coefficients (Configuration B - splash grids at distance 0.57 m beneath trickle pack)

Test	T_{aidb}	T_{aiwb}	T_{wi}	T_{wo}	L/G	KaV/L	N_p
	℃	℃	℃	℃	–	–	*1/m*
1	21.72	19.66	50.24	42.33	3.447	0.1921	11.429
2	21.21	19.12	49.42	38.95	2.366	0.2042	6.620
3	20.99	18.71	49.02	36.03	1.723	0.2148	4.590
7	21.34	19.01	46.49	36.24	1.898	0.2367	6.133
8	21.35	19.27	46.03	38.62	2.761	0.2251	10.471
9	21.22	19.17	45.56	36.98	2.168	0.2202	8.351
10	21.31	19.03	45.33	34.27	1.485	0.2334	4.972
15	21.52	18.99	43.98	32.88	1.163	0.2529	4.121
16	21.53	19.19	43.72	34.84	1.628	0.2402	6.475

(P_{atm} = 100526 Pa, T_{atm} = 24.0 °C)

Table B.4 Simulation transfer characteristic and pressure loss coefficient for 8 *m* rain zone.

			A		B	
L	G	L/G	KaV/L	N_p	KaV/L	N_p
kg/m^2s	kg/m^2s	-	-	*1/m*	-	*1/m*
1.446	1.185	1.220	0.546	3.173	0.883	8.809
1.446	1.785	0.810	0.588	1.463	0.949	1.984
1.446	2.370	0.610	0.633	0.95	1.019	1.37
1.446	2.951	0.490	0.680	0.729	1.096	1.153
1.506	1.186	1.270	0.546	3.313	0.883	9.942
1.506	1.772	0.856	0.588	1.522	0.949	2.063
1.506	2.390	0.630	0.633	0.998	1.019	1.425
1.506	2.953	0.510	0.680	0.759	1.096	1.201
1.566	1.186	1.320	0.545	3.455	0.882	9.313
1.566	1.780	0.880	0.587	1.581	0.948	2.143
1.566	2.373	0.660	0.632	1.037	1.020	1.481
1.566	2.955	0.530	0.680	0.789	1.100	1.248

(A : Drop size distribution of Configuration A, B : Drop size distribution of Configuration B4)

APPENDIX C

SPLASH PACK SIMULATION PROGRAM (SPSIM)

The following assumptions were made in the mathematical model used in the program:

- The enthalpy potential model for simultaneous heat and mass transfer, proposed by Merkel [26ME1] is valid. This implies that Le = 1 and that evaporation is negligible.
- The air is thoroughly mixed, i.e., the air enthalpy is constant in any given horizontal plane.
- Radiation effects are negligible.
- The initial drop size distribution and drop velocities are known at the water inlet side
- The transient problem of modelling accelerating drops may be approximated as a succession of steady states.
- The drop drag coefficients and heat/mass transfer coefficients experienced by each drop in the splash pack is not influenced by the proximity of other drops.
- The effect of free stream turbulence on the drag of individual drops is assumed to be negligible. The effect of free stream turbulence on the heat and mass transfer from the drops is taken into account.

General

For integration purposes, the packing zone is divided into a number of layers. The number of layers correspond to the number of splash grids. These imaginary layers in the packing are selected in such a way as to ensure that every grid (if any) falls on the boundary of a layer. If a spray zone and a rain zone are to be evaluated as well, they each represent another layer. Every layer is divided into a number of elements, each with a thickness of ∂z. For a typical element, the following governing equation for the total heat transfer from the water to the air can be derived from the Merkel theory:

$$\partial \dot{Q} = K \partial A (i_{asw} - i_a) = Ka A_{fr} \partial z (i_{asw} - i_a) \qquad (5.x)$$

An energy balance gives

$$\partial \dot{Q} = \dot{m}_a \partial i_a = \dot{m}_w c_{pw} \partial T_w \qquad (5.x)$$

The temperature drop of the water and the air enthalpy gain can be calculated from the equations above.

The equation of motion of a given drop falling through an element is solved to determine the average velocity of the drop through the element. The drop velocity is then used to calculate the heat and mass transfer coefficients. From these coefficients, the cooling rate of the drop in

the element is calculated. The integration process is started at the top of the packing zone (at the water inlet side) since the initial drop size and velocity distributions are known there. The outlet air enthalpy, i_{ao}, is not known and an initial value of i_{ao} is assumed. After the integration downwards through the packing, the calculated air inlet enthalpy should correspond with the ambient air enthalpy (if the initial choice of i_{ao} was correct). If it does not agree, a new value of air outlet enthalpy has to be assumed and the integration process repeated until a solution is reached. Upon completion of the integration process the average outlet water temperature can be calculated. The overall transfer characteristic of the packing can then be calculated using the Tchebycheff integration method.

To simplify and reduce the number of calculations required to evaluate a given element, the collection of drops in each element is divided into discrete packets. These packets allow drops of similar diameter, temperature and velocity to be lumped together. Each packet has a unique combination of drop size, velocity and temperature. To specify the number of drops per packet, the mass flow rate represented by each packet is used.

Options

The current program makes provision for the following conditions and options:

- The inlet drop distribution can be mono- or polydispersed (Rosin-Rammler distribution).
- The inlet mass mean drop size and velocity can be user-specified or approximated for a full cone spray nozzle.
- Three drop drag models can be used:
  1. No drag
  2. Spherical drops
  3. Deformed non-oscillating drops
- Dripping of water below grids is modeled with the Yung [80YU1] model or using interpolation from tabulated experimental data.
- Splashing of drops on grids are modelled using
  a) a model based on data by Mutchler [71MU1], Scriven et al. [72SC1] and Stedman [79ST1], or
  b) a model based on experimentally determined Rosin-Rammler experimental data.
- Cutting of drops near the edges of slats are taken into account using a simple model based on that proposed by Yao et al. [88YA1].
- Aerodynamic break-up of drops are modelled using the Wierzba [90WI1] model.
- Upward flow of small drops are taken into account assuming:
  a) drop loss, or
  b) redistribution of mass between down-flowing drops, or
  c) the dripping of large cold drops from the drift eliminators.
- Drop-drop collisions (assuming coalescence).
- Heat and mass transfer from the grids.